POLITECNICO
MILANO 1863

SCUOLA DI INGEGNERIA INDUSTRIALE
E DELL'INFORMAZIONE

Thermodynamic analysis and optimization of improved Heat Pump architecture for Carnot battery based energy storage system

ENERGY ENGINEERING –INGEGNERIA ENERGETICA

Author: **Sobhan Amini Harandi** and **Masoud Mohammadi**

Student ID:	10757854, 10761679
Advisor:	Prof. Marco Astolfi
Co-advisor:	Dario Alfani
Academic Year:	2022-23

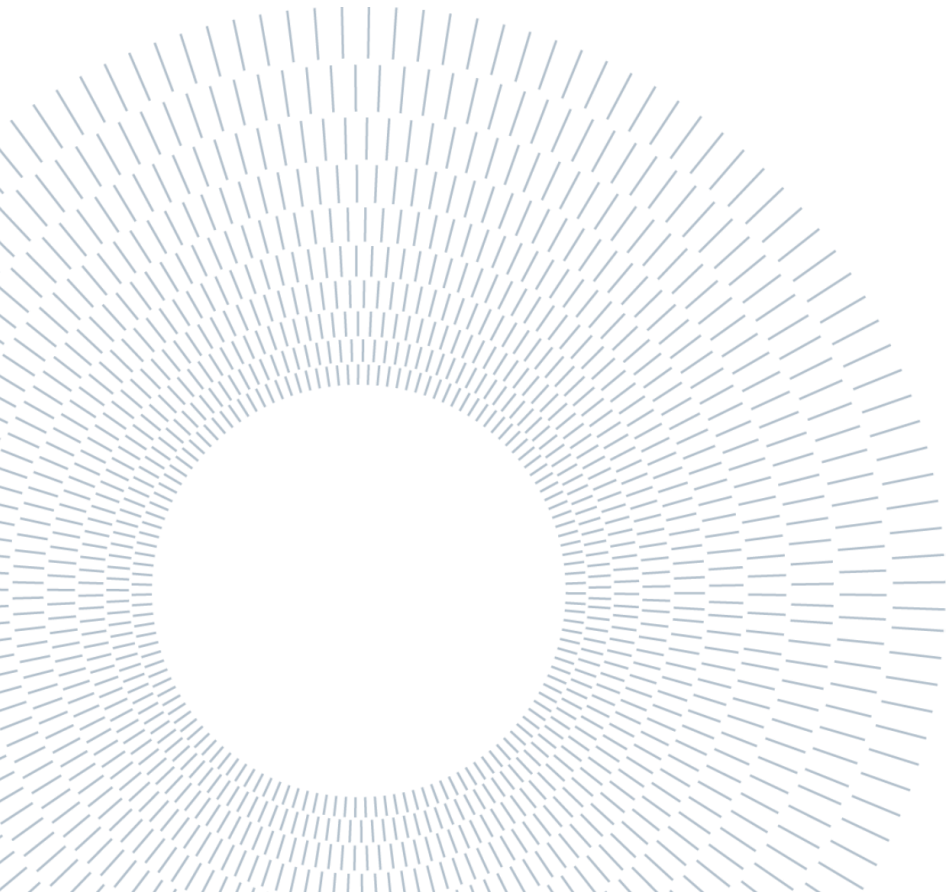

To our parents and partners,

For their endless love, support and encouragement

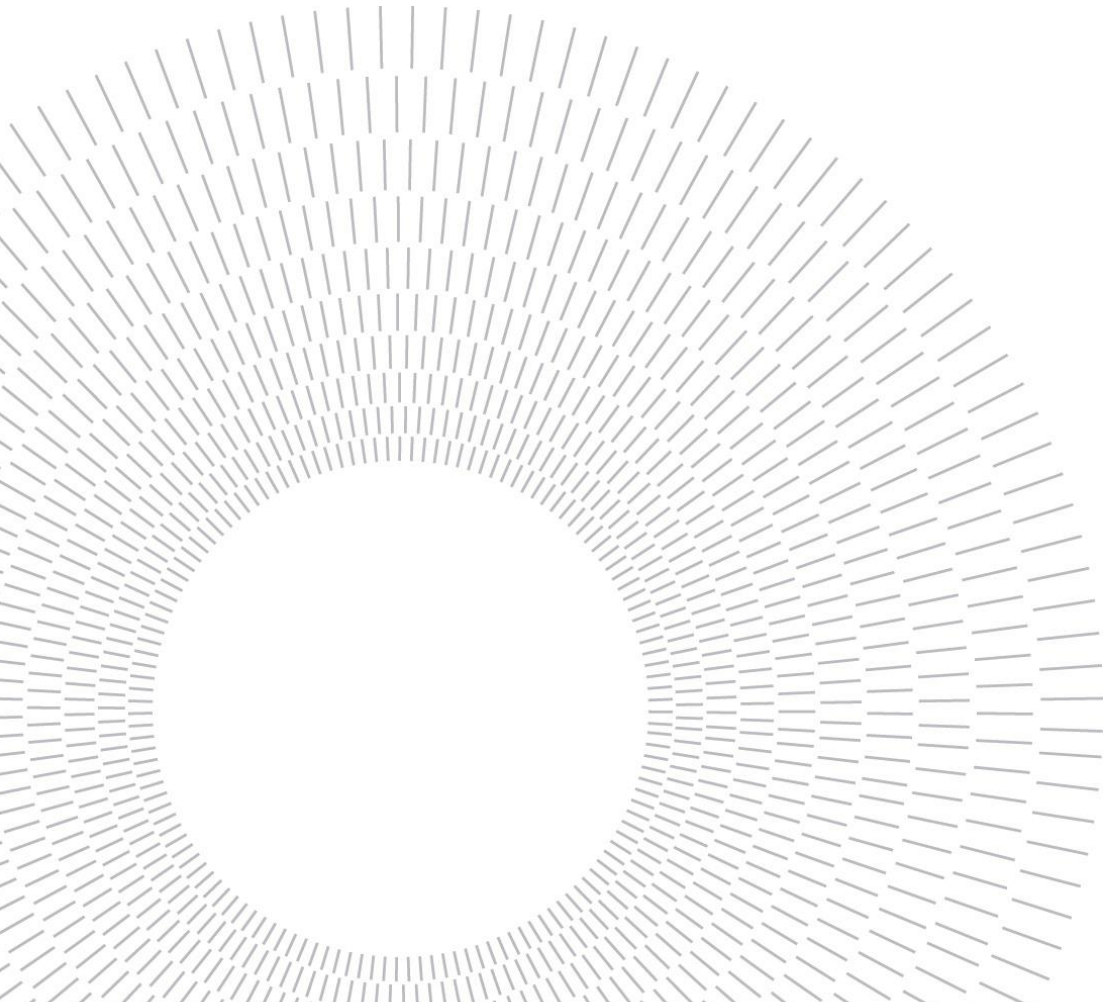

"Out of clutter, find simplicity. From discord, find Harmony. In the middle of difficulty lies opportunity"

Albert Einstein

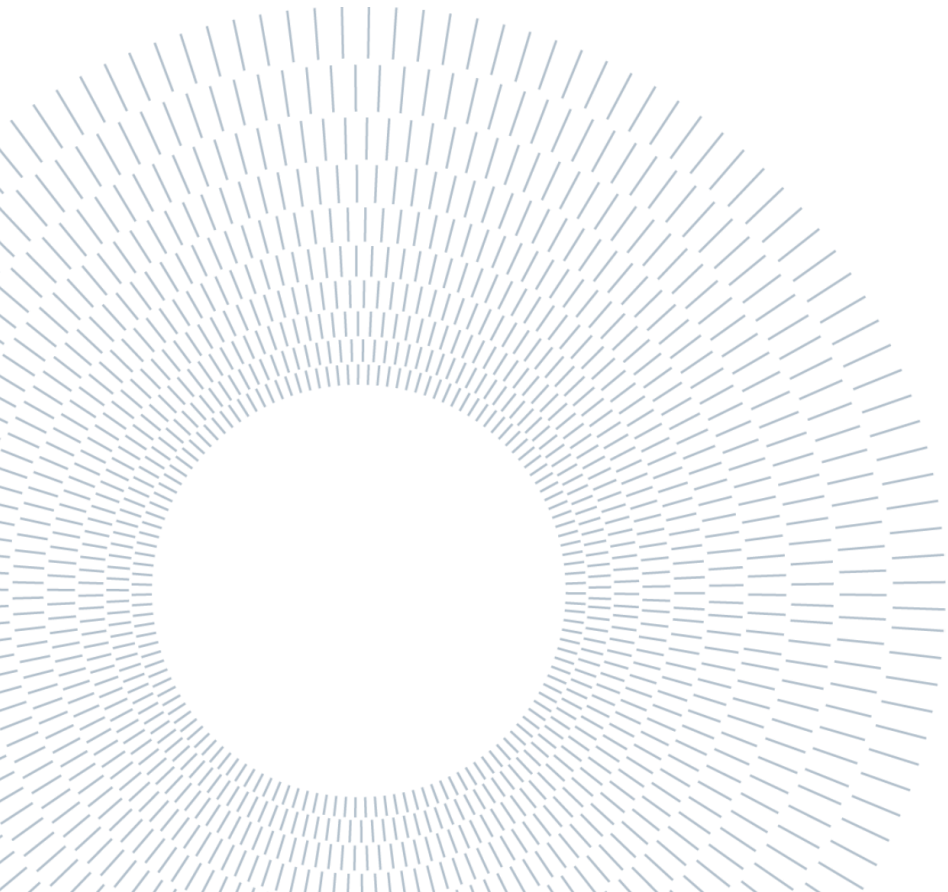

Acknowledgements

We want to express our gratitude to Professor Astolfi for his consistent presence, invaluable guidance, and assistance throughout this thesis. His ability to anticipate the expected outcomes has been particularly noteworthy.

Notes

As a general remark, it should be noted that certain sections of the Matlab code are derived from prior collaborative work by the Professor Astolfi with his colleagues such as Dario Alfani, Simone Montozzi at the Energy Department of Politecnico di Milano.

Abstract

In the current research project, the author analyzes an improved typed of Heat Pump cycle, which is used in a new method of energy storage systems; a heat pump cycle including a drain cooler is coupled to Rankine cycle based on a thermochemical storage system. This innovative system uses a low-temperature heat source, which can come from sources such as industrial waste or renewable heat, to evaporate the operating fluid in a low-pressure heat exchanger. After compression, the fluid undergoes condensation in a high-pressure exchanger, releasing heat that supplies the thermochemical reactor where the endothermic reaction takes place. When power is needed, a reverse exothermic reaction occurs, releasing heat for the Rankine cycle. To analyze the thermodynamics of the heat pump cycle and determine the most efficient fluid in terms of coefficient of performance, the author created a set of Matlab® codes.

Thanks to the sensitivity analysis involving different fluids PXYLENE, Ebenzene, C3CC6 and Toluene are the best fluid in terms of having largest coefficient of performance and hydrocarbons are the best organic chemicals in terms of adding a drain cooler to simple heat pump cycle.

Key-words: Heat Pump, Organic Rankin Cycle, Coefficient of Performance, Thermochemical storage, Heat Exchangers

Sommario

Nel presente progetto di ricerca, l'autore analizza un tipo migliorato di ciclo della pompa di calore, che viene utilizzato in un nuovo metodo di sistemi di accumulo dell'energia; un ciclo a pompa di calore comprendente un raffreddatore di scarico è accoppiato al ciclo Rankine basato su un sistema di accumulo termochimico. Questo sistema innovativo utilizza una fonte di calore a bassa temperatura, che può provenire da fonti come rifiuti industriali o calore rinnovabile, per evaporare il fluido operativo in uno scambiatore di calore a bassa pressione. Dopo la compressione, il fluido subisce condensazione in uno scambiatore ad alta pressione, liberando calore che alimenta il reattore termochimico dove avviene la reazione endotermica. Quando è necessaria energia, si verifica una reazione esotermica inversa, che rilascia calore per il ciclo Rankine. Per analizzare la termodinamica del ciclo della pompa di calore e determinare il fluido più efficiente in termini di coefficiente di prestazione, l'autore ha creato una serie di codici Matlab®.

Grazie all'analisi di sensibilità che coinvolge diversi fluidi, PXYLENE, Ebenzene, C3CC6 e Toluene sono i migliori fluidi in termini di coefficiente di prestazione più elevato e gli idrocarburi sono i migliori prodotti chimici organici in termini di aggiunta di un raffreddatore di scarico al semplice ciclo della pompa di calore.

Parole chiave: Pompa di calore, Ciclo Rankin organico, Coefficiente di prestazione, Accumulo termochimico, Scambiatori di calore

Contents

1.Introduction

1.1 Transition Towards Renewables

The urgent need to transition towards cleaner and more sustainable energy sources has never been more apparent. With the relentless rise of carbon emissions and their devastating impact on global ecosystems, the harnessing of renewable energy has garnered immense attention. In addition, as the global population continues to increase, along with its energy demands, a critical shift from fossil fuels to renewable sources has become imperative. This transition not only addresses pressing ecological challenges but also promises a myriad of social, economic, and environmental benefits. Renewable energy sources, such as solar, wind, hydroelectric, and geothermal power, offer a beacon of hope by providing energy that is both abundant and environmentally friendly.

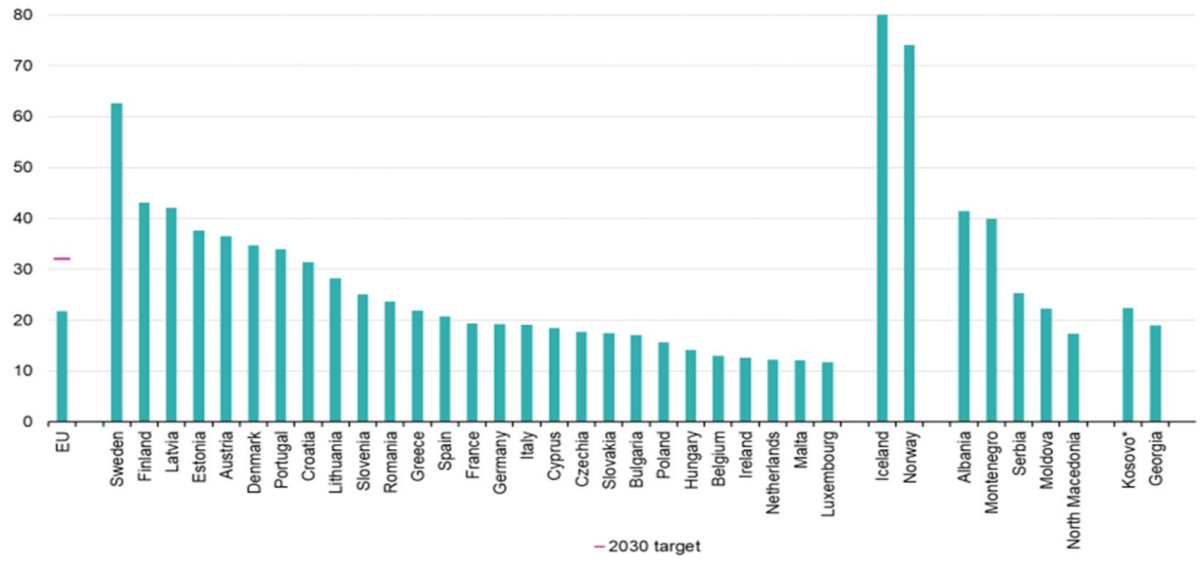

Figure 1-1: Share of energy from renewable sources, 2021 (% of gross final energy consumption)

In 2021, the EU used renewable sources for about 21. 8% of its gross final energy consumption, which was slightly less than the previous year. The removal of the rules related to the COVID-19 pandemic may have contributed to this decrease. Moreover, the change in the laws and the way we do our accounting has also played

a role in this progress [1]. Figure 1-1 displays the most recent information on the proportion of renewable energies used in total energy consumption [1]

1.2 Importance of Energy Storage Systems (ESS)

The importance of renewable energy transcends its role as an alternative energy source; it embodies a transformative shift towards a more sustainable, equitable, and resilient future. By mitigating climate change, conserving resources, stimulating economic growth, fostering innovation, and safeguarding public health and the environment, renewable energy serves as a catalyst for positive change on a global scale. As nations continue to recognize the imperative of this transition, investing in and embracing renewable energy emerges as a critical pathway towards a brighter and more sustainable tomorrow.

With the increment of the generation of power/energy from renewables it gets to be much vital to see at strategies and strategies to store this energy. In guideline, the renewable energy can be changed into another shape of storable energy and to be changed back when required. When we are talking about energy storage systems, we should consider the criteria of selection for method and technique of storing this energy. Researchers and scientists have classified different criteria in selecting the energy storage techniques, the main points to be considered are: 1) the available energy resources, 2) energy requirement and application, 3) energy storage efficiency, 4) energy storage cost, 5) energy storage infrastructure, 6) other factors [2].

In the realm of contemporary energy systems, the importance of energy storage cannot be overstated. As the world moves towards greater reliance on renewable energy sources and grapples with the challenges posed by intermittency and fluctuating demand, energy storage systems emerge as a linchpin to ensure a reliable, stable, and sustainable energy supply.

- Renewable energy sources, such as solar and wind, are inherently intermittent, generating power only when environmental conditions permit. This variability poses a challenge to the consistent supply of electricity, often leading to imbalances between generation and demand. Energy storage systems play a pivotal role in bridging this gap by capturing surplus energy during periods of high generation and releasing it during peak demand or low generation times. This ensures a steady and predictable power supply, enhancing grid stability and minimizing disruptions.

- The integration of renewable energy into existing energy grids is essential for reducing carbon emissions and curbing the effects of climate change. However, the intermittent nature of renewables makes seamless integration a complex endeavor. Energy storage systems act as a buffer, enabling excess energy to be stored and used when needed, thereby facilitating the reliable integration of variable renewable sources. This synergy transforms intermittent renewables into a dependable energy source, reducing the reliance on fossil fuels and advancing the transition to cleaner energy systems.
- Modern energy grids are complex networks that require precise balance between supply and demand. Energy storage systems enhance grid flexibility by providing rapid response to fluctuations in demand or supply. This capability is crucial for maintaining grid stability, avoiding blackouts, and accommodating unforeseen events. Moreover, energy storage systems enhance grid resilience by offering backup power during emergencies, strengthening the overall reliability of energy supply.
- Energy storage systems have the potential to reshape energy markets and economics. They can store excess energy during periods of low demand when electricity prices are lower and release it when demand is high and prices are elevated. This practice, known as peak shaving or demand response, optimizes energy consumption patterns and reduces the need for costly peaking power plants. Additionally, energy storage systems can provide grid services, such as frequency regulation and voltage support, creating new revenue streams for system operators and investors.
- The rise of distributed energy resources, including rooftop solar panels and residential wind turbines, has transformed the energy landscape. Energy storage systems complement these resources by allowing homeowners and businesses to store surplus energy for use when their generation capacity is limited. This fosters greater energy self-sufficiency, reduces strain on centralized grids, and empowers consumers to actively participate in the energy transition.
- The electrification of transportation, particularly electric vehicles (EVs), introduces new dynamics to energy systems. Energy storage systems can play a critical role in supporting EV charging infrastructure. They can store energy during off-peak hours and deliver it to charging stations during peak demand, reducing strain on the grid and minimizing infrastructure upgrades.

Moreover, used EV batteries can find a second life as stationary energy storage units, extending their lifecycle and contributing to overall sustainability.

- The importance of energy storage systems extends beyond their current applications. Ongoing research and development hold the promise of new storage technologies with higher efficiency, longer lifespans, and lower costs. Additionally, the synergy between energy storage and other emerging technologies, such as advanced materials, artificial intelligence, and blockchain, can unlock novel solutions for energy management, distribution, and consumption.

1.3 Different Types of Energy Storage Systems

These systems bridge the gap between energy generation and consumption, providing the reliability and flexibility necessary to accommodate the intermittency of renewable energy sources and ensure grid stability. This part provides a comprehensive overview of different types of energy storage systems, ranging from traditional to cutting-edge technologies, each offering unique advantages and applications.

1.3.1 Electrochemical Energy Storage Systems:

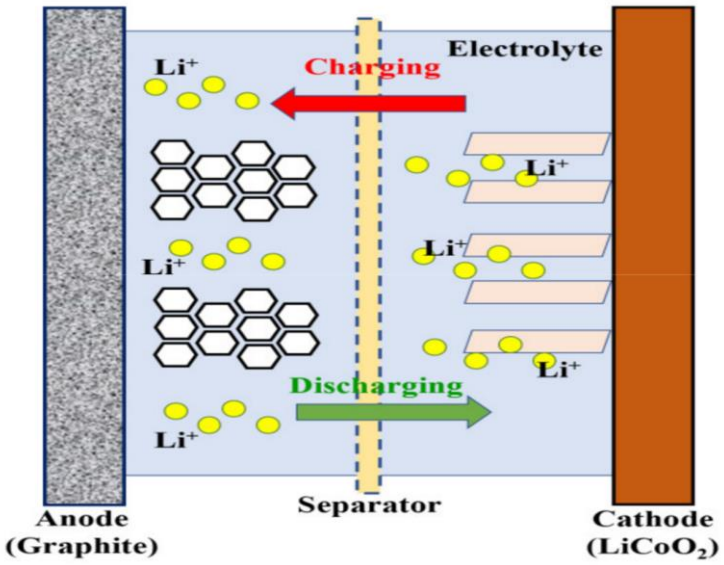

Figure 1-2: Schematic of the structure and working mechanism of Li-ion batteries

These power sources use chemical reactions to produce an electric current. At least two things react together to create a chemical change [3, 4].

- Battery Technology: Batteries are among the most well-known and widely used energy storage systems. They store energy through electrochemical reactions and are prevalent in various applications, from consumer electronics to grid-scale installations. Lithium-ion batteries, for instance, power electric vehicles and enable residential energy storage. Lithium-ion batteries have four main parts: a cathode, an anode, an electrolyte, and a separator. This can be seen in Figure 1-2 [5]. Vanadium redox flow batteries excel in grid applications, offering scalability and long cycle life. Emerging technologies like solid-state batteries hold promise for higher energy density and safety.

1.3.2 Mechanical Energy Storage Systems:

Mechanical energy storage can be divided into different types based on how they work: using pressurized gas, springs that are activated by a force, storing energy in movement (kinetic), and storing energy in a stationary position (potential). The best advantage of mechanical energy storage is that it can easily provide the energy needed for mechanical tasks whenever needed [6].

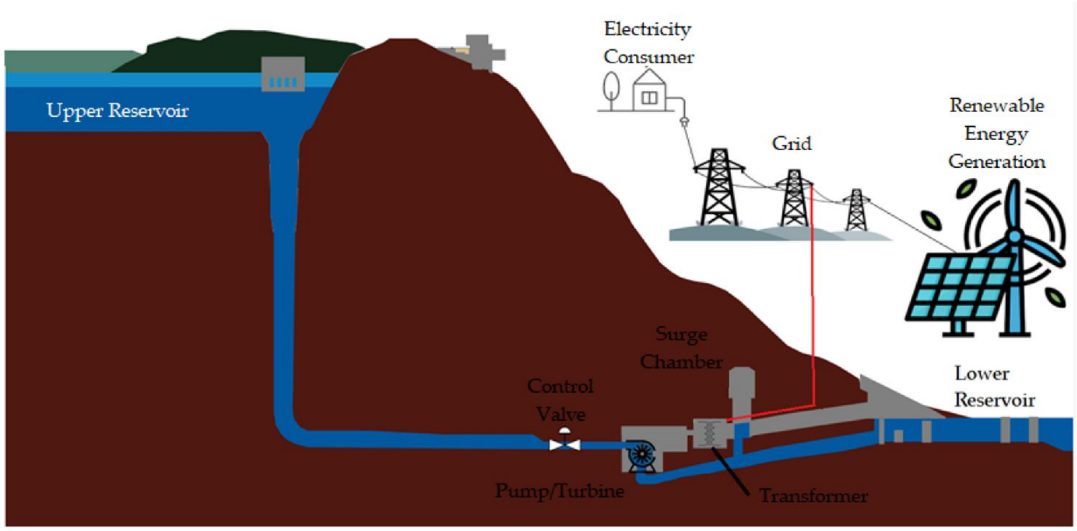

Figure 1-3: layout of a PHS system

- **Pumped Hydro Storage:** Pumped hydroelectric storage is a mature and effective technology that utilizes two reservoirs at different elevations to store and release energy. It is shown in Figure 1-3. During periods of low demand, excess electricity pumps water from the lower reservoir to the upper reservoir. When demand peaks, the stored water is released, flowing downhill and

driving turbines to generate electricity. This system offers high efficiency and large storage capacity, making it a significant contributor to grid stability.

1.3.3 Thermal Energy Storage Systems:

- **Latent and Sensible Heat Storage:** Thermal energy storage systems capture and release heat energy to provide heating, cooling, or power generation when needed. Latent heat storage uses materials that change phase (such as solid to liquid) to store or release heat [7]. Sensible heat storage systems use the change in temperature of a material to store or release heat [7]. Figure 1-4 [8] shows the relation between temperature heat stored in these systems. These systems find applications in industrial processes, district heating, and concentrated solar power plants.

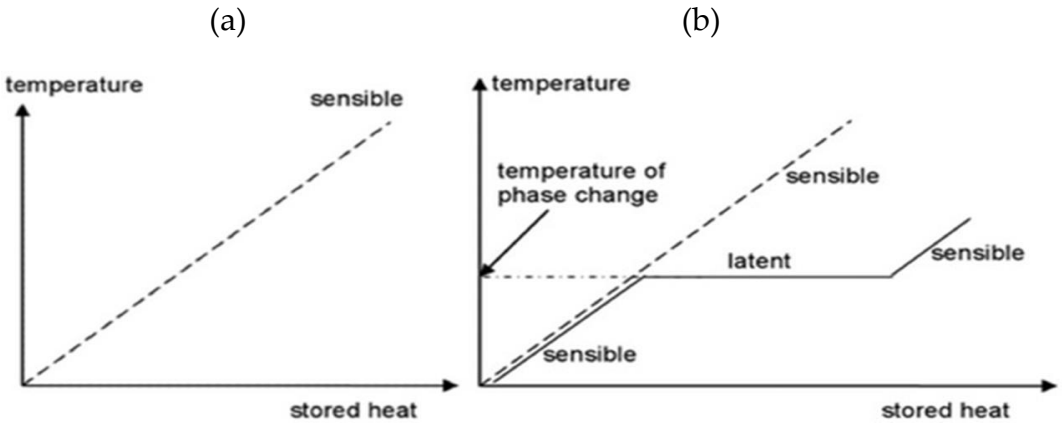

Figure 1-4: a) Temperature increase during sensible heat storage; b) Heat storage as latent heat for the case of solid-liquid phase change

1.3.4 Chemical Energy Storage Systems:

Chemical energy is put away within the chemical bonds of molecules and particles, which can as it were be seen when it is discharged in a chemical response. After the discharge of chemical energy, the substance is regularly changed into totally distinctive substance. Chemical energy storage is rather suitable for storage of large amounts of energy and for greater durations [9, 10].

- **Hydrogen and Fuel Cells:** Hydrogen is an energy carrier that can be produced using renewable sources and stored for later use. It can be converted back to electricity using fuel cells, which combine hydrogen with oxygen to generate electricity and water. Hydrogen storage technologies include compressed

hydrogen, liquid hydrogen, and solid-state hydrogen storage. Fuel cells find applications in stationary power generation, transportation, and even backup power systems.

1.3.5 Electrostatic and Electromagnetic Energy Storage Systems:

Electrical energy storage systems can be divided into two types: electrostatic, which includes capacitors and supercapacitors, and magnetic/current storage systems [11]. Capacitors can be used when there is a lot of electrical flow but they can only stay for a very short time. Capacitance generation means the creation of electrical capacitance. A capacitor is a device that can store electrical energy, but a supercapacitor is a special type of capacitor that can store a lot of energy in a small size. Superconducting magnetic energy storage systems are a good choice for the exit of power plants to keep a consistent amount of energy or at big work locations [9].

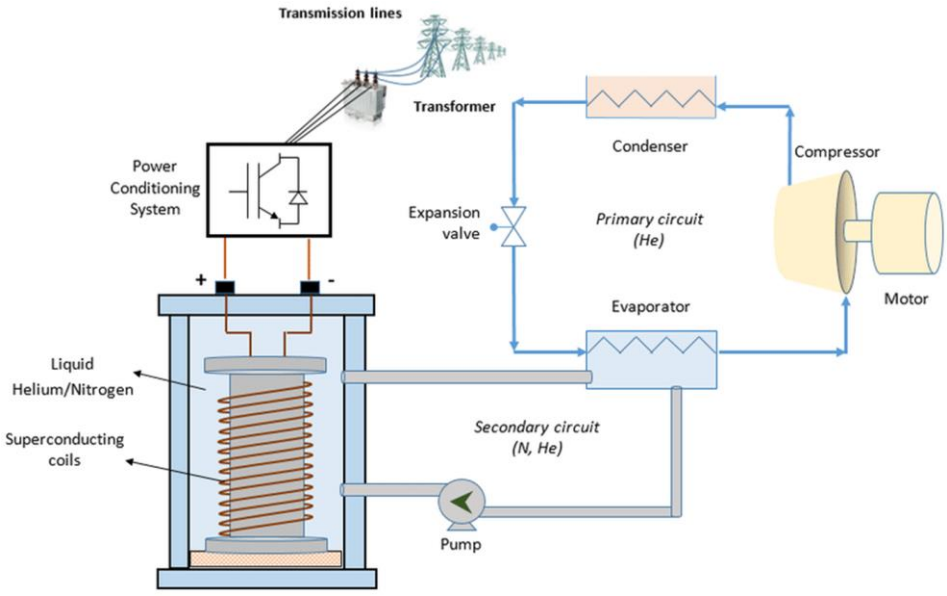

Figure 1-5: Schematic diagram of superconducting magnetic energy storage system

- **Capacitators:** A capacitor is made up of two pieces of metal that are kept apart by a material that doesn't conduct electricity which is called dielectric that is a special layer. When one plate gets electricity from a direct-current source, the other plate will get a charge with the opposite sign [11].
- **Super-capacitors:** Super-capacitors, also known as ultra-capacitors, store energy through the separation of charges at an electrode-electrolyte interface. They offer rapid charge and discharge capabilities and are suitable for short

bursts of energy, such as regenerative braking in electric vehicles and providing quick power support to stabilize grids.

- **Superconducting Magnetic Energy Storage (SMES) systems:** They use electrodynamics to store energy. The energy is kept in a magnetic field made by a strong current in a cold coil [11, 12]. Figure 1-5 shows a superconducting magnetic energy storage system [13].

1.3.6 Emerging and Innovative Energy Storage Systems:

- **Flywheel Energy Storage:** Flywheels store energy in the form of rotational kinetic energy [14]. They involve a spinning rotor in a vacuum or in an enclosed space with minimal air resistance. When energy is supplied, the rotor speeds up, and when energy is discharged, the rotor's kinetic energy is converted back into electricity. Flywheels are quick to respond and can provide short-duration power support. Figure 1-6 [15] Shows an example of a flywheel-based energy storage system.

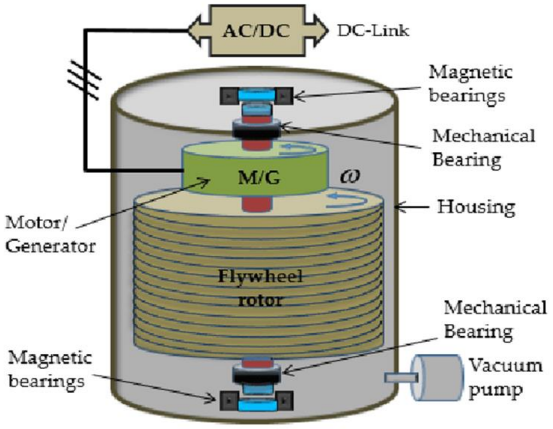

Figure 1-6: Structure and components of flywheel energy storage system

- **Thermochemical Energy Storage (TCES):** Thermochemical energy storage systems utilize reversible chemical reactions to store and release energy. This involves absorbing heat to induce a chemical change and releasing heat when the process is reversed. Reaction can proceed in both the forward and backward directions. Material C absorbs heat energy to undergo a chemical conversion. Into two parts (A and B). The opposite reaction can happen if these parts A and B are put together again, they make a changed form called C

[16]. The procedure of a TCES is shown in the Figure 1-7 [17].Such systems hold promise for high energy density and long-duration storage, making them suitable for industrial processes and concentrated solar power plants.

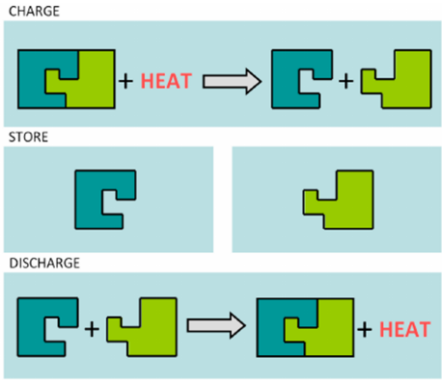

Figure 1-7: Concept of thermochemical heat storage

1.4 Carnot Batteries

Nevertheless, many of the mentioned storage options are ideal for brief periods of charge and discharge because of their elevated per-unit capacity expenses [18] and the current connection between power and energy storage capability. Carnot Batteries (CB) emerge as a potential collection of technologies with economical specifics, unaffected by the interdependence of capacity and power, or geographical limitations.

CBs transform electrical energy into heat, as demonstrated by a heat pump, and preserve it as thermal energy. During discharge, the stored heat is utilized to operate a power cycle that generates electricity. In cases where both the heat pump and power cycle possess reversibility, a CB can achieve a perfect roundtrip efficiency of 100% [19]. Furthermore, CBs incorporate thermal storage into their operations, enabling them to either absorb or supply heat for heating/cooling needs in addition to electricity. Consequently, they serve as a distinct resource for comprehensive multi-vector energy management [20]. Thus, first, a brief classification of CB will be explained; second, a general classification of input heat to CB will be stated.

The label CB encompasses various thermo-mechanical storage ideas, including liquid air energy storage (LAES) and pumped thermal energy storage (PTES), along with their adaptations [21]. It also encompasses Lamm-Honigmann storage (LHS) [22], systems that combine resistive heating with power cycles [23], and assorted hybrid concepts. In contrast, CAES does not fall under the category of CB [24].

1.4.1 Brayton PTES

Brayton PTES functions through a reversible Brayton cycle, connecting a cold and a hot thermal reservoir, as depicted in Figure. During the charging phase, the cycle proceeds in a clockwise direction. It involves compressing a gaseous working fluid (1–2), transferring compression heat to the hot TES (2–3), and then expanding the gas (3–4), resulting in low outlet pressure and lower temperatures at point 4. This decrease in temperature in the cold TES (4–1) establishes a positive temperature difference between the two thermal reservoirs. In the discharge phase, the cycle is reversed. Heat is transferred from the hot TES to the pressurized fluid (3'-2') to drive turbine expansion (2'-1'), and the cold energy is utilized (1'-4') to reduce compression work (4'-3'). Brayton PTES operates as a closed-loop cycle, necessitating one or two additional heat exchangers (illustrated in Figure 1-8.) to dissipate heat generated by irreversibilities and ensure cyclic operation [25]. Furthermore, a buffer vessel may be included or eliminated through suitable adjustments of the storage media packing in the TES (process flow diagrams for these two solutions can be found, respectively, in [26, 27]).

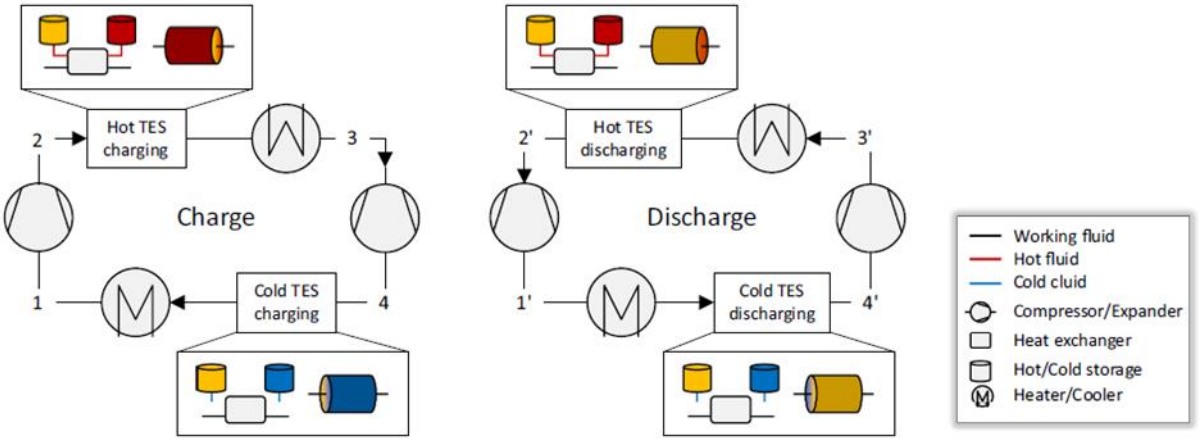

Figure 1-8: Process flow diagram of Brayton PTES

Typical temperature and pressure ranges for Brayton PTES range from approximately -170 to 950 degrees Celsius and from 1 to 20 bar. The most commonly used working fluids for Brayton PTES are monoatomic gases like argon and helium. These gases, with a fixed compression ratio, allow for higher process temperatures, thus improving system efficiency [28].

1.4.2 Rankine PTES

The schematic diagram illustrating a Rankine PTES is presented in Figure 1-9. This system comprises a vapor compression heat pump, a power recovery unit utilizing a Rankine cycle, and a thermal energy storage (TES) component. During the charging phase, the working fluid undergoes evaporation (1–2) and subsequent compression to achieve high pressures and temperatures (2–3). This process releases both sensible and latent heat, transferring it to the hot storage unit during condensation (3–4), before finally expanding to lower pressures (4–1). In the discharging or power generation phase, the liquid fluid is pumped to a high pressure (1′-4′), evaporated using energy obtained from the TES (4′-3′), and expanded through a turbine (3′-2′). Ultimately, it undergoes condensation through an auxiliary heat exchanger and the cold storage (2′-1′).

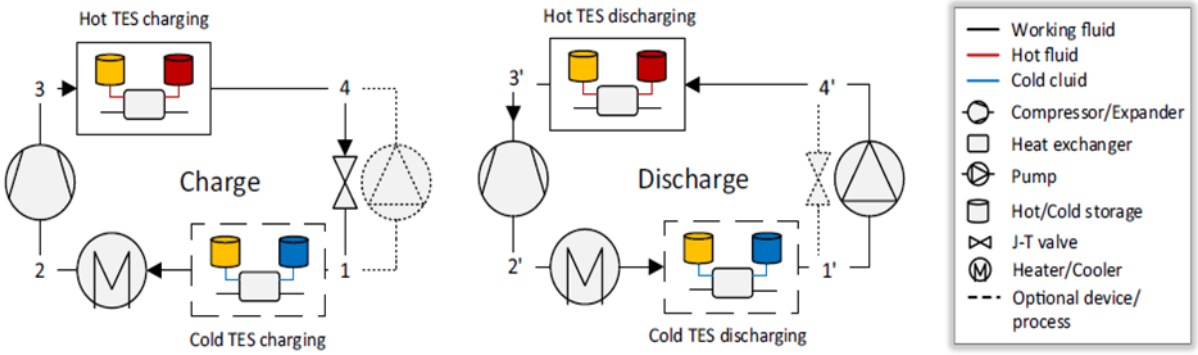

Figure 1-9: Process flow diagram of Rankine PTES

Temperature and pressure ranges applicable to Rankine PTES systems extend from approximately -30°C to 400°C and from 1 to 200 bar. There are two different types of Rankine PTES including the steam Rankine cycle [29, 30] and the organic Rankine cycle [31, 32]. The decision regarding the choice of the working fluid hinges on the system's scale and the temperature ranges encountered during its operation. When dealing with cycle temperatures exceeding 200°C, water is the preferred option, although this is contingent upon the availability of an external heat source. Conversely, for smaller-scale systems and different temperature profiles, organic fluids like R1233zd(E) are generally favored [33]. In both scenarios, the phase transition of the working fluid reduces the work input but concurrently results in less efficient heat transfer processes.

1.4.3 LAES

Illustrated in the process flow diagram in Figure 1-10, LAES operates within an open cycle. During the system's charging phase, an air liquefaction process is executed. This process involves the compression of ambient air (1–2), followed by cooling to cryogenic temperatures accomplished through: i) the return of the air gas stream, ii) a portion of air subjected to external expansion, and iii) high-grade cold recovered from air evaporation (2–3). Subsequently, an expansion device partially liquefies the air (3–4), with a gas fraction recirculated to provide process cooling. Liquid air is then stored in a vacuum-insulated vessel at close-to-ambient pressure. During the discharging phase, liquid air undergoes high-pressure pumping (5–6), evaporation (6–7), and eventual expansion in a turbine (7–8) to produce the required power output. Notably, the very low temperatures of liquid air allow the ambient environment to serve as the hot reservoir for the expansion process. However, it's worth noting that this scenario may lead to suboptimal plant efficiency [34]. As a result, the heat released during the compression phase of LAES charging is stored and recycled to provide hot thermal energy for the subsequent expansion. Similarly, cold generated during evaporation is utilized to enhance the cooling process during air liquefaction.

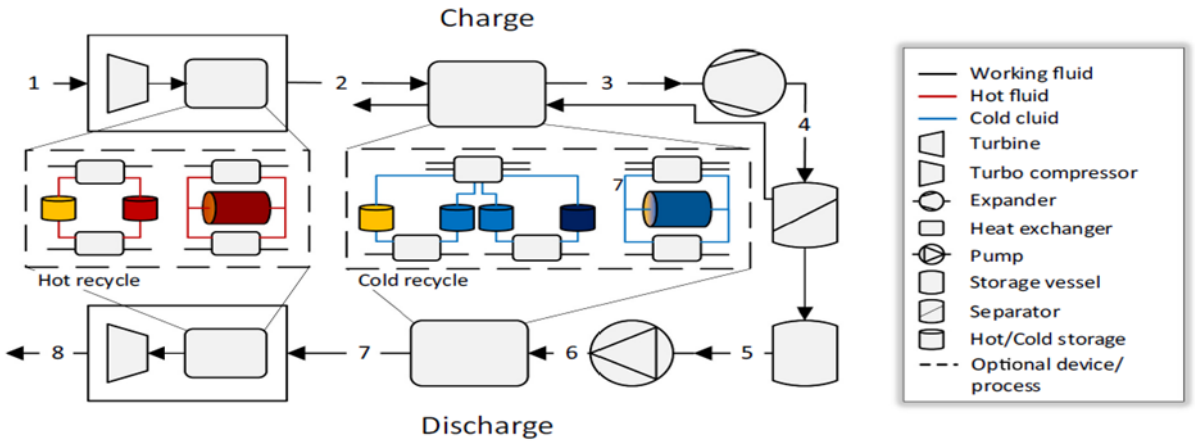

Figure 1-10: Process flow diagram of LAES

For standalone LAES systems, it is commonly recommended to maintain charging pressures within the range of 10–18 MPa, with recommended discharging pressures falling between 7–12 MPa. Temperature variations span from -196°C (the saturation point for air at ambient pressure) to 400°C.

1.4.4 District heating system

As it was said in the last section, the low temperature heat source in heat pump cycle can be supplied by the waste heat gases. Here, a short definition and classification of district heating systems will be carried out.

A district heating system, sometimes referred to as a heat network, is an innovative and effective way to produce and distribute heat for domestic, commercial, and industrial uses within a small geographic region. In this cutting-edge system, heat is generated centrally at one or more heat producing facilities and then distributed to numerous end customers via a network of insulated pipes. The idea behind a district heating system is to provide a dependable and affordable solution for heating needs in densely populated urban areas as well as in areas where energy resources may be plentiful but otherwise underutilized. It also revolves around maximizing energy efficiency and minimizing environmental impact.

Based on a variety of factors, such as heat sources, distribution networks, and system designs, district heating systems can be categorized into a number of unique groups.

- Heat sources
    i. Conventional fossil fuel based systems
    ii. Combined heat and power (CHP) plants
    iii. Renewable energy based systems
- Distribution network
    i. Two pipe systems
    ii. Single pipe system
    iii. Direct system
    iv. Indirect system
- System configurations
    i. Decentralized system
    ii. Centralized system
- Operation Temperature
    i. First generation of district heating systems (1GDH)
    ii. 2GDH
    iii. 3GDH
    iv. 4GDH
    v. 5GDH

1.5 Scope of Work

One of the essential processes of the CBs is the charging cycle that can be done through a heat pump (HP). Heat pumps are essential devices in various applications, known for their ability to efficiently transfer heat from one location to another. When integrated into Carnot batteries, these systems offer a revolutionary approach to energy storage, leveraging thermodynamics to store and retrieve energy.

The objective of this dissertation is to determine the most suitable working fluid for the different configurations under examination and also improve performance of the HP by evaluating a multi-stage cycle rather than the single-stage one. The primary criterion being considered is the Coefficient of Performance (COP). The COP is calculated using the (1. 1) equation. Additionally, the effect of COP on the whole system is shown using the (1. 2) equation. It should be noted that there is no economic analysis in this study. Nevertheless, heat exchanger area variation will be analyzed to check if the optimal temperature of the cycle matches the minimum heat exchanger area or not.

$$COP_{HP} = \frac{Q_{cond}}{P_{total}} \tag{1. 1}$$

$$\eta_{roundtrip} = COP_{HP} \times \eta_{TCS} \times \eta_{PC} \tag{1. 2}$$

In the above equations Q_{cond} is the heat from the condenser and P_{total} is total power input of the cycle. $\eta_{roundtrip}$ is the roundtrip efficiency of cycle that is calculated based on COP and heat storage efficiency (η_{TCS}) and discharge or power cycle efficiency (η_{PC}).

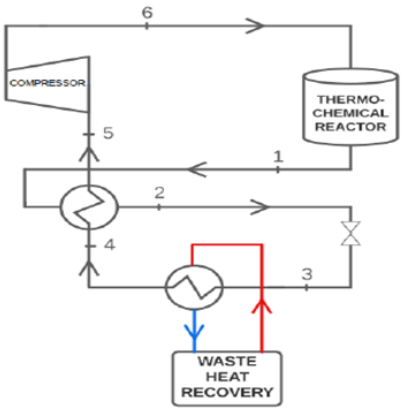

Figure 1-11: Charging cycle scheme

In the Figure 1-11 the charging cycle of a simple recuperated-HP is shown. The low-temperature heat source, denoted as "waste heat recovery", injects energy into the cycle, leading to the evaporation of the working fluid (from 3 to 4). Subsequently, the fluid undergoes preheating in the recuperator, reaching point 5 before entering the compressor. At the turbomachine's outlet, denoted as point 6, the fluid, now at high temperature and pressure, condenses to release the heat required for the chemical reaction. Ultimately, the condensed fluid (point 1) experiences cooling, reducing its temperature to point two within the recuperator, before being compressed to complete the cycle.

In this dissertation, it is tried to improve the performance of cycle by evaluating and optimizing a two-stage HP based on Organic Rankine Cycle. To illustrate the system's configuration under investigation, Figure 1-12 provides insight into the charging phase. In this phase, a heat source, which operates at low temperatures and can originate from either a renewable energy source (RES) or industrial waste heat (WH), supplies energy to the system, causing the working fluid to evaporate. Subsequently, the fluid undergoes compression and eventual condensation. The heat released during the condensation phase serves as the energy source for the chemical reactor, initiating an endothermic reaction.

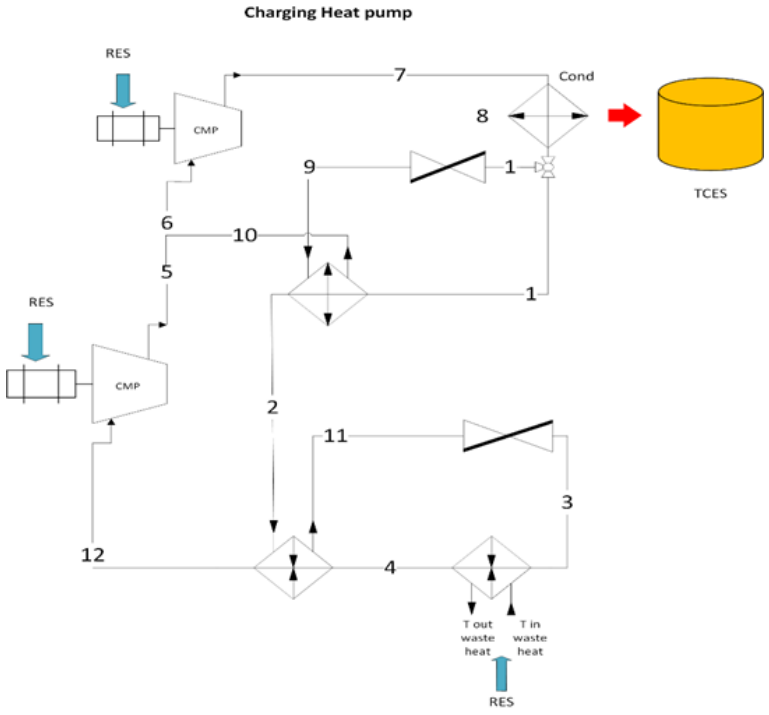

Figure 1-12: Improved charging cycle scheme

Connecting an appropriate heat pump to a low-temperature heat offers the advantage of elevating the heat's temperature to a higher level. When there is a need to initiate the reverse reaction, the products of the previous reaction are stimulated to interact, resulting in the release of heat. This liberated heat energy is then integrated into the discharge cycle, commonly referred to as the power cycle, facilitating the vaporization of the working fluid.

2.Literature Review

Heat pumps are widely recognized for their energy-efficient heating and cooling capabilities. They operate on the principle of transferring heat from a low-temperature source to a high-temperature sink. One of the limitations of conventional heat pump systems is their dependence on external conditions, such as weather and electricity prices. To address these limitations, the integration of heat pump Rankine cycles with thermal heat storage systems has gained increasing attention. This coupling allows for the storage of excess thermal energy when it is abundant and its retrieval when needed, thus optimizing energy utilization.

2.1. Brief History of Heat Pumps

Before actually starting to delve into the literature review of heat pump systems, a brief history of heat pumps during 19th and 20th century is given below:

- **First Practical Applications (Early 20th Century):** The early 20th century marked the emergence of practical heat pump applications. In 1907, American engineer Albert Marsh patented a household heat pump system that used ammonia as a refrigerant. This innovation allowed homes to be heated more efficiently.
- **Growth during World War II and Post-War Period (20th Century):** World War II spurred further developments in heat pump technology, as military efforts required efficient heating and cooling systems. After the war, these technologies were adapted for civilian use, leading to the widespread adoption of heat pumps in homes and businesses.
- **The Expansion of Heat Pumps (Mid-20th Century):** In the mid-20th century, heat pump technology continued to advance. The development of new refrigerants and improved compressor designs led to more efficient and

reliable systems. This period saw the integration of heat pumps into various applications, including residential heating and cooling, industrial processes, and commercial buildings.

- **Air-Source Heat Pumps (1970s):** The 1970s marked a significant milestone in the history of heat pumps with the widespread adoption of air-source heat pumps for residential heating and cooling. These systems used the ambient air as a heat source during the heating season and a heat sink during the cooling season. They offered improved energy efficiency compared to traditional heating and cooling methods.
- **Ground-Source Heat Pumps (Geothermal) (1970s):** Around the same time, ground-source heat pumps, also known as geothermal heat pumps, gained popularity. These systems utilized the stable temperature of the Earth's subsurface as a heat source in the winter and a heat sink in the summer. While initially more expensive to install, geothermal heat pumps offered higher energy efficiency and lower operating costs over time.
- **Environmental Considerations (Late 20th Century):** As concerns about energy efficiency and environmental impact grew, heat pumps gained further attention. The Montreal Protocol of 1987 led to the phase-out of ozone-depleting refrigerants, such as CFCs and HCFCs, in favor of more environmentally friendly options like HFCs. This shift had a direct impact on the design and efficiency of heat pump systems.
- **Modern Advancements (21st Century):** The 21st century brought continued innovation in heat pump technology. Advances included the development of variable-speed compressors, smart thermostats, and integrated control systems. These improvements allowed for more precise temperature control, increased energy efficiency, and enhanced user convenience.
- **Hybrid Heat Pump Systems:** Hybrid heat pump systems emerged as a solution that combined the benefits of both electric heating and heat pumps. These systems automatically switched between conventional heating methods and heat pumps to optimize energy efficiency based on outdoor temperatures and energy costs.
- **Heat Pump Integration with Renewable Energy (21st Century):** As renewable energy sources gained prominence, heat pumps found new applications in conjunction with solar panels and wind turbines. These systems allowed homeowners and businesses to harness renewable energy for heating and cooling, reducing their reliance on fossil fuels.

With the increasing price of fuel and the growing concern about global warming, people have become more interested in using HP as a way to save energy. Heat pumps are a good way to help with the greenhouse effect. This process is the only one we know of that takes heat from the environment and waste heat and uses it to produce more heat. It is a good way to heat and cool buildings and industries without using too much energy or harming the environment [35]. It can be used in houses, offices, and factories. Unlike heat-powered systems, mechanical vapor compression heat pumps are commonly used in various manufacturing industries.

Numerous heat pump variations are available, with some necessitating external mechanical effort, while others rely on external thermal energy. In various industries, commercial heat pumps employing either the vapor compression cycle or the absorption cycle are currently in use for various applications. Although emerging heat pump technologies like the adsorption cycle or the chemical reaction cycle are advancing swiftly, they have not yet found widespread use in major industrial sectors [36]. Next, comes a section outlining various methods that are currently being used to enhance heat pump performance. The following section includes a number of hybrid heat pump systems with the ability to recover heat from a variety of thermal sources. Finally, it provides some fresh uses for heat pump systems in a variety of energy-intensive industries.

Sustained endeavors will continue to focus on enhancing the efficiency of heat pumps, leading to direct improvements in energy utilization and the reduction of carbon emissions in numerous energy-intensive industries.

2.2. Improving Energy Efficiency

2.2.1. Multistage Cycles

Multistage systems employ multiple compression stages, and they can be categorized as compound or cascade systems. In a compound system, as depicted in Figure 2-1 [37], two or more compression stages are connected in series. This configuration can include a high-stage compressor (operating at higher pressure) and a low-stage compressor (operating at lower pressure) or several compressors linked in series. Multistage systems, in contrast to single-stage ones, offer advantages such as a reduced compression ratio and enhanced compression efficiency at each stage, resulting in a greater refrigeration effect, lower high-stage compressor discharge

temperatures, and increased flexibility [38, 39]. The pressure between the high-stage compressor's discharge pressure and the low-stage compressor's suction pressure in a multistage system is referred to as interstage pressure. For a two-stage system, interstage pressure is typically adjusted to ensure nearly equal compression ratios between the two stages, aiming for an improved coefficient of performance (COP) [39].

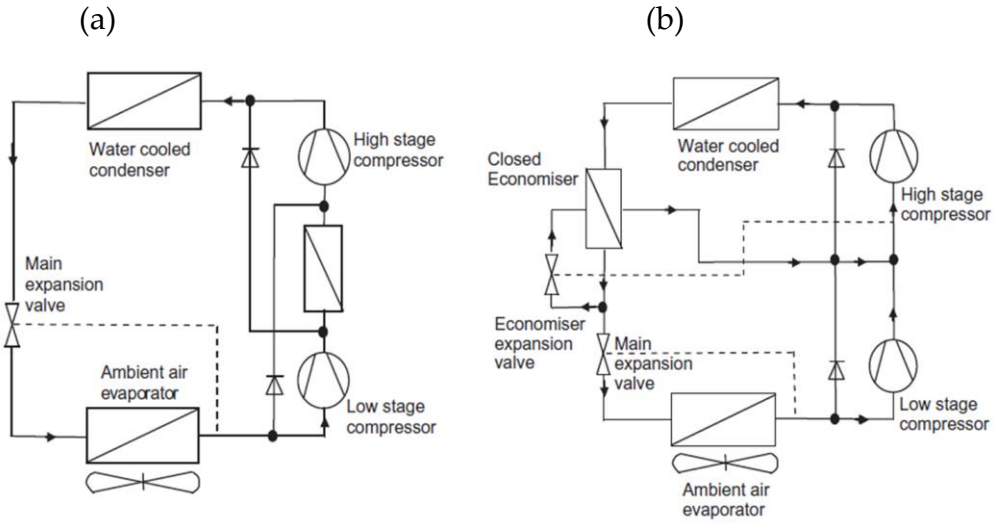

Figure 2-1: Diagrams of (a) a two-stage cycle with an intercooler and (b) a two-stage cycle with a closed economizer

In a study by Tanaka and Kotoh [40] on double-stage compressor heat pump water heaters using CO2 refrigerant in cold regions of Japan, they observed that the ratio of the compressor's suction pressure (low pressure) to its discharge pressure (high pressure) is substantial, subjecting the compressor to harsh conditions in cold districts where temperatures can drop as low as -10 to -20 degrees Celsius. This adversely impacts both water heating capacity and system COP. To enhance the performance and reliability of their heat pump system, they introduced a two-stage compression stroke and refrigerant injection at intermediate pressure [40]. Therefore, a compound multistage heat pump system emerges as a viable choice for improving system COP when operating in extremely cold environments.

A cascade system is comprised of two independent refrigeration systems. The first maintains a lower evaporating temperature, generating refrigeration. In contrast, the second operates at a higher evaporating temperature, as seen in Figure 2-2 [37]. These two distinct systems are interconnected through a cascade condenser, where the lower system's condenser releases heat, which is then absorbed by the higher system's evaporator.

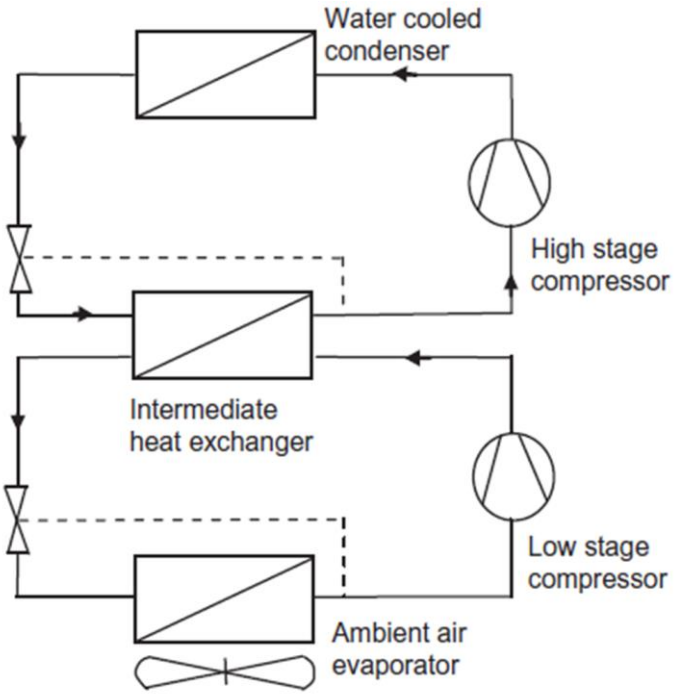

Figure 2-2: Schematic of a cascade cycle

In a study conducted by Wang et al. [41], they investigated the potential of a double-stage coupled heat pump heating system. In this setup, an air source heat pump was integrated with a water source heat pump. Their findings indicated a substantial enhancement in energy efficiency, boasting a 20% improvement when compared to the performance of a standalone air source heat pump [41].

2.2.2. Compressor Performance

To reduce the energy usage of the vapor compression cycle, one effective strategy involves minimizing the energy consumption of the compressor while maintaining the required compression ratio. In simpler terms, enhancing the compressor's performance is the goal. In recent times, a significant advancement in compressor technology has been the development of the scroll compressor [42], which is roughly 10% more efficient than the conventional reciprocating compressor. This improvement can be attributed to three main factors [43].

Firstly, in the scroll compressor, the suction and discharge processes are isolated, preventing the introduction of heat into the suction gas as it enters the compressor. This is in contrast to reciprocating compressors, where heat is added. Secondly, the compression process in the scroll compressor occurs gradually over 540 degrees of

rotation, as opposed to the 180-degree rotation in reciprocating compressors. Consequently, torque fluctuations are only about 10% of what is experienced in reciprocating compressors. Thirdly, the scroll compression mechanism allows for the elimination of suction and discharge valves, which are sources of pressure losses in reciprocating compressors.

Additionally, scroll compressors offer improved reliability due to their fewer moving parts and their ability to operate more effectively under liquid slugging conditions. Recent studies combining heat pumps with scroll compressors have demonstrated the energy efficiency benefits of such integration [44, 45].

An alternative, less active approach for enhancing compressor performance revolves around maintaining the compressor's temperature at a lower level while it operates. Wang and colleagues [46] explored two methods to achieve this goal.

The initial approach centered on cooling the compressor's motor through external means, avoiding the use of suction gas for cooling. The second method involved subjecting the compressor to an isothermal process by transferring heat from the compression chamber. Their findings indicate that this approach has the potential to reduce compression work by as much as 14% compared to the isentropic compression process used in an R22 refrigeration system. By combining both techniques, it is possible to achieve energy savings of up to 16%, depending on the operating conditions and the choice of fluid [46].

2.2.3. Ejector

The ejector is a crucial component at the core of the jet refrigeration system and was originally conceived by Sir Charles Parsons around 1901. Its initial purpose was to eliminate air from the condenser of a steam engine. In 1910, Maurice Leblanc employed an ejector in the very first steam jet refrigeration system [47]. The ejector holds immense significance in a wide array of applications, including refrigeration, air conditioning, desalination, petroleum refining, and the chemical industry [48]. Moreover, it plays an integral role in distillation columns, condensers, and various other heat exchange processes. Recent publications have delved into different facets of the ejector-compression system, including topics like the ejector-expansion trans-critical CO2 heat pump cycle [49], the two-phase ejector system [50, 51], the utilization of ejectors in a multi-vaporator refrigeration context [52], and the performance of ejector refrigeration systems driven by low-grade waste heat or solar energy [53, 54]. The subsequent section will highlight a notable recent advancement in ejector heat pump systems.

Depending on the specific design aspects related to geometry, aerodynamics, and mechanics of the ejector, theoretical investigations have indicated that the coefficient of performance (COP) of an ejector-compression heat pump can achieve a notable performance enhancement of up to 21% compared to the standard vapor compression cycle [55]. In order to validate the energy efficiency of an ejector-compression heat pump, Chaiwongsa and Wongwises [51] executed an experiment using motive nozzles with three different outlet diameters. In Figure 2-3, you can observe the COP of their ejector-HP (heat pump) system as it operates at varying heat sink temperatures [51]. Their study indeed showcased a significant enhancement in energy efficiency, with the COP reaching as high as 6 in some instances.

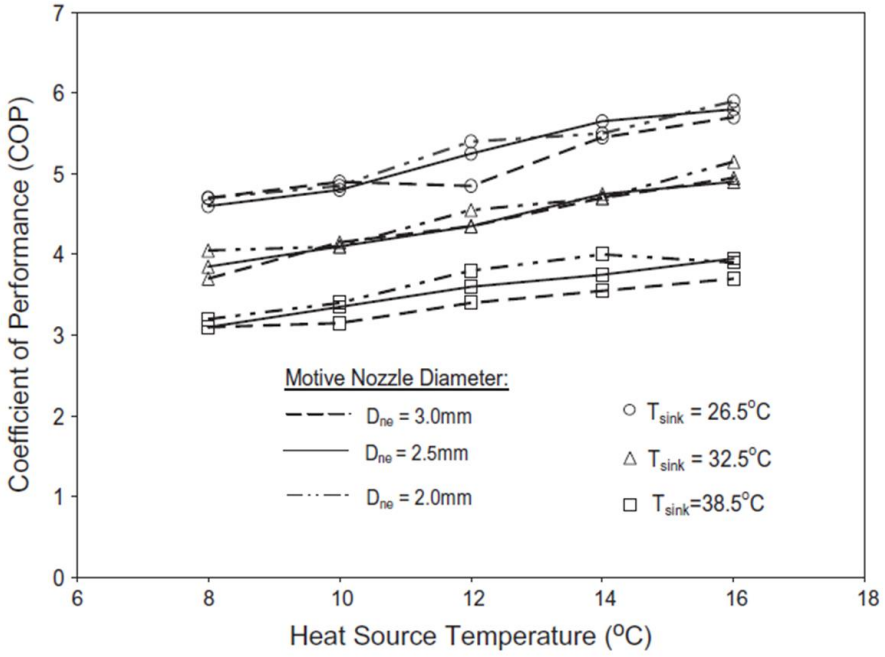

Figure 2-3: The performance coefficient of an ejector-HP system when operated with varying nozzle diameters and under different heat sink temperatures

2.2.4. New Refrigerants

HCFC-22 is a commonly utilized refrigerant in heat pump and air conditioning systems. While it possesses a relatively low potential for ozone depletion, its chlorine content necessitates the search for an alternative refrigerant. Lately, performance evaluations have been carried out on a variety of novel refrigerant blends.

In Chen's study [56], a performance assessment of R410A was carried out, revealing that the efficiency of an air conditioning unit using R410A was approximately 12%

higher than that of a unit utilizing R22. This improvement in efficiency can be attributed to the fact that compressors running on R410A operate at lower temperatures, resulting in reduced energy consumption and a decreased likelihood of burnout. Additionally, R410A exhibits superior heat absorption and release characteristics, leading to reduced electricity usage and enhanced operational efficiency [57]. Furthermore, R410A has the potential to reduce the size of heat exchangers, particularly evaporators and condensers, due to its superior heat transfer properties compared to R22 [56]. Another promising refrigerant, R433A, has also shown significant potential for enhancing the energy efficiency of heat pumps.

Park et al. [58] conducted a comparative examination between R433A and R22 using a heat pump bench testing facility. The primary findings from their research indicated that R433A achieved a higher coefficient of performance (COP) than HCFC-22 and also exhibited notably lower discharge temperatures. Furthermore, as an extension of their research, they investigated the thermodynamic performance of an R170/R290 blend as a potential replacement for R22 [59]. In terms of energy efficiency, their results showed that, under typical heat pump operating conditions, the COP of the R170/R290 mixture outperformed that of R22 within a composition range of up to 6% R170.

Researchers, including Atipoang et al. [60] and Gorozabel Chata et al. [61], have conducted investigations into the effectiveness of hybrid heat pump systems that utilize refrigerant blends. They successfully identified the optimal system performance by determining the appropriate mass mixture of refrigerants.

2.3. Using Hybrid Systems

2.3.1. A Desiccant Hybrid System

A hybrid desiccant heat pump system is an efficient solution for managing indoor humidity levels and controlling air temperature. These systems integrate an electric vapor compression cycle with desiccant materials to achieve this dual functionality. A desiccant heat pump hybrid system offers several notable advantages:

- **Independent Control:** It enables separate and precise control of both humidity and temperature, enhancing overall comfort and allowing for more precise regulation of indoor conditions.

- **Improved Comfort:** By reducing humidity levels in occupied spaces, these systems maintain comfort levels at a given temperature, improving overall comfort for occupants.
- **Cost Efficiency:** These systems can reduce capacity costs by eliminating the need for expensive over-cooling and reheat devices that are typically required for dehumidification processes. This results in more cost-effective operation.

Lazzarina and Castellotti [62] investigated the operation of a desiccant heat pump hybrid system in a supermarket environment. In their setup, they combined a cooling system worked with a self-regenerating liquid desiccant and an electric heat pump. Their study revealed the potential for energy savings with this hybrid system when contrasted with traditional mechanical dehumidification techniques [62]. In a separate study, researchers conducted performance assessments of a desiccant heat pump [62]. The attainable coefficient of performance (COP) for the unit, when targeting low dehumidification capacities (between 4 to 6 grams of moisture per kilogram of air), ranged from approximately 5 to 6. However, it was noted that the COP decreased as the dehumidification capacity increased.

Researchers led by Aynur et al. [63] explored an innovative hybrid system that merged variable refrigerant flow technology with a heat pump desiccant (HPD) system. They conducted field performance assessments throughout a heating season and presented outcomes illustrating that this novel system offers significant energy conservation benefits, all while ensuring superior indoor thermal comfort and indoor air quality conditions.

2.3.2. Solar-assisted Heat Pumps (SAHP)

Combining a heat pump with solar technology introduces an innovative hybrid system that has the potential to substantially boost the heat pump's performance by harnessing energy from a readily available natural source: solar energy [64]. Pei and collaborators [65] have introduced an innovative system known as the photovoltaic solar-assisted heat pump (PV-SAHP). In this setup, they integrated a Photovoltaic Thermal (PVT) component onto the evaporator, effectively creating a combined evaporator and collector plate. Within this configuration, a portion of the received solar energy was converted into electricity, while the remaining energy was transformed into heat. The heat energy was absorbed by the refrigerant and then transferred to the condenser. The electricity generated served to supplement the power required for the compressor. This utilization of solar energy led to a significant enhancement in the coefficient of performance (COP) of the heat pump [65]. The study's findings demonstrated that the PV-SAHP system not only

outperformed conventional heat pump systems but also achieved a higher level of photovoltaic efficiency.

Recent studies have focused on examining the effectiveness of a Solar-Assisted Heat Pump (SAHP) (shown as an example in Figure 2-4 [66]) for the purpose of hot water production [67, 68]. These investigations specifically applied the SAHP technology to water heating applications in Hong Kong. Researchers developed a mathematical model to assess its performance across various operating conditions. The model's results highlighted several key findings:

- The performance of the SAHP system was notably influenced by changes in circulation flow rate, the surface area of the solar collector, and the initial water temperature in the preheating solar tank.
- The study demonstrated that the SAHP system could achieve an annual average Coefficient of Performance (COP) of 6.46. This COP value is significantly higher than that of conventional heat pump systems [67].

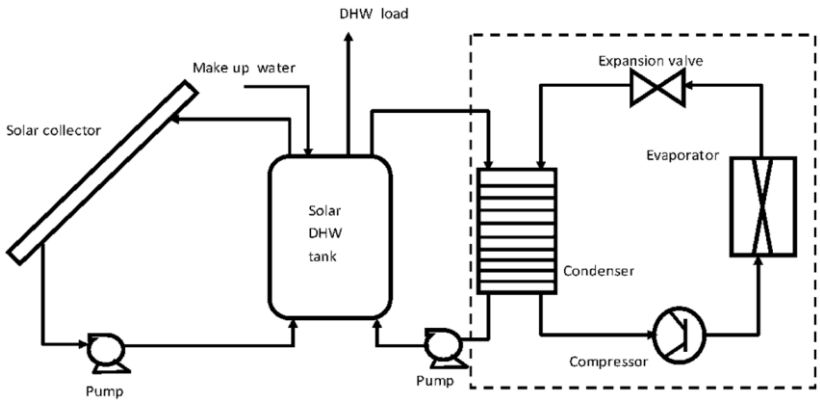

Figure 2-4: A Hybrid Direct Expansion Solar-Assisted Heat Pump Water Heater

2.4. Innovative Applications and Solutions

2.4.1. Drying

Heat pump dryers are acknowledged for their energy-saving attributes when utilized in drying operations [69]. The primary advantages of heat pump dryers result from their capability to recover energy from exhaust gases and their control over both drying gas temperature and humidity levels [70, 71]. The heat pump dryer offers several notable advantages [36]:

- **High Specific Moisture Extraction Ratio (SMER):** Heat pump drying (HPD) achieves one of the highest SMER values, often falling within the range of 1.0 to 4.0. This is possible because heat can be reclaimed from the moisture-laden air.
- **Enhanced Product Quality:** Heat pump dryers have the capability to significantly enhance product quality by operating at low temperatures. These lower temperatures allow for the preservation of the drying potential of the air through further reduction of air humidity.
- **Versatile Drying Conditions:** Heat pump dryers can generate a wide range of drying conditions, typically spanning temperatures from -20 to 100°C (with auxiliary heating) and relative humidity levels from 15% to 80% (with a humidification system).
- **Precise Environmental Control:** They provide excellent environmental control, making them suitable for high-value products, while also reducing electrical energy consumption for less valuable products.

Numerous researchers in the field of drying have found that HPD exhibit more efficient energy utilization compared to traditional drying systems [36]. Hepbasli and colleagues [72] introduced a gas engine-driven heat pump (GEHP) for food drying, marking the first application of its kind. This system comprises four essential components:

1. A GEHP unit with a heating capacity of 18 kW.
2. A Heat Pump (HP) unit equipped with a scroll compressor modified for enhanced vapor injection.
3. An air solar collector.
4. A band conveyor dryer.

Initial investigations have indicated that approximately 30% of the total heating capacity for GEHP systems can be supplied through heat recovery [72].

2.4.2. Desalination

Desalination is the process of transforming seawater into freshwater. Heat pumps (HPs) are effectively utilized in desalination facilities to capture heat energy. Several research efforts have been conducted to investigate the application of heat pump systems in freshwater production [73]. Among the various technologies used in desalination plants, mechanical vapor compression (MVC) is acknowledged as the most thermodynamically efficient option [74].

In 2008, Gao et al. conducted research demonstrating the energy-efficient operation of an MVC system for freshwater production [75]. Their experimental setup showed that it was feasible to generate 60 kg of freshwater daily while utilizing a conservative power input of 500 watts.

Hawlader and co-researchers [76] conducted an assessment of a unique solar-assisted heat pump system test-rig and achieved favorable water production results. Their experimental system had the capacity to produce 1 liter of water per hour. In terms of energy efficiency, this hybrid system exhibited effective performance, with a Coefficient of Performance (COP) ranging from 5 to 9, and a performance ratio within the range of 0.6 to 1.38. By combining the heat pump (HP) and solar energy, this hybrid system offered the advantage of reducing operational costs, while also providing the convenience of simple maintenance [76].

2.4.3. Geothermal Heat Pump

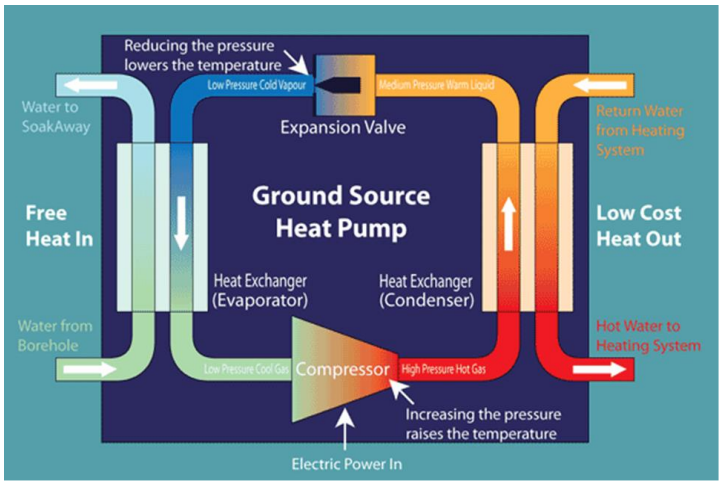

Figure 2-5: A Ground Source Heat Pump

A geothermal heat pump, often referred to as a ground-source heat pump (GSHP) as shown in Figure 2-5 [77], is a centralized heating and cooling system. Its function involves moving heat to or from the ground to provide both heating and air conditioning, and in most instances, it also supplies hot water.

Zamfirescu and Dincer [78], as well as Granowskii et al. [79], have pioneered the creation of novel mechanical compression heat pump systems employing organic fluids. These systems are designed to elevate the temperature, making it suitable for operating thermochemical or hybrid cycles. Their heat pump technologies have showcased impressive efficiency when applied in scenarios featuring a temperature

difference of approximately 50°C and a consistent heat source, such as ground-source applications.

The main benefit of GSHP technology lies in the fact that both the earth and water sources offer a relatively stable temperature for heat exchange. This characteristic enhances the energy efficiency, as measured by the COP, compared to conventional air-based systems. Moreover, efforts have been made to integrate ground-coupled heat pump (GCHP) systems with additional components like a fluid cooler, cooling tower, or surface heat rejecters in buildings where cooling demands are predominant [80].

2.4.4. Heating and cooling systems

Heat pumps used for heating and cooling buildings can be categorized into four primary groups based on their operational functions and requirements. These categories encompass:

- Heating-focused heat pumps, which supply space heating and/or water heating.
- Dual-purpose heat pumps, providing both space heating and cooling.
- Integrated heat pump systems, offering space heating, cooling, water heating, and sometimes even exhaust air heat recovery.
- Specialized heat pump water heaters, exclusively designed for water heating purposes [81].

While exploring the performance traits of an R134a automotive air conditioning system that can double as an air-to-air heat pump using outdoor air as a heat source, researchers Hosoz and Direk [82] noted that the heat pump function adequately delivered heating but was more effective in milder weather conditions. As the outdoor temperature decreased, the heating capacity significantly declined. Additionally, the heat pump exhibited a higher coefficient of performance when compared to running the system solely for air conditioning, resulting in lower exergy destruction per unit capacity.

2.4.5. Combined HP-ORC (also coupled to Energy Storages)

First, it is essential to understand the basics of heat pump Rankine cycles. These cycles are a variation of the well-known Rankine cycle, typically used in power generation. In a heat pump Rankine cycle, the working fluid undergoes a phase change from liquid to vapor and vice versa, enabling the transfer of heat from a low-

temperature source to a high-temperature sink. Key components of a heat pump Rankine cycle include:

- **Evaporator:** Where the working fluid absorbs heat from the low-temperature source, causing it to evaporate.
- **Compressor:** The vaporized working fluid is then compressed, increasing its temperature and pressure.
- **Condenser:** In the condenser, the hot, pressurized vapor releases heat to the high-temperature sink and condenses back into a liquid.
- **Expansion Valve:** The liquid working fluid is then expanded, reducing its pressure and temperature, and the cycle repeats.

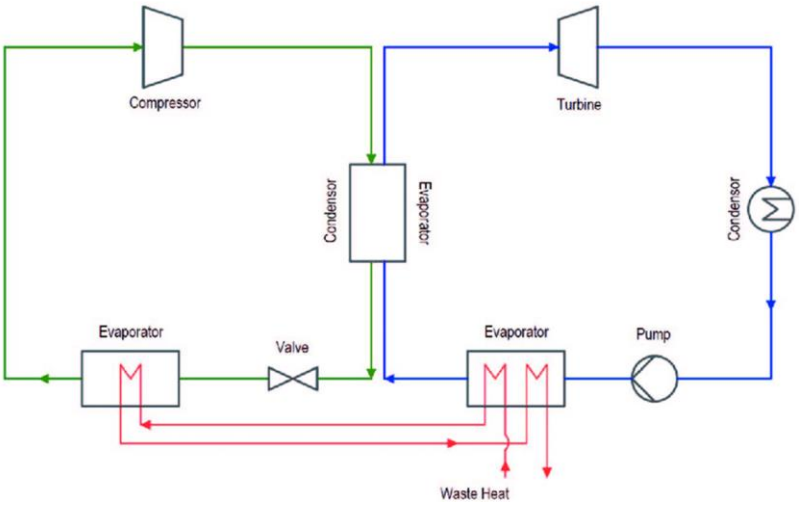

Figure 2-6: Diagram illustrating the integrated HP-ORC system: (left); (right): ORC

The combination of heat pump and ORC (e.g. in Figure 2-6 [83]) systems offers several advantages. Firstly, it allows for the efficient utilization of waste heat, as the heat pump can upgrade the temperature of the heat source before it enters the ORC system. This improves the thermal match between the waste heat source and the working fluid, enhancing overall system efficiency. Additionally, the heat pump can provide heating and cooling services, reducing the need for separate heating and cooling systems. This leads to energy savings and improved comfort in buildings.

Steger and colleagues [84] examined a reversible system that combines a heat pump with an organic Rankine cycle, as illustrated in the accompanying diagram (Figure 2-7). The system relies on identical components, including the turbomachinery, making the pressure ratio a critical parameter. After evaluating numerous fluids,

they determined that R1233ZD(E) is a suitable choice for the pilot plant configuration, taking into account its low GWP (Global Warming Potential) and other favorable fluid properties.

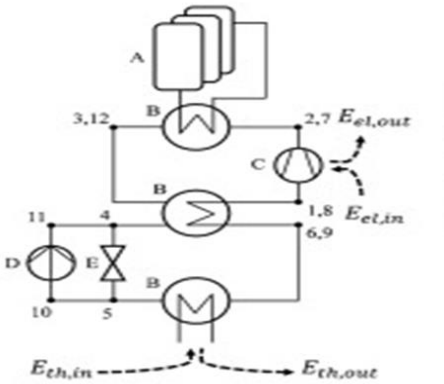

Figure 2-7: Flow Diagram of a Reversible HP

In their study, Eppinger and colleagues [85] pinpoint the most suitable fluids for a heat storage setup linked to a heat pump that draws energy from a low-temperature source and is connected to an organic Rankine cycle. They assess both latent and sensible storage systems using various fluids, analyzing their appropriateness for diverse operational scenarios. Their primary focus is on Cyclopentane, R1233zd(E), Novec649, and R365mfc. Among these options, R1233zd(E) emerges as the most favorable choice, striking a balance between slightly lower efficiency and considerations for environmental sustainability and safety.

Abarr and colleagues [86] introduced a concept known as the Pumped Thermal Energy Storage and Bottoming System (Bot-PTES). By connecting this Bot-PTES system to a natural gas peaker plant, it becomes capable of capturing and utilizing heat that would otherwise go to waste from the peaker plant. Consequently, the Bot-PTES system can function as a large-scale energy storage system during periods when the peaker plant is idle, including times with excess power generated from solar or wind sources. The primary advantage of the Bot-PTES system lies in its ability to operate for more hours per day, resulting in a higher capacity factor compared to alternative energy storage systems. This increased operational time leads to greater revenue generation from the initial capital investment.

Also Simone Montozzi [87]evaluated and optimized a single-stage reversible charge and discharge cycle of CB that is shown in Figure 2-8.

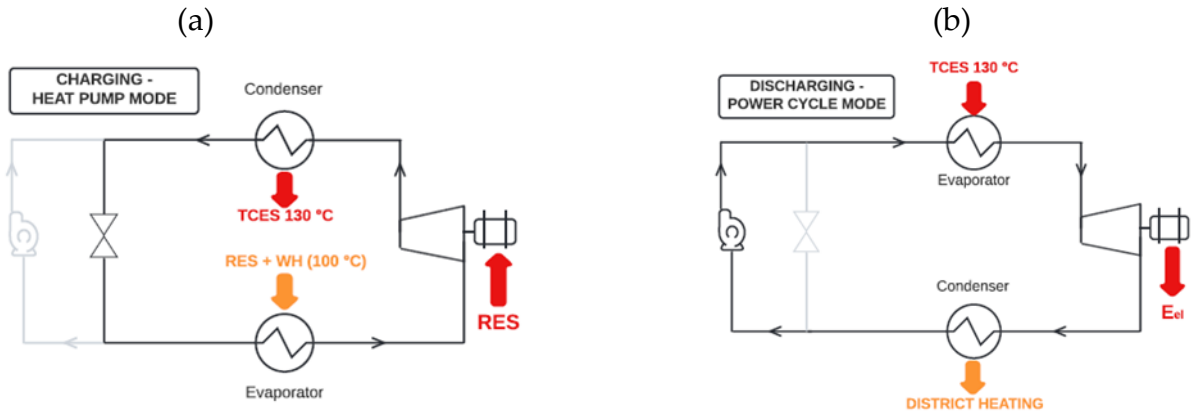

Figure 2-8: charging and discharge cycles of CB

In this dissertation only the charging cycle is going to changed to a multi-stage in order to have larger COP compared to a single-stage cycle.

3.Methodology

This chapter provides a comprehensive explanation of both the system under study and the methodology used for the calculations. The assumptions made for the simulations and the basic components within the code are examined. MATLAB software is used to perform the simulations, while all the essential fluid properties required for the simulations are obtained from REFPROP.

3.1 Plant Layout

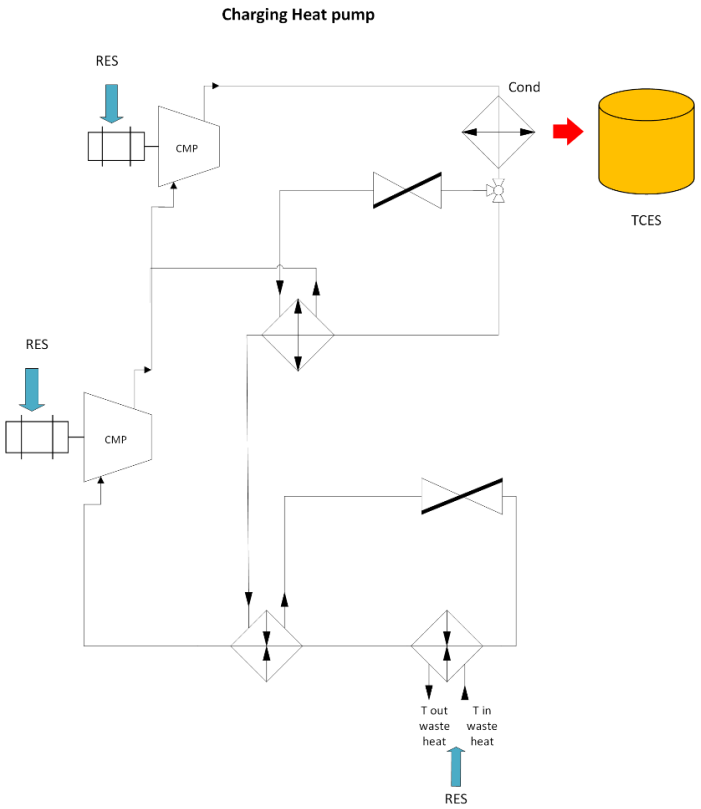

Figure 3-1: Plant configuration: Heat pump cycle

To illustrate the structure of the system under study Figure 3-1 can be referred, which shows the charging phase.

A heat source, which operates at low temperatures and can come from a renewable energy source (RES) or industrial waste heat (WH), supplies energy to the system, resulting in the evaporation of the working fluid. The fluid is then compressed and eventually condenses. The released heat during condensation is used in the chemical reactor to initiate an endothermic reaction.

The advantage of connecting a suitable heat pump to a low-temperature heat source is its ability to raise the temperature of that heat to a higher level.

It is visible that proposed plant is different in some components compared to simple heat pump cycle. In fact, a drain cooler (heat exchange) is added in the middle of cycle having middle temperature. Moreover, second compressor is added to compress the fluids more. To better understand the difference with respect to simple heat pump cycle, T-S diagram of both cycles including Recuperator are drawn in Figure 3-2 and Figure 3-3.

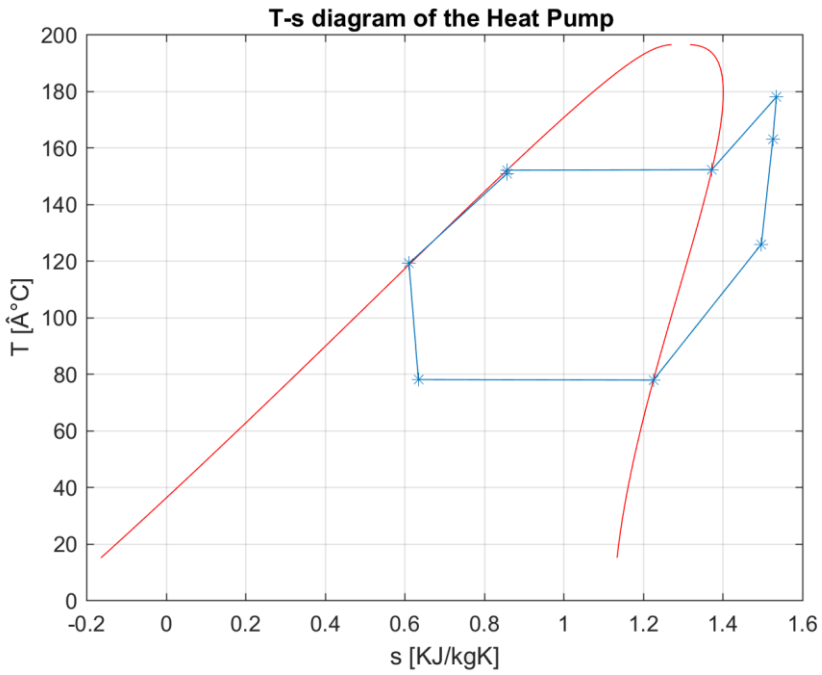

Figure 3-2: T-S diagram of simple Heat pump cycle

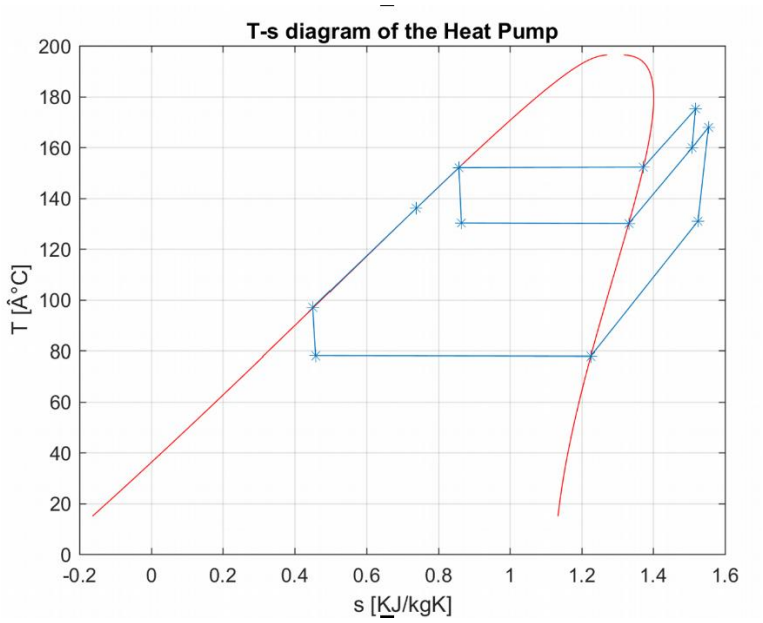

Figure 3-3: T-S diagram of improved Heat pump cycle

3.2 Model Assumption

Regarding the assumption, it is divided into two groups; first, fixed assumptions that are constant in whole project. Second, varriable assumptions that will change in sensitivity analysis to check their effect on the study.

3.2.1 Fixed assumption

3.2.1.1 Turbomachinery

The efficiency of the equipment used has a great influence on the COP. At the first attempt, some experimental efficiency correlations of volumetric machines were used; but there were some problems to use them: Firstly, there are not enough relations to cover all the volumetric machines. Secondly, formulas are different from one volumetric machine to the other one makes it a bit complex.

In addition, there are some attempts to use efficiency relation for reversible machines; similarly, there are some problems to use them: there are not equations for all types of volumetric machines in which the efficiency of turbine and compressor can be calculated;

The values used in all the simulations performed in this work are consistent with those used in numerous studies that examined storage systems similar to the one considered here.

For a more comprehensive analysis, a more detailed study of the fluid dynamics of the processes involved is needed. This would lead to more reliable efficiency values for the system components. However, the assumed values are not expected to differ significantly.

The efficiency values for the isentropic performance of the compressor are considered reasonable only if the components operate in the superheated steam region where no liquid phase is present. Consequently, scenarios involving conversions within the saturation dome are excluded. This is due to the fact that in such cases the efficiency drops significantly and other turbomachinery blades are required that are able to absorb and remove liquid droplets.

Consequently, in all cases studied, the heat pump cycles are designed so that the compression process takes place outside the saturation dome, in the superheated steam region.Table 3-1 contains a list of the efficiency values used.

	Compressor 1	**Compressor 2**
Isentropic efficiency	80%	80%
Mechanical efficiency	99%	99%

Table 3-1: Compressor Efficiencies

3.2.1.2 Heat Exchangers

The heat exchangers exert a significant impact on the overall efficiency of the system over a complete cycle. The parameters that possess the potential to substantially influence both the system's performance and cost encompass the temperature difference at the pinch point, the overall heat transfer coefficient, and the pressure losses experienced within the component.

In this section, heat transfer coefficient will be introduced briefly and much in detail about the two others:

Regarding global heat transfer coefficients, it is mainly influenced by internal and external heat transfer coefficients, internal and external fouling coefficient and a geometric factor. This relationship is shown in the following equation (3. 1) and (3. 2)

$$U = f(h_{in}, h_{ext}, C_{in}^{fouling}, C_{out}^{fouling}, Area\ Ratio) \quad (3.\ 1)$$

$$U = \left(\frac{1}{h_{in}\frac{A_{int,pt}}{A_{ext,pt}}} + \frac{1}{h_{ext}\frac{A_{ext,t}}{A_{ext,pt}}} + \frac{R_{f,int}}{\frac{A_{int,pt}}{A_{ext,pt}}} + \frac{R_{f,ext}}{\frac{A_{ext,t}}{A_{ext,pt}}}\right)^{-1} \left[\frac{W}{m^2K}\right] \quad (3.\ 2)$$

The coefficients $R_{f,int}$ and $R_{f,ext}$represent anti-fouling ability, simulating the accumulation of dirt during operation. These factors are defined as the average value obtained between two cleaning cycles. Actual values obtained from bibliographic sources are attributed to these coefficients and are presented in Table 3-2. The same applies to the area ratio of the heat exchanger, as shown in references [88, 89].

Regarding the heat transfer coefficients, their value is said to depend on the specific cross-section of the heat exchanger [90]. Indeed, heat transfer is affected by the conditions of the two fluids involved in the heat exchanger. A detailed study of these coefficients for each part of each heat exchanger is available in the literature [91, 92].

Parameter	Value	Parameter	Value
$\frac{A_{int,pt}}{A_{ext,pt}}$	0.87	$R_{f,ext,Cond}$	0.0004
$\frac{A_t}{A_{ext,pt}}$	1	$R_{f,int,Rec}$	0.00018
$\frac{A_t}{A_{ext,pt}}(rec)$	14	$R_{f,ext,Rec}$	0.00018
$\frac{A_t}{A_{ext,pt}}(Dc)$	10	$R_{f,int,Drain}$	0.00018
$R_{f,int,Cond}$	0.0002	$R_{f,ext.Drain}$	0.00018

Table 3-2: Area Ratio and fouling factor assumption

The assumed values are reported in Table 3-3:

Parameter	**Value** ($\frac{W}{m^2K}$)	**Parameter**	**Value** ($\frac{W}{m^2K}$)
$h_{i,eva}$	2000	$h_{i,rec}$	600
$h_{e,eva}$	5000	$h_{e,rec}$	1900
$h_{i,cond}$	2000	$h_{i,Drain}$	600
$h_{e,cond}$	1000	$h_{e,Drain}$	1900

Table 3-3: Heat transfer coefficient for heat exchanger's surfaces

Another important factor related to heat exchangers has to do with the pressure drop they experience. These losses have the potential to significantly affect the overall efficiency of the system. To accurately estimate the pressure loss in the heat exchanger, a computer-based fluid dynamics simulation is required. However, such an analysis is beyond the scope of this project, as it requires precise knowledge of component geometry. Therefore, these losses are assumed and incorporated in the next equations.

$$\Delta P_{liquid} = 0.5\ [bar] \tag{3. 3}$$

$$\Delta P_{gas} = 0.02 \times P_{inlet} \tag{3. 4}$$

Even with phase transition, pressure drop still occurs. In an ideal phase change scenario, pressure and temperature remain constant. However, this ideal condition is not met due to the presence of irreversible phenomenon and pressure drop.

Typically, the loss experienced during a phase change is not quantified in bar or as a percentage of the inlet pressure; rather, they are expressed as temperature differences.

The values used in the simulations are as followed:

$$\Delta T_{HP_{sat,Cond}} = 0.5 \tag{3. 5}$$

$$\Delta T_{HP_{sat,eva}} = 0.2 \tag{3. 6}$$

3.2.1.4 Low Temperature Heat source

The heat source is a low temperature heat source, that could be a waste heat or a low temperature energy source. The thermal energy source used for this investigation is predicted to be water, which may be heated to a temperature of 100°C by a solar collector or by industrial waste gases. This water must then cool to 80°C in order to facilitate the evaporation of the working fluid during the heat pump cycle.

3.2.2 Variable assumption

These are assumptions that are subject to change in sensitivity analysis to assess their impact on results. They are divided into two parts.

3.2.2.1 Maximum Temperature of Cycle

First variable assumption is the maximum temperature of cycle. In order to understand how worthy the improved cycle is compared to a simple heat pump cycle, the comparison should be made fair. Indeed, changing T_{10} leads to different values of T_7 which is not a fair comparison with respect to a simple heat pump cycle. In fact, the higher T_7 leads to higher COP. In this regard, T_7 should be keep constant.

3.2.2.2 Working Fluid

37 fluids were initially chosen from the REFPROP database as the working fluid. The thermodynamic properties of pure fluids and mixtures are provided by the computer software REFPROP, which is available through the Standard Reference Data program of NIST, for a variety of fluid conditions, including liquid, gas, and supercritical phases [93].

It has proven to be a very helpful tool that is utilized by business, the government, and academia, and it is the main way that the Thermophysical Properties of Fluids Group's research is disseminated.

Moreover, there are some thermodynamic criteria to choose an ideal fluid. It should have appropriate critical parameter (temperature and pressure). In other words, it should be high enough to enable condensation in heat pump cycle. Therefore, fluids having critical temperatures below the reaction's temperature have been left out of the equation. Additionally, only those having a critical pressure below 50 bar are taken into account, according to a study aimed at determining the optimal fluids for heat pumps [94].

Moreover, the following features play role to decide a suitable fluid:

1) Thermodynamic Efficiency: High thermodynamic efficiency should be present throughout the heat pump cycle in the fluid. This factor may be seen in the fluid's capacity to transfer heat efficiently through compression, condensation and evaporation.

2) Low Viscosity: Lower viscosity causes the heat pump's components to experience less friction loss, which enhances energy transfer and reduces energy loss.

3) Non-Toxic and Non-Flammable: Because safety must come first, the fluid must be non-toxic and non-flammable to protect the environment and system operators.

4) Chemical Stability: The fluid must maintain its chemical stability throughout the operating temperature and pressure range to avoid deterioration or production of unfavorable byproducts that might compromise the integrity or performance of the system.

5) Cost-Effective and Abundant: These two characteristics are essential. An ideal fluid should be easily accessible, economically viable, and not susceptible to supply restrictions that might harm the heat pump system's long-term sustainability.

6) Compatible with System Materials: To ensure long-term dependability and durability, the fluid must be compatible with the components of the heat pump system.

7) Optimal operating range: an important feature for this study is COP; So choosing a fluid with higher COP would be prioritized.

8) Ease of Maintenance: To reduce operational complexity, a perfect fluid should not need regular maintenance or difficult handling methods.

9) Minimal Environmental Impact: the fluid should have a negligible effect on ecosystems, water supplies, and air quality during manufacture, use, and disposal. It also should exclude from the following groups of fluid:

- Fluids with high ODP (Ozone Depletion Potential): It is defined as the ratio of the worldwide ozone loss caused by a particular chemical to the global ozone loss caused by the discharge of a certain amount of CFC-11 [95].
- Fluids with high GWP (Global warming potential): This criteria makes it possible to compare how various gases affect global warming. It is a measurement of the amount of energy that 1 ton of gas will absorb over a certain amount of time in comparison to 1 ton of carbon dioxide (CO2) [96].

The refrigeration and air conditioning industry has used a class of fluids known as CFCs (chloro-fluoro-carbons), sometimes referred to as "freons," for many years. They were perfect in many ways, including low flammability, low toxicity, low cost,

and good thermodynamic properties, but they suffer from the major drawback of a high ODP. They are not featured in the table because they were gradually prohibited as a result.

The Hydro Fluoro Carbons (HFCs) family of refrigerants was subsequently created. They are nonflammable, recyclable, and nontoxic, and have a low ODP value. Despite the widespread usage of HFCs, current legal requirements call for a GWD significantly lower than what HFCs demonstrate.

All the initial fluids are summarized in Table 3-4:

Fluid	***Critical Pressure*** [***bar***]	***Critical Temperature*** [°***C***]	**High GWP**	**High Flammable**
$R125$	36.2	66	Yes	No
$R128$ $(Perfluoro\ propane)$	26.4	71.9	Yes	No
$R143a$	37.6	72.7	Yes	Yes
$R32$	57.8	78.1	Yes	Yes
$R1234yf$	33.8	94.7	No	Yes
$R134a$	40.6	101	Yes	No
$R227ea$	29.3	102	Yes	No
$R161$	50.1	102	No	Yes
$R1234ze$	36.3	109	No	Yes
$perfluoro\ butane$	23.2	113	Yes	No
$R152a$	45.2	113	Yes	Yes
Perfluoro cycle propane	27.8	115	Yes	No
$R236fa$	32	125	Yes	No
$R236ea$	34.2	139	Yes	No
$RE347MCC$	24.8	164.55	*Yes*	No

R1233ZD	36.2	165.6	No	No
RE245FA2	34.3	171.73	Yes	No
R245CA	39.4	174.42	Yes	No
R123	36.6	183.681	Yes	No
R365MFC	32.7	186.85	Yes	Yes
IPENTANE	33.8	187.2	No	Yes
PENTANE	33.7	196.55	No	Yes
IHEXANE	30.4	224.55	No	Yes
HEXANE	30.3	234.67	No	Yes
MM	19.4	245.6	No	Yes
HEPTANE	27.4	266.98	No	Yes
IOCTANE	25.7	270.85	No	Yes
CYCLOHEXANE	40.8	280	No	Yes
DMC	49.1	283.85	No	Yes
*B*enzene	48.9	288.85	No	Yes
MDM	14.2	290.94	No	Yes
OCTANE	25	296.17	No	Yes
C1CC6	34.7	299.05	No	Yes
Toluene	41.3	318.85	No	Yes
Nonane	23.11	321.4	No	Yes
PXYLENE	35.3	343.018	No	Yes
C3CCC6	28.6	357.65	No	Yes

Table 3-4: Critical properties of initial fluids

It should be noted that flammability itself does not consider being only reason to select or reject a fluid in this study. Additionally, among the initial fluids, refrigerant fluids are not considered for this study. In fact, they often have high ODP and GWP causing environmental problem. Among them $R1234yf$,$R161$, $R1234ze$ have low values of ODP and GWP, but they are flammable.

Finally, all fluids except the refrigerant fluids are selected and simulation will be carried out.

3.3 Model Description

This paragraph describes a MATLAB script developed to simulate the various configurations tested in this thesis. First, it provides a general explanation of how the code works, providing an overview of the inputs, the variables selected for sensitivity testing, and the outputs. Next, the heat pump cycle simulation procedure is given.

3.3.1 General Description of the Code

The charging cycle needs following requirements to be simulated:

- Fixed Assumption
- Temperature of the heat sources
- Working Fluid

Among these three terms, working fluid is variable parameter that should be optimized.

Then, heat pump calculation function starts and coefficient of performance will be calculated.

Therefore, the final result is the COP, running the code for each fluid as a sensitivity analysis, and for different maximum temperature of cycle, an optimized condition of each fluid and finding the best fluids will be obtained.

3.3.2 Plant Configuration

Figure 3-4 illustrates the heat pump cycle:

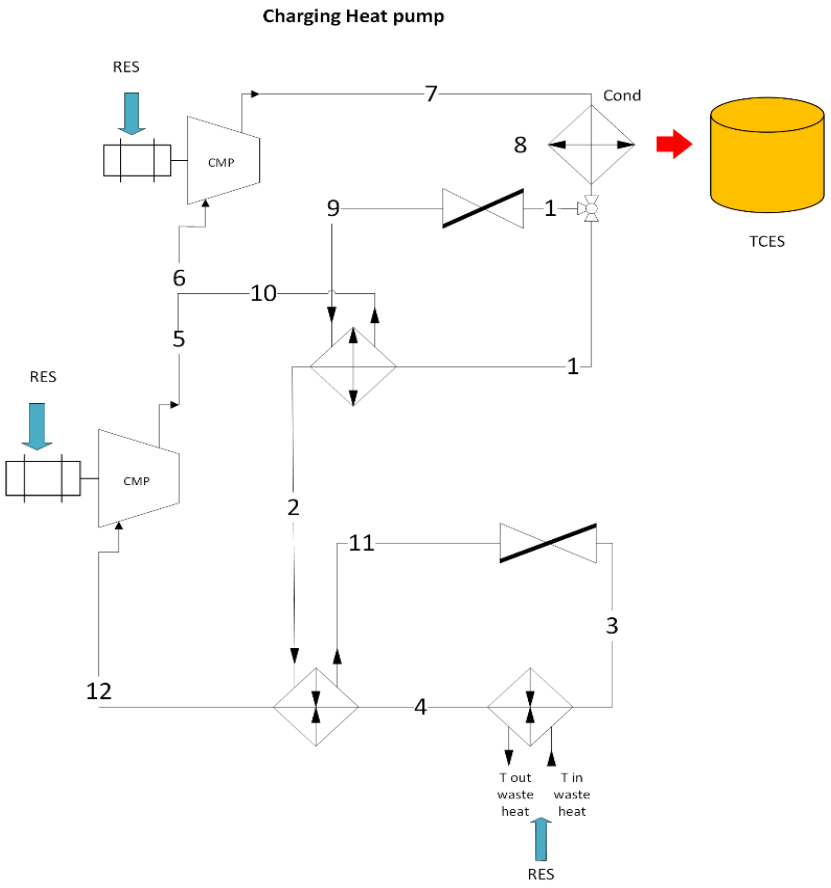

Figure 3-4: Heat Pump Cycle

The low temperature heat source including waste heat recovery and renewable sources which is shown as RES supplies heat to the system. It leads to evaporating the fluid from point 3 to 4. Subsequently, the fluid undergoes a preheating process within the Recuperator, raising its temperature to point 12. Then it enters the first compressor. At the outlet of first compressor, point 5, fluid reaches high temperature and pressure. Then, there is an intersection of streams 10, 5 and 6. More specifically, streams 10 and 5 are mixed making point 6 ready to enter the second compressor. Through the second compressor fluid reaches the maximum temperature of the cycle, point 7. Then, the fluid is condensed to liberate the heat for the thermochemical storage.

Then the fluid, in point 1, splits to two streams:

- One goes directly to drain cooler, becoming cooler and gives the heat to cold side of the drain cooler, point 2. Then, stream 2 is ready to goes through the Recuperator and preheat cold side, reaching point 11. Then the fluid losses the pressure through isenthalpic process of the valve reaches point 3.

- One goes through the valve by losing pressure, point 9. Then the stream of 9 enters a drain cooler absorb the heat and reach the saturated vapor in point 10.

The thermodynamic cycles is shown in Figure 3-5.

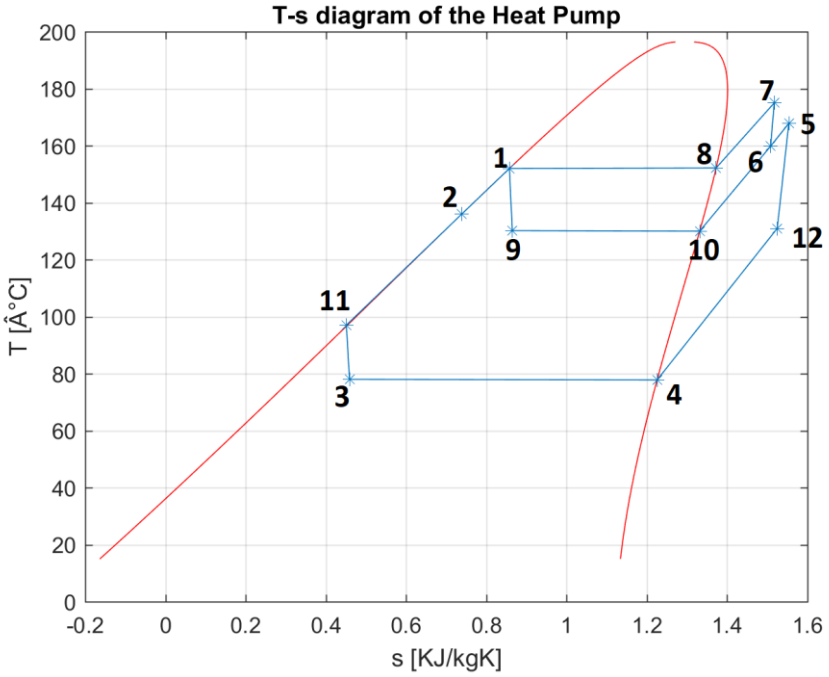

Figure 3-5: T-S diagram of HP cycle

It is needed to mentioned that heat in condensation step supply the heat of endothermic reaction in thermochemical storage. When it is needed, the reaction can take place in the reverse exothermic reaction. This energy supplies the evaporation process of power cycle.

3.4 Heat Pump Simulation

A mid temperature level of streams are added compared to simple heat pump cycle to increase the COP of cycle. However, finding a temperature which makes an ideal situation for the cycle to reach its objective is the goal of optimization procedure. In fact, in this section, temperature of point 10 which is between the temperature of point 1 and 3 is varying in order to find optimum T_{10} for the cycle, Figure 3-6. More specifically, starting T_{10} from the largest value very close to T_1 with the step of one degree all the thermodynamic properties calculated and the COP is stored in a matrix. Then the second T_{10} and so on till the temperature very close to T_3. At the end, the maximum COP among all COP is found and the temperature of T_{10} is the optimized and is introduced as the best for that cycle and fluid.

Regarding the margin that is set for T_{10} it should be said that for the maximum T_{10}, based on the order of thermodynamic property calculation, Point 2 is calculated based on point 9 and the pinch point temperature. So considering a minimum of 5 degree for the pinch point temperature leads the starting point to a temperature very close to T_1 and not the equal one.

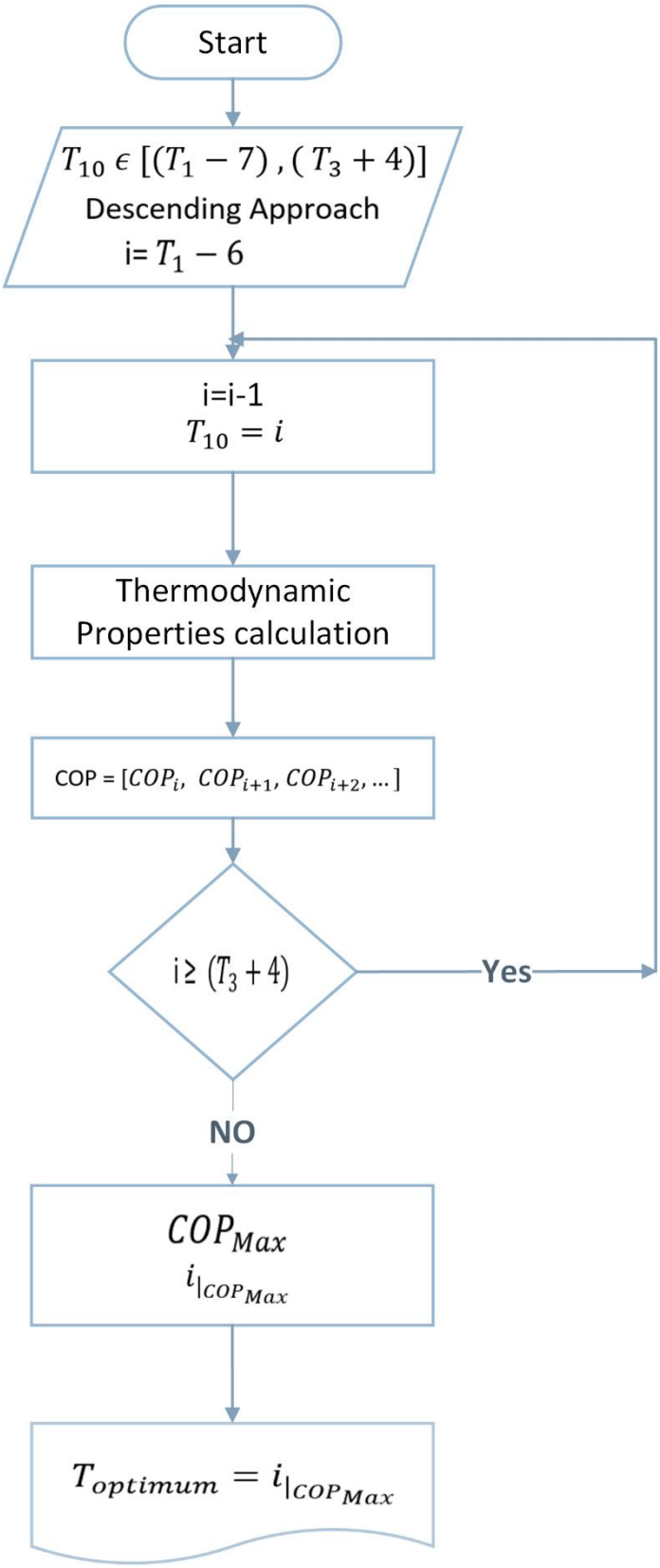

Figure 3-6: Simulation Flow chart

3.4.1 Compressor inlet and outlet checking

There are some issues about the cycle and simulation process that should be explained:

2.4.1.1 Compressor Inlet and outlet Regulation

The first concern about the cycle is related to compressor inlet and outlet. The compressors shall not:

- End inside the saturation bell
- End outside the saturation but passing through it

These two conditions are unacceptable. Before proposing a solution for that, the problem should be clearly explained. This situation takes place when T_{12} (the inlet temperature of the first compressor) and T_6 (the inlet temperature of the second compressor) are too low or based on the complexity of the fluid the bell is too curved. In the optimization process of T_{10}, when T_{10} gets too close to T_3, it exaggerate this condition.

To solve it, different actions are done: firstly, a Recuperator is proposed; indeed, the Recuperator preheat the cycle and push the inlet of first compressor to right side of T-S diagram. In this situation, the probability of first compressor to end inside the domain decreases. Figure 3-7 shows the effect of Recuperator. The cycle without the Recuperator is drawn in blue and the one with Recuperator is sketched in red.

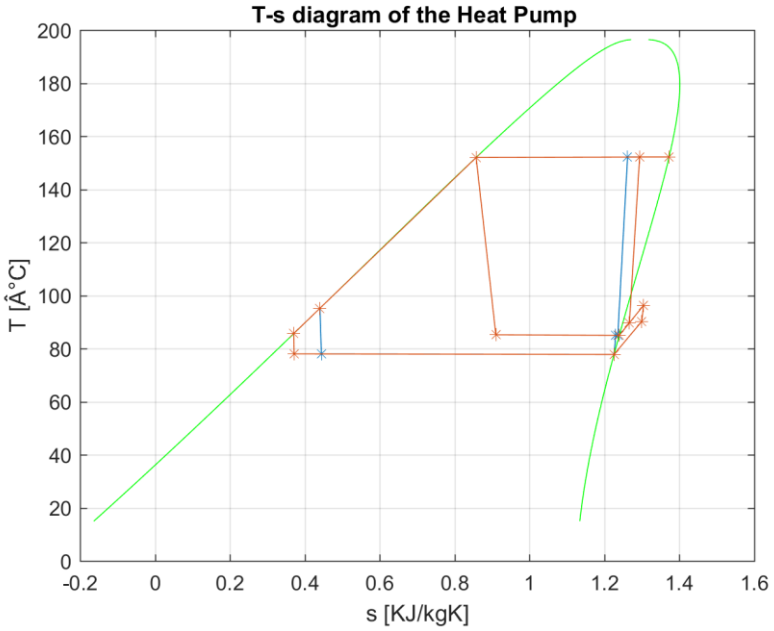

Figure 3-7: Recuperator effect

In this figure, it is visible that Recuperator may work for the first compressor and the problem for the second compressor still exists. In addition, probability of the first compressor to end inside the bell or cross it stills is not zero, because it mainly depends on saturation domain and the complexity of the fluid

Secondly, changing the pinch point temperature of drain cooler can be a suitable tool to counteract this issue. More specifically, increasing the pinch point temperature of drain cooler will disappear the role of drain cooler and shifting the second compressor to the right side of T-S diagram. Figure 3-8 shows the effect of drain cooler on compressor inlet and outlet temperature.

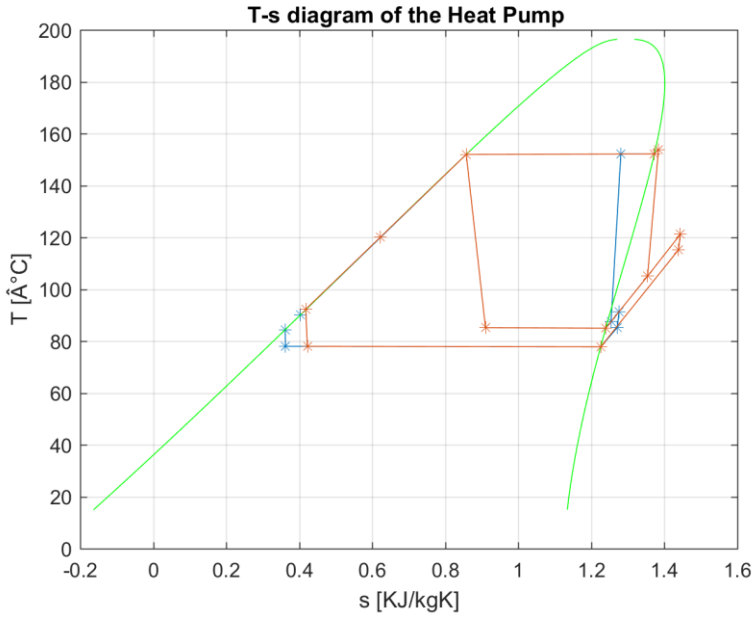

Figure 3-8: pinch point temperature of drain cooler effect

Heat pump cycle with high pinch point temperature of drain cooler is plotted in red and low value of it is plotted in blue. According to graph, from a certain value of pinch point temperature of drain cooler, both compressor shifts right and prevention of neither crossing nor ending inside the bell ensured.

Before keeping on, it should be mentioned that two proposed solutions solve the aforementioned problem but there should be a monitoring function to be sure about it. The only concern is the second compressor, so the function is designed for that.

In this regard, a function is created in which accepts the inlet and outlet coordinates of the compression process as inputs and calculates the closest distance between the compression line and the saturation curve.

In addition, this function provides information on whether compression ends in saturation bells. From a thermodynamic point of view, this scenario is characterized by the Algorithm 1:

Algorithm 1: Monitoring function of compressor distance from the bell

1: ***if*** $h_7 < h_8$ ***do***

2: $distance = 0;\ Break = 1;$

3: ***Else*** $h_8 \leq h_7$ ***do***
$Break = 0;$

$h_{CMP} = linspace\ (h_6, h_7, 10);$

$s_{CMP} = linspace(s_6, s_7, 10);$

4: ***For*** $i = 1: length\ (h_{CMP})$

$T_{CMP}\ (i) = refpropmm(\ h_{CMP}(i), s_{CMP}\ (i))\ ;$

P_{CMP} (i) = $refpropmm(T_{CMP}\ (i),\ h_{CMP}\ (i));$

$h_{vapor\_bell}\ (i) = refpropmm(P_{CMP}\ (i),\ Q = 1);$

5: **End for**

6: Error = h_{CMP}-h_{vapor_bell};

Distance = min (error);

7: **End if**

If the enthalpy of point eight is higher compared to point seven, it means that the compressor crosses the bell and ends inside the bell so $distance = 0$ and $break = 1$. The else case is related to situation in which the compressor crosses the bell but ends outside the bell; in this condition, the enthalpy of inlet and outlet of compressor is subdivided into ten intervals among them. Then, the enthalpy of saturated vapor of bell at the same pressure of those 10 points are calculated; finally, the difference of these enthalpies are computed. The minimum could be the worst case, as named distance will be reported.

3.4.1.2 Maximum temperature of cycle Regulation

The third concern is about the outlet temperature of second compressor. In fact, because of thermal limitation of components the maximum temperature that cycle can tolerate is $200\ °C$. In addition, there is a minimum threshold for T_7; In fact, to maintain a suitable temperature difference (ΔT) from the reaction temperature, the decision is made to establish the minimum outlet temperature of the compressor equal to$155°C$.

To control minimum and maximum value of T_7, the pinch point temperature of Recuperator is changed; so that the increase of pinch point temperature of Recuperator is accompanied with the decrease of T_7. In other words, it can be an appropriate tool to diminish the maximum value of T_7 and reaching the minimum one.

3.4.2 Optimization Framework

Considering the previous parts, optimization consists of three variables:

- T_{10}
- ΔT_{pp_rec}
- ΔT_{pp_dc}

More specifically, T_{10} was already explained in Figure 3-6. Considering the issues of inlet and outlet temperature of compressor in 3.4.1 Compressor inlet and outlet checking, two pinch point temperatures of Recuperator and drain cooler should be added to variables. Changing two pinch point temperature while keeping constant T_7 makes a new optimization progress. More in detail, a multi variable optimization approach is needed.

To solve this optimization two approaches are suggested, but just one of them is used.

- Multi variable optimization of multi objectives: In this solution, both pinch point temperature of Recuperator and drain cooler are variables; T_7 and COP are the objectives of optimization function.
- Multi variable optimization of one objective: In this solution, both pinch point temperature of Recuperator and drain cooler are variables and the combination of T_7 and COP provide one objective output to be optimized. In other words, two objectives in the first solution are merged in one objective.

Comparing both solutions ends up choosing the second solution. In fact, the second solution outweighs the first one:

- Both solutions depend on initial guess of variables; but in the first case, the sensibility to initial guess increase a lot; so that it makes the solving process more complex.
- The time of solving is another important aspect. In one-objective optimization, it is much faster.
- The trends are smoother and more stable in one-objective optimization.

Therefore, in general optimization flow chart will be like Figure 3-9.

More specifically, starting point and the steps of T_{10} are similar to Figure 3-6 For a certain T_{10}, in case of constraint existence, it should be defined. In the next section, constraints, it will be explained in detail.

Initial values should be given. Giving correct initial values is really important. In fact, the fmincon finds the local minimum of the function and not the absolute one. Therefore, the initial value should be close enough to the solution. To have better initial values the trends of both pinch point temperature and the their role in optimization should be considered.

Three other inputs should also be given: the maximum number of iteration, the tolerance of the iteration from a solution and the constant value of T_7. The iteration begins and it will be continued until the iteration reaches the maximum number or the solution gets too close and lower than the tolerance.

Furthermore, the objective function, j, is a combination of two outputs. The solver function that minimize the output should have high COP and very close T_7 to T7_obj to get larger negative values. With the help of $weight$ coefficient, there could be prioritization of one output over the other one.

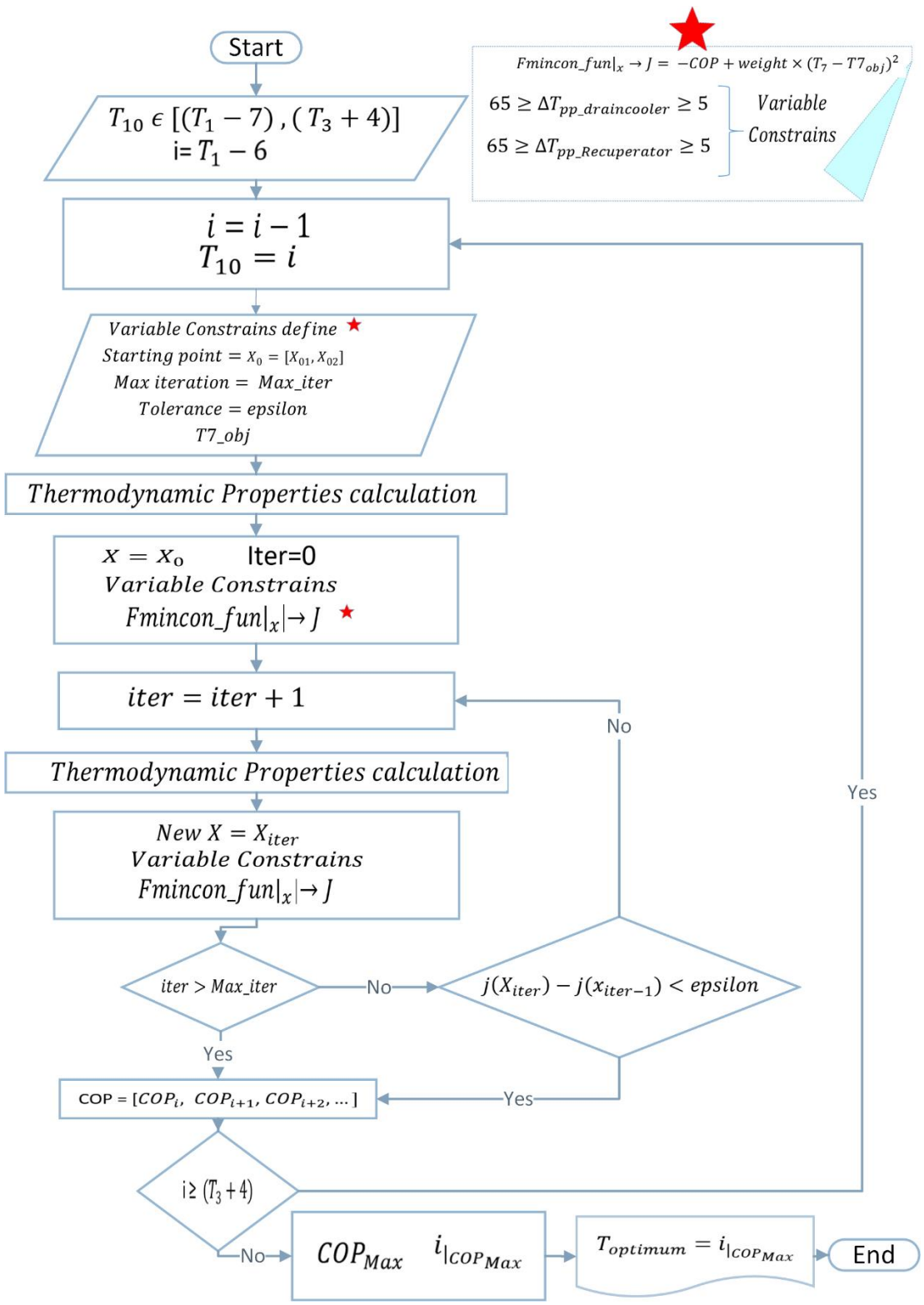

Figure 3-9: Optimization framework

3.4.3 Constraints

As can be seen in Figure 3-9, variables have some constraints that should be respected in the optimization.

Working range of T_{10} is clearly shown which is $[(T_1 - 7)\ , (\ T_3 + 4)]$.

As for two pinch point temperatures, there is a minimum threshold of 5 degree; pinch point value below minimum threshold are not acceptable for a working of heat exchanger. In addition, there is a maximum value of 65 degree based on the evaporation and condensation temperature of heat pump cycle. In other words, difference of those aforementioned values put a maximum threshold for pinch point temperatures. Following equation shows the working range of both pinch point temperature of heat exchangers.

$$\begin{aligned} 65 \geq \Delta T_{pp\_draincooler} \geq 5 \\ 65 \geq \Delta T_{pp\_Recuperator} \geq 5 \end{aligned} \tag{3. 7}$$

3.4.4 Properties calculation

Beginning with the understanding of the reaction's operating temperature ($T_{reactor} = 150°C$) and the temperature limit to which the energy source is cooled($T_{Wh\_out} = 80°C$), the condensation outlet temperature and the initiation temperature of evaporation are promptly computed:

$$\begin{aligned} T_1 = T_{reactor} + \Delta T_{pp,cond} \\ T_3 = T_{wh,out} + \Delta T_{pp,liq-liq} \end{aligned} \tag{3. 8}$$

Where $\Delta T_{pp,cond}$ and $\Delta T_{pp,liq-liq}$are supposed to be equal to 2 $°C$.

Using these temperatures as reference points, the temperature at the start of condensation and the temperature at the end of evaporation are calculated, taking into account the losses that occur during the phase transition.

$$\begin{aligned} T_8 = T_1 + \Delta T_{cond,HP} \\ T_4 = T_3 + \Delta T_{eva,HP} \end{aligned} \tag{3. 9}$$

Concerning the points situated along the saturation curve, the corresponding thermodynamic properties are computed based on the known vapor quality. This is achieved by invoking the REFPROP software:

$$[P_1, h_1, s_1] = refpropm(T_1, Q = 0) \tag{3. 10}$$

$$[P_4, h_4, s_4] = refpropm(T_4, Q = 1)$$

$$[P_8, h_8, s_8] = refpropm(T_8, Q = 1)$$

Then temperature of point 10 is assumed equal to 145 as the first value for the loop. According to T-S diagram, point 10 is coincident on saturation bell with the vapor quality equal to one. As a result, other properties will be calculated based on equation (3. 11).

$$[P_{10}, h_{10}, s_{10}] = refpropm(T_{10}, Q = 1) \tag{3. 11}$$

Going to the mid-pressure stream inlet of drain cooler, point 9, Similar to condensation and evaporation there a very small difference temperature of phase change in saturation bell equal to 0.2 based on equation (3. 12)

$$T_9 = T_{10} + \Delta T_{dc\_HP} \tag{3. 12}$$

Then, by knowing the isenthalpic process of valve, the enthalpy of point 9 is known. In addition, other thermodynamic properties are calculated, based on equation (3. 13)

$$h_9 = h_1$$
$$[P_9, s_9] = refpropm(T_9, h_9) \tag{3. 13}$$

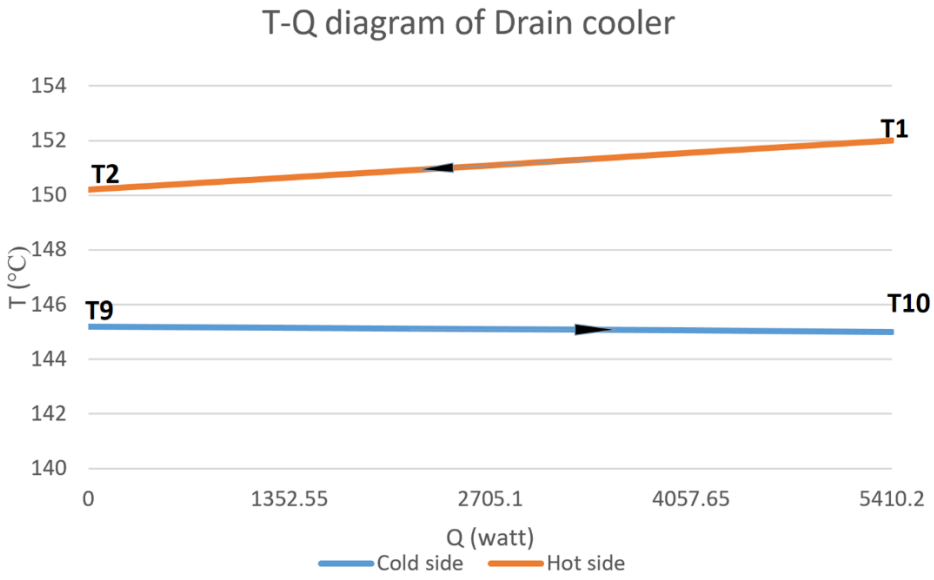

Figure 3-10: T-Q diagram of drain cooler

Then, according to T-Q diagram of drain cooler, Figure 3-10 and equation (3. 14) the temperature of low-pressure stream, inlet of the hot side of the Recuperator, point 2,

is calculated. By knowing the quality of point 2, which is equal to zero other thermodynamic properties are provided (equation (3. 14)).

$$T_2 = T_9 + \Delta T_{pp\_dc}$$
$$[P_2, h_2, s_2] = refpropmm(T_2, Q = 0) \quad (3.\ 14)$$

Regarding the junction between two compressors, all the streams enter at the same pressure; thus, based on equation (3. 15), pressure of point five, 6 and 10 are equal.

$$P_5 = P_{10}$$
$$P_6 = P_{10} \quad (3.\ 15)$$

According to Figure 3-11, the temperature of point 12 (inlet of first compressor) is calculated with the help of temperature pinch point of Recuperator. Moreover, considering the pressure drop equal to 0.02 of the inlet pressure, the pressure of point 12 will be calculated. Then, all other thermodynamic properties obtained easily based on equation (3. 16).

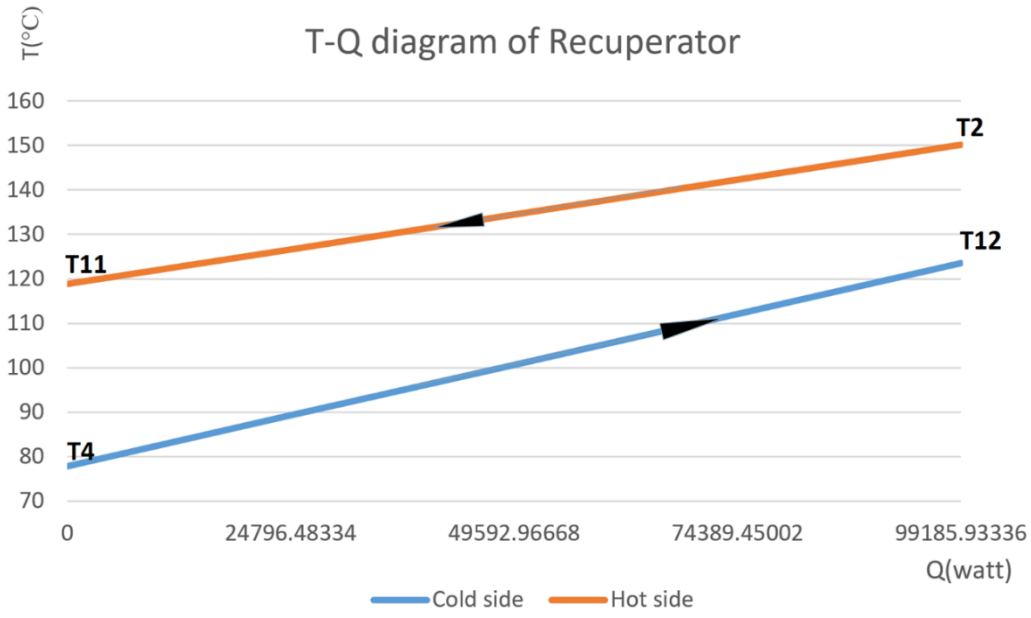

Figure 3-11: T-Q diagram of Recuperator

$$T_{12} = T_2 - \Delta T_{pp\_rec}$$
$$\Delta P_{HX\_gas} = 0.02\ [kpa] \quad (3.\ 16)$$

$$P_{12} = P_4 \times (1 - \Delta P_{HX\_gas})$$

$$[\, h_{12}, s_{12}] = refpropm(T_{12}, P_{12})$$

Then, with the help of energy balance on Recuperator, the enthalpy of point 11 (the outlet of liquid side of Recuperator) is calculated. Similar to point 12, the pressure of point 11 is obtained considering the pressure loss in the liquid side of Recuperator equal to 50 $[kPa]$. Then all other thermodynamic properties will be calculated based on equation (3. 17).

$$\begin{aligned} h_{11} &= h_2 + h_4 - h_{12} \\ \Delta P_{HX\_liquid} &= 50\ [kpa] \\ P_{11} &= P_2 - \Delta P_{HX\_liquid} \\ [\, T_{11}, s_{11}] &= refpropm(P_{11}, h_{11}) \end{aligned} \tag{3. 17}$$

Knowing that isenthalpic valve provides the enthalpy of point 3 equal to 11. All other properties using the equation of (3. 18) will be obtained easily.

$$\begin{aligned} h_3 &= h_{11} \\ [\, P_3, s_3] &= refpropm(T_3, h_3) \end{aligned} \tag{3. 18}$$

As for the first compressor, first it is needed to calculate the isentropic enthalpy of point 5 (the outlet of first compressor). Then, with the help of isentropic efficiency, enthalpy of point 5 is computed. Finally, other properties will be calculated. Equation (3. 19) summarizes all calculation.

$$\begin{aligned} [\, h_{5s}] &= refpropm(P_5, s_{12}) \\ h_5 &= \frac{h_{5s} - h_{12}}{\eta_{CMP1}} + h_{12} \\ [\, T_5, s_5] &= refpropm(P_5, h_5) \end{aligned} \tag{3. 19}$$

Before going on, three mass flow rate should be explained: according to Figure 3-4, the outlet of condenser is splitted into two parts:

- the mid-pressure steam passing the valve from 1 to 9
- the low-pressure steam passing from 1 to 2

The mass flowing in the low-pressure side is called $\dot{m}_{LP}$ and the one going in mid-pressure side is called $\dot{m}_{MP}$. The summation of the aforementioned mass flow rates is $\dot{m}_{total}$.

Then, by writing energy balance on drain cooler; mass fraction is defined as equation (3. 20);

$$\begin{aligned} \dot{m}_{MP}.(h_{10}-h_9) &= \dot{m}_{LP}.(h_1-h_2) \\ \rightarrow \dot{m}_{ratio} &= \frac{h_{10}-h_9}{h_1-h_2} = \frac{\dot{m}_{LP}}{\dot{m}_{MP}} \end{aligned} \tag{3. 20}$$

Again, by writing an energy balance on the junction between two compressor, using the $\dot{m}_{ratio}$, the enthalpy of point 6 is computed. Equation (3. 21) shows all the procedure:

$$\begin{aligned} \dot{m}_{total}.h_6 &= \dot{m}_{MP}.h_{10} + \dot{m}_{LP}.h_5 \\ h_6 &= \frac{\dot{m}_{MP}.h_{10} + \dot{m}_{LP}.h_5}{\dot{m}_{MP} + \dot{m}_{LP}} \\ \xrightarrow{\times\frac{\dot{m}_{MP}}{\dot{m}_{MP}}} h_6 &= \frac{h_{10} + \dot{m}_{ratio}.h_5}{1 + \dot{m}_{ratio}} \end{aligned} \tag{3. 21}$$

Then other properties of point 6 is calculated as following equation:

$$[T_6, s_6] = refpropm(P_6, h_6) \tag{3. 22}$$

Going to the last point of cycle, point 7, pressure is equal to the pressure of point 8. Similar to the first compressor, the procedure for the second compressor takes place based on equation (3. 23).

$$\begin{aligned} P_7 &= P_8 \\ [h_{7s}] &= refpropm(P_7, s_6) \\ h_7 &= \frac{h_{7s}-h_6}{\eta_{CMP2}} + h_6 \\ [T_7, s_7] &= refpropm(P_7, h_7) \end{aligned} \tag{3. 23}$$

With knowledge of the thermodynamic states at each point in the cycle, various relevant parameters can be calculated. The heat released in condensing is equivalent to the heat required to allow an endothermic reaction in the reactor. Using equations (3. 24), the total rate of fluid circulation within the charging cycle can be determined.

$$Q_{cond\_HP} = Q_{reaction} \tag{3. 24}$$

$$\dot{m}_{total} = \frac{Q_{reaction}}{h_7 - h_1}$$

With the combination of $\dot{m}_{ratio}$ and $\dot{m}_{total}$ formula, the mass flow rate of mid-pressure ($\dot{m}_{MP}$) and low-pressure streams ($\dot{m}_{LP}$) can be calculated:

$$\dot{m}_{MP} = \frac{\dot{m}_{total}}{1 + \dot{m}_{ratio}} \qquad (3.\ 25)$$

$$\dot{m}_{LP} = \dot{m}_{total} - \dot{m}_{MP}$$

Continuing the process of determining the desired parameters, the electrical powers consumed by both compressors are acquired.

$$W_{CMP1} = \dot{m}_{LP} \times (h_5 - h_{12}) \qquad (3.\ 26)$$

$$W_{CMP2} = \dot{m}_{total} \times (h_7 - h_6)$$

Finally, the most significant parameter for heat pump cycle, COP, is calculated as follows:

$$COP = \frac{Q_{reaction}}{W_{CMP1} + W_{CMP2}}$$

Concerning the heat input into the cycle, it originates from the low-temperature source. This thermal energy is utilized to vaporize the working fluid within the charging cycle. Thus, mass flow rate of water for the vaporization is obtained. Mathematically, this relationship is represented by the subsequent pair of equations:

$$\dot{m}_{LP}.(h_4 - h_3) = \dot{m}_{water\_wh} \times 4.2 \times \left(T_{in_{wh}} - T_{out\_wh}\right) \qquad (3.\ 27)$$

$$\dot{m}_{water\_wh} = \frac{\dot{m}_{LP}.(h_4 - h_3)}{4.2 \times \left(T_{in_{wh}} - T_{out\_wh}\right)}$$

3.4.5 Heat Exchangers Areas

The code proceeds by calculating the area of the heat exchanger. This is done using the overall basic heat transfer equation for the heat exchange process in the heat exchanger:

$$Q = UA\Delta T_{ml} \tag{3. 28}$$

That ΔT_{ml} represents the logarithmic mean temperature difference, which is defined as equation below:

$$\Delta T_{ml} = \frac{\Delta T_A - \Delta T_B}{ln\frac{\Delta T_A}{\Delta T_B}} \tag{3. 29}$$

3.4.3.1 High pressure Heat exchanger (Condensation)

The T-Q diagram of the high-pressure heat exchanger (condenser) is illustrated in the Figure 1-12.

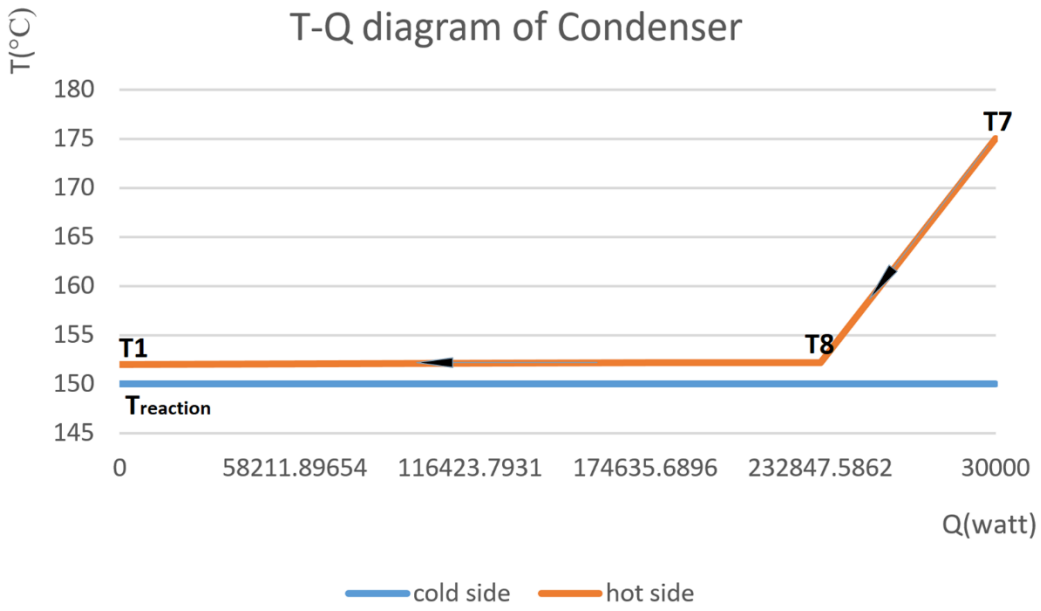

Figure 3-12: T-Q diagram of condenser

To begin with, the heat transferred in the condenser and the desuperheater are computed.

$$\begin{aligned} \dot{Q_{Cond}} &= \dot{m}_{total}.(h_8 - h_1) \\ \dot{Q_{DSH}} &= \dot{m}_{total}.(h_7 - h_8) \end{aligned} \tag{3. 30}$$

Subsequently, the logarithmic mean temperature difference, ΔT_{ml}, for both parts are computed.

$$\Delta T_{ml\_cond} = \frac{(T_8 - T_{reaction}) - (T_1 - T_{reaction})}{ln\frac{T_8 - T_{reactio}}{T_1 - T_{reactio}}}$$
$$\Delta T_{ml\_DSH} = \frac{(T_7 - T_{reaction}) - (T_8 - T_{reaction})}{ln\frac{T_7 - T_{reaction}}{T_8 - T_{reaction}}} \quad (3.\ 31)$$

Finally, the UA parameter of the high-pressure heat exchanger is derived.

$$UA_{cond} = \frac{\dot{Q}_{Cond}}{\Delta T_{ml\_cond}} + \frac{\dot{Q}_{DSH}}{\Delta T_{ml\_DSH}} \quad (3.\ 32)$$

The overall heat transfer coefficient, U, can be calculated with the help of Table 3-2 and Table 3-3. Therefore, the area of heat exchanger is computed easily.

3.4.3.2 Low pressure Heat exchanger (evaporation)

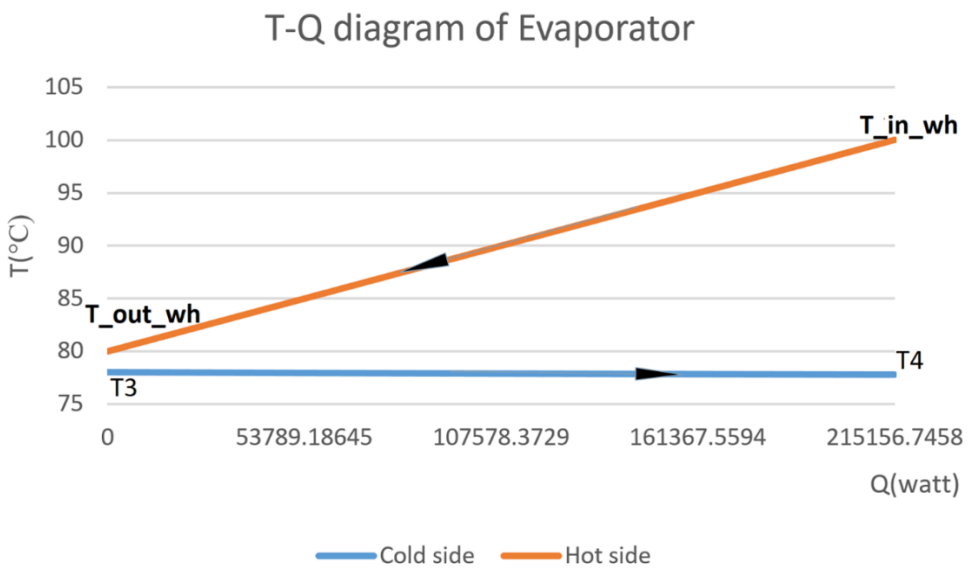

Figure 3-13: T-Q diagram of evaporator

Figure 3-13 shows a T-Q diagram of evaporation process. The required heat for the evaporation process is calculated according to Equation (3. 33).

$$\dot{Q}_{eva\_HP} = \dot{m}_{LP}.(h_4 - h_3) \tag{3. 33}$$

Similar to the previous heat exchanger, the U parameter is calculated. Following this, the surface area of the low-pressure heat exchanger (evaporation) is calculated.

$$\Delta T_{ml\_eva} = \frac{(T_{in\_wh} - T_4) - (T_{out\_wh} - T_3)}{ln\frac{T_{in,Wh} - T_4}{T_{out\_wh} - T_3}}$$
$$UA_{eva} = \frac{\dot{Q}_{eva\_HP}}{\Delta T_{ml\_eva}} \tag{3. 34}$$

3.4.3.3 Recuperator

T-Q diagram of Recuperator has already drawn in Figure 3-11. Consequently, the exchanged heat, ΔT_{ml_rec} and the UA parameter are calculated based on following equations:

$$\dot{Q}_{rec\_HP} = \dot{m}_{LP}.(h_{12} - h_4)$$
$$\Delta T_{ml\_rec} = \frac{(T_2 - T_{12}) - (T_{11} - T_4)}{ln\frac{T_2 - T_{12}}{T_{11} - T_4}} \tag{3. 35}$$
$$UA_{rec} = \frac{\dot{Q}_{rec\_HP}}{\Delta T_{ml\_rec}}$$

3.4.3.4 Drain cooler

T-Q diagram of drain cooler has already drawn in Figure 3-11. Consequently, the exchanged heat, ΔT_{ml_dc} and the UA parameter are calculated based on following equations:

$$\dot{Q}_{dc\_HP} = \dot{m}_{LP}.(h_1 - h_2)$$
$$\Delta T_{ml\_dc} = \frac{(T_2 - T_9) - (T_1 - T_{10})}{ln\frac{T_2 - T_9}{T_1 - T_{10}}} \tag{3. 36}$$
$$UA_{dc} = \frac{\dot{Q}_{dc\_HP}}{\Delta T_{ml\_dc}}$$

4.Results

After explaining the method and using the MATLAB code to perform the simulation on the Heat pump cycle, reference case will be defined; then, the results of reference case will be provided. At the end, sensitivity analysis will be carried out to show the effect of different parameter such as maximum temperature of cycle and fluid type.

4.1 Reference case definition

According to Methodology chapter, simulation is done on the constant temperature of T_7. Now, as a reference case, one temperature should be selected. As it was said before, the possible range of T_7 is$[155°C\,, 200°C]$. Choosing a temperature in this range is based on different criteria.

Firstly, the larger T_7 brings larger COP system. However, in reality the maximum temperature (200 °C) cannot be a good representative of the range of COP of the system specially for low value of T_7. Secondly, considering the simulation variables' constraints, equation (3. 7), the optimization does not work properly in higher values of T_7. Thirdly, one of the analysis of results is related to the behavior of optimization solver, when the constraints reach the extremum. Therefore, the mid temperature of T_7, $[200 + 155]/2 \cong 175,$ would be a suitable case for the reference case.

	Chemical formula	$\boldsymbol{T_{critical}}$	$\boldsymbol{P_{critical}}$	**ODP**	**GWP**
$\boldsymbol{Methyl - cyclo - hexane}$ **(C1CC6)**	$cycle\ (CH_2)_6 - CH_3$	299	34.7	0	3

Table 4-1: C1CC6 chemical properties

Next, a suitable fluid as a reference case should be selected. Among different fluids of Table 3-4, an appropriate fluid should follow the criteria in section *3.2.2.2 Working*

Fluid. As a result, C1CC6 is selected. Having a high critical temperature and pressure along with low GWP and ODP and large COP makes this fluid unique. All the properties are summarized in the Table 4-1 [97] . The only concern of this fluid is the high rate of flammability.

4.2 Reference case outcomes

In this section, results of C1CC6 will be obtained. Results are divided into three parts; firstly, general results such as COP, mass flow rate and variables variation will be computed. In the second part, heat exchangers' area will be obtained.

4.2.1 General outcomes

In the first place, COP of cycle is shown in Table 4-1. It shows how COP is affected by T_{10}, at a constant T_7.

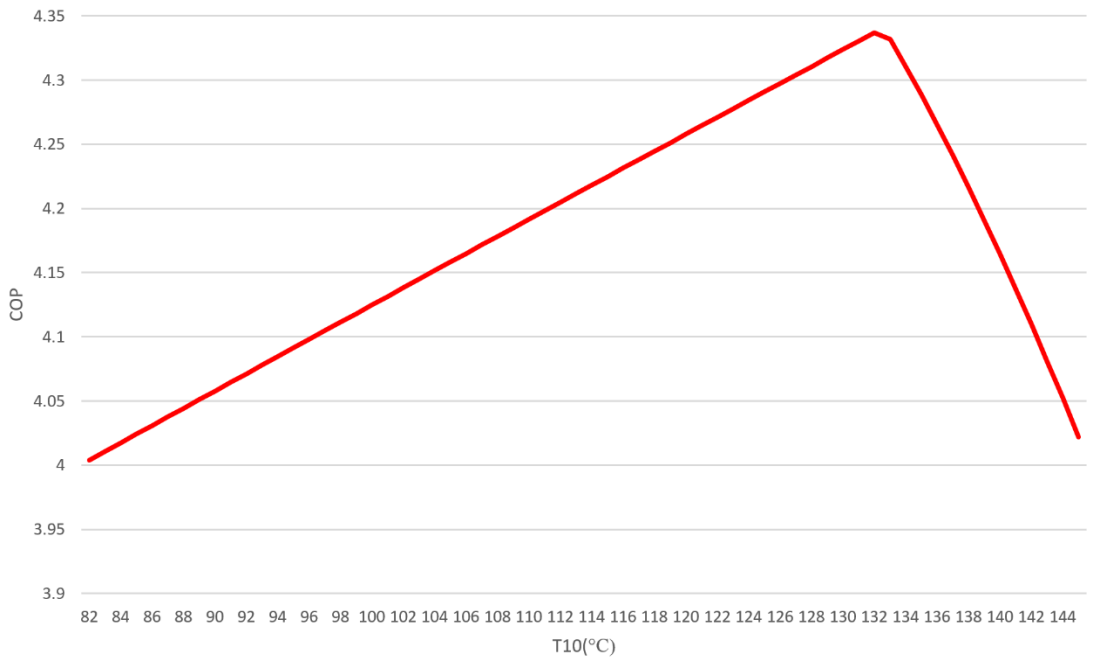

Figure 4-1: COP variation of the reference case

Starting from the high temperature of T_{10}(descending approach), COP increases. Then, it reaches the maximum one at 132℃. T-S diagram of reference case at 132℃ is shown in Figure 4-2. After that, it decreases linearly reaching the same value of COP as starting point with the negligible tolerance as following equation:

$$COP_{start} - COP_{end} \leq 0.06 \quad (4\text{- }1)$$

According to equation (4- 1), as thermodynamic point of view (without considering other perspectives), heat pump cycle has almost the same COP when T_{10} is at the maximum or the minimum value.

Moreover, when T_{10} is at the maximum value, it is almost the same as the simple heat pump cycle; in other words, at high value of T_{10}, drain cooler's role is disappeared and it seems like a heat pump cycle with two compressor and one Recuperator without drain cooler. Thus, higher value of COP for mid temperature of T_{10} compared to the maximum one clearly justifies that the proposed cycle is worthy to used. Defining relative increase of coefficient of performance as $(COP_{optimum} - COP_{simple_{HP}})/COP_{simple_{HP}}$ repeats the previous statement numerically. For the reference case, the relative increase of COP is 7.8%.

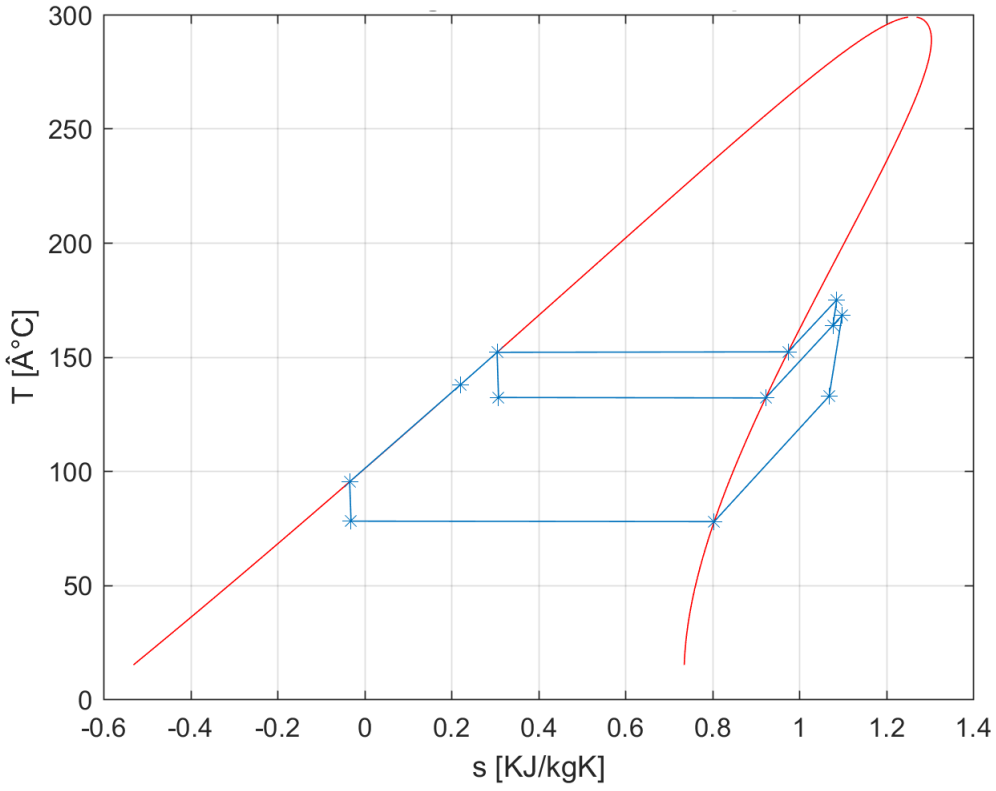

Figure 4-2: T-S diagram of Optimized temperature of the reference case

Next, the pinch point temperatures as the main variables in the optimization should be monitored. Pinch point temperature variation has significant effect on all other

parameters. For example, the heat exchanger area is affected by the pinch point temperatures. The fluctuation of Recuperator's and drain cooler's pinch point temperatures are illustrated in Figure 4-3.

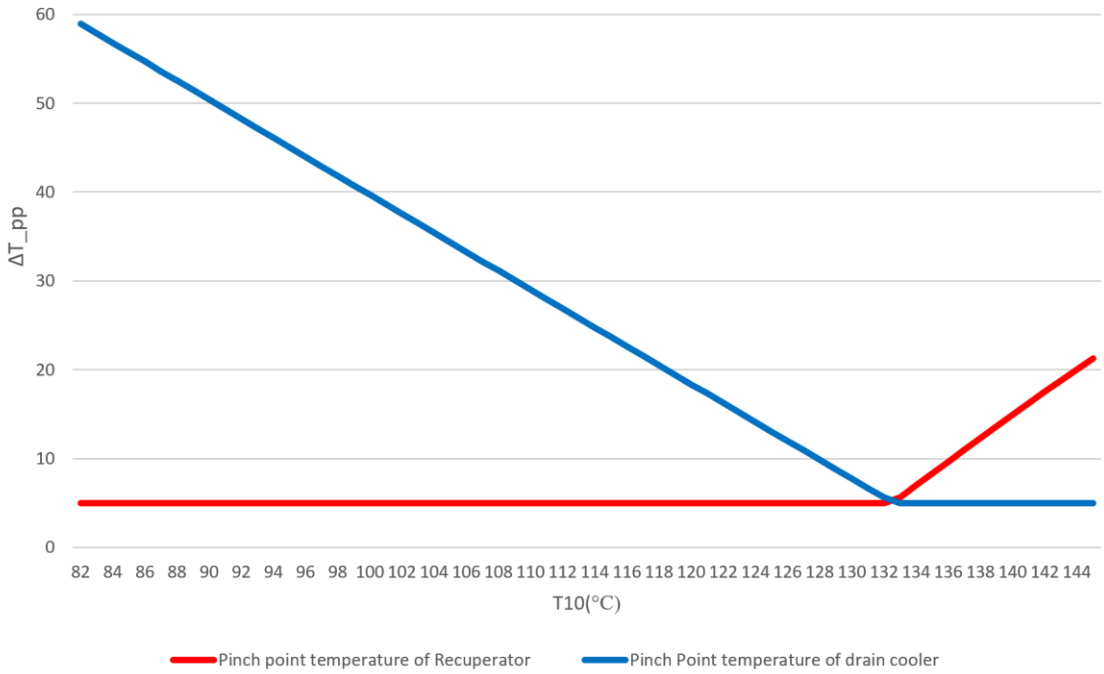

Figure 4-3: Pinch Point temperature of drain cooler and Recuperator variation of a reference case

In accordance with section 3.4.1 Compressor inlet and outlet checking, for low value of T_{10} high value of $\Delta T_{pp_dc}$is needed to prevent crossing the bell or ending inside the bell. Therefore, the figure above demonstrates that in descending approach (155 to 82) from a certain value, S, the pinch point temperature of drain cooler increases. Comparing the value of S with Figure 4-1, signifies that S is the optimal value of cycle (equation (4- 2))

$$S = T_{10\_optimum} \tag{4- 2}$$

Again, in compliance with section 3.4.1.2 Maximum temperature of cycle Regulation, increasing the ΔT_{pp_rec} is used to control T_7. In fact, in order to keep a constant T_7 especially when T_{10} is a high temperature, ΔT_{pp_rec} is needed. ΔT_{pp_rec} increases after the optimal temperature.

To sum up, the point in which both pinch point temperatures have the lowest value (5 degree) is an optimal condition.

Additionally, the role of drain cooler is going to be analyzed; indeed, monitoring the mass fraction indicates how mass flow rate is splitted in drain cooler branch and main branch. Therefore, the mass flows in drain cooler indicates how drain cooler plays role in optimized conditions. Besides, checking the mass flow variation is beneficial for heat exchangers' area. Figure 4-4 shows the mass flow rate of low pressure, high pressure.

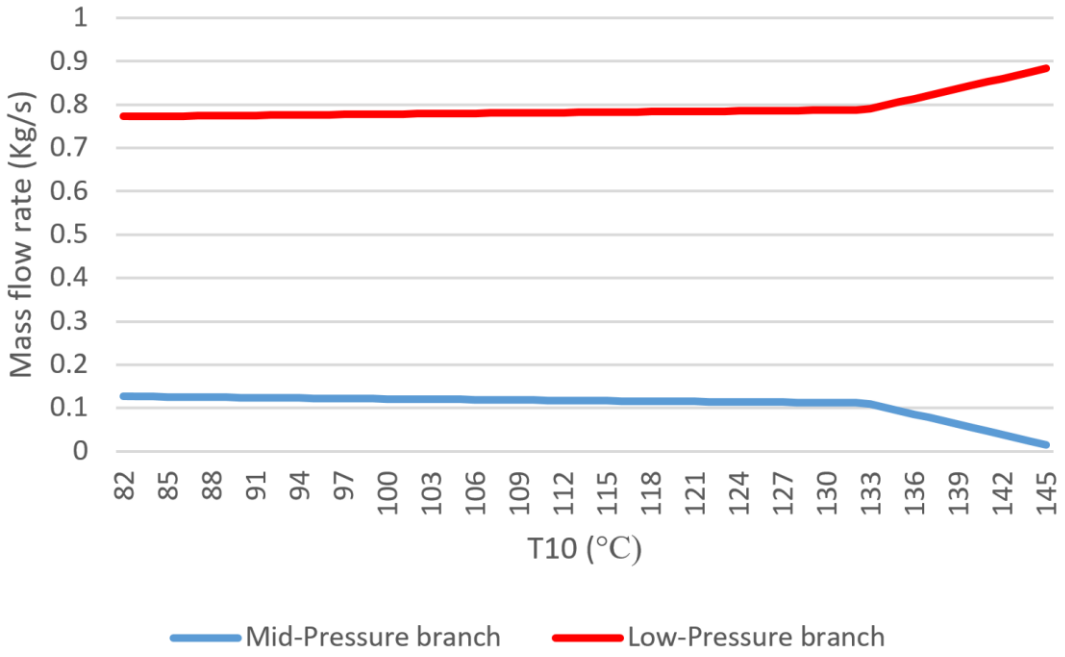

Figure 4-4: Mass flow rate variation for the reference case

It is evident that for large T_{10}, $\dot{m}_{MP}$ becomes very small while $\dot{m}_{LP}$ increases; As a result, the cycle looks like a simple heat pump cycle and the role of drain cooler is faded.

4.2.2 Heat exchangers' Area

In this section, the effect of optimization on all heat exchangers' area will be checked. There are four heat exchangers: high-pressure heat exchanger, evaporator, Recuperator and drain cooler. High-pressure heat exchanger, itself, consists of condenser and desuperheater parts.

To have a better view on heat exchangers' charts, the variation of basic parameters is summarized in Table 4-2.

$T_{10\_optimum}$ splits the table into two parts. Considering the descending approach (starting point 145℃) the first part of is a range of $[T_{10_{opt}}, 145]$ and the range of second part is [82, $T_{10_{opt}}$]. Table provides all the essential parameter affecting the heat exchange area.

Increase of a parameter is shown in blue, while decrease of that is illustrated in red. When two parameters have counter effect, the one that has the stronger effect is shown with two arrows. In other words, the number of arrows show the intensity of the parameter in the calculation.

T_{10_opt}		
Component	$T_{10} = 82℃$ $\overset{T_{10}}{\leftarrow}$	$\overset{T_{10}}{\leftarrow}$ $T_{10} = 145℃$
HX_{Cond}	$\dot{Q}_{Cond} = \dot{m}_{total}.(h_8 - h_1)$ & $UA_{cond} = \frac{\dot{Q}_{Cond}}{\Delta T_{ml\_cond}}$	
	$h_8 = const$ $h_1 = const$ $\dot{m}_{total} = const$ } $\dot{Q}_{Cond} = const$ $\Delta T_{ml_{cond}} = const$ $\Rightarrow A_{cond} = const$	$h_8 = const$ $h_1 = const$ $\dot{m}_{total} = const$ } $\dot{Q}_{Cond} = const$ $\Delta T_{ml_{cond}} = const$ $\Rightarrow A_{cond} = const$
HX_{DSH}	$\dot{Q}_{DSH} = \dot{m}_{total}.(h_7 - h_8)$ & $UA_{DSH} = \frac{\dot{Q}_{DSH}}{\Delta T_{ml\_DSH}}$	
	$h_8 = const$ $h_7 = const$ $\dot{m}_{total} = const$ } $\dot{Q}_{DSH} = const$ $\Delta T_{ml_{DSH}} = const$ $\Rightarrow A_{DSH} = const$	$h_8 = const$ $h_7 = const$ $\dot{m}_{total} = const$ } $\dot{Q}_{DSH} = const$ $\Delta T_{ml_{DSH}} = const$ $\Rightarrow A_{DSH} = const$
Evaporator	$\dot{Q}_{eva\_HP} = \dot{m}_{LP}.(h_4 - h_3)$ & $UA_{eva} = \frac{\dot{Q}_{eva\_HP}}{\Delta T_{ml\_eva}}$	

	$h_4 = const$ $h_3 \uparrow$ $\dot{m}_{LP} \downarrow$ $\} \dot{Q}_{eva\_HP} \downarrow$ $\Delta T_{ml\_eva} = const$ $\Rightarrow A_{eva} \downarrow$	$h_4 = const$ $h_3 \downarrow\downarrow$ $\dot{m}_{LP} \downarrow$ $\} \dot{Q}_{eva\_HP} \uparrow$ $\Delta T_{ml\_eva} = const$ $\Rightarrow A_{eva} \uparrow$
Recuperator	$\dot{Q}_{rec\_HP} = \dot{m}_{LP}.(h_{12} - h_4)$ & $UA_{rec} = \frac{\dot{Q}_{rec\_HP}}{\Delta T_{ml\_rec}}$	
	$h_4 = const$ $h_{12} \uparrow\uparrow$ $\dot{m}_{LP} \downarrow$ $\} \dot{Q}_{rec_{HP}} \uparrow\uparrow$ $\Delta T_{ml\_rec} \uparrow$ $\Rightarrow A_{rec} \uparrow$	$h_4 = const$ $h_{12} \uparrow$ $\dot{m}_{LP} \downarrow\downarrow$ $\} \dot{Q}_{rec_{HP}} \downarrow$ $\Delta T_{ml_{rec}} \downarrow\downarrow$ $\Rightarrow A_{rec} \uparrow$
Drain Cooler	$\dot{Q}_{dc\_HP} = \dot{m}_{LP}.(h_1 - h_2)$ & $UA_{dc} = \frac{\dot{Q}_{dc\_HP}}{\Delta T_{ml\_dc}}$	
	$h_1 = const$ $h_2 \uparrow$ $\dot{m}_{LP} \downarrow$ $\} \dot{Q}_{dc\_HP} \downarrow$ $\Delta T_{ml\_dc} \uparrow$ $\Rightarrow A_{dc} \downarrow$	$h_1 = const$ $h_2 \downarrow\downarrow$ $\dot{m}_{LP} \downarrow$ $\} \dot{Q}_{dc\_HP} \uparrow\uparrow$ $\Delta T_{ml\_dc} \uparrow$ $\Rightarrow A_{dc} \uparrow$

Table 4-2: Basic parameters variation

Going through the heat exchangers' variation, the effect of optimization on surface area is monitored. They are displayed as following figures.

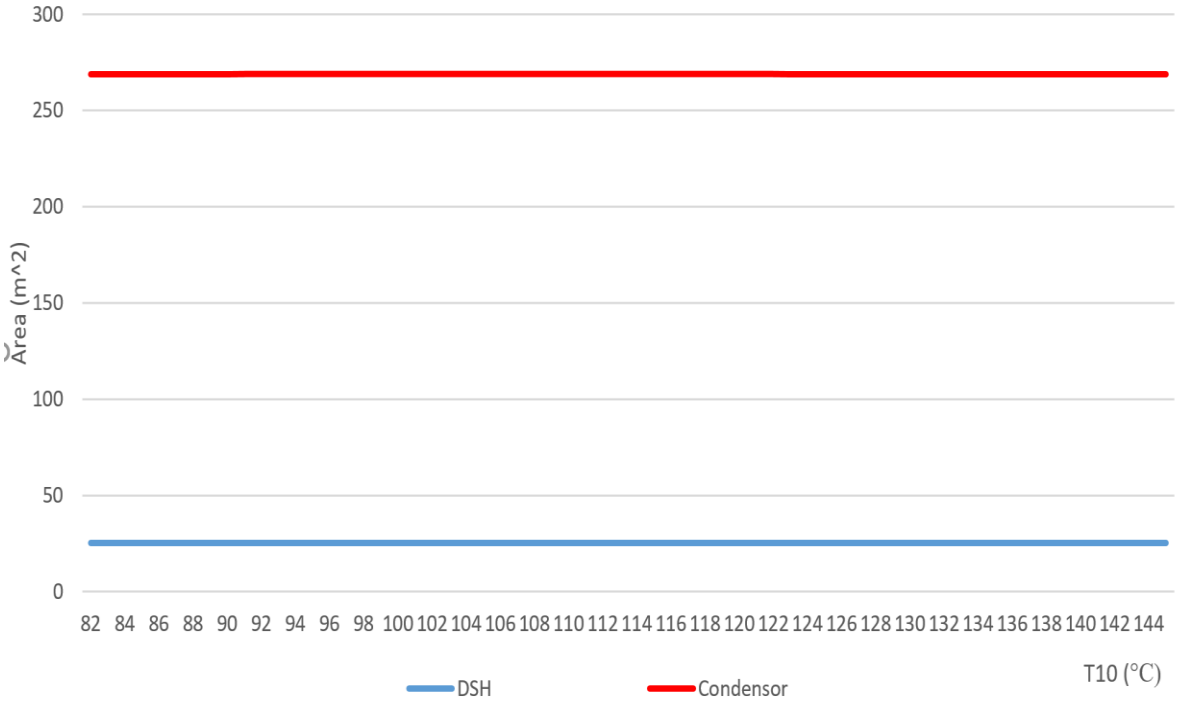

Figure 4-5: The variation of condenser and desuperheater heat exchanger's surface area for the reference case

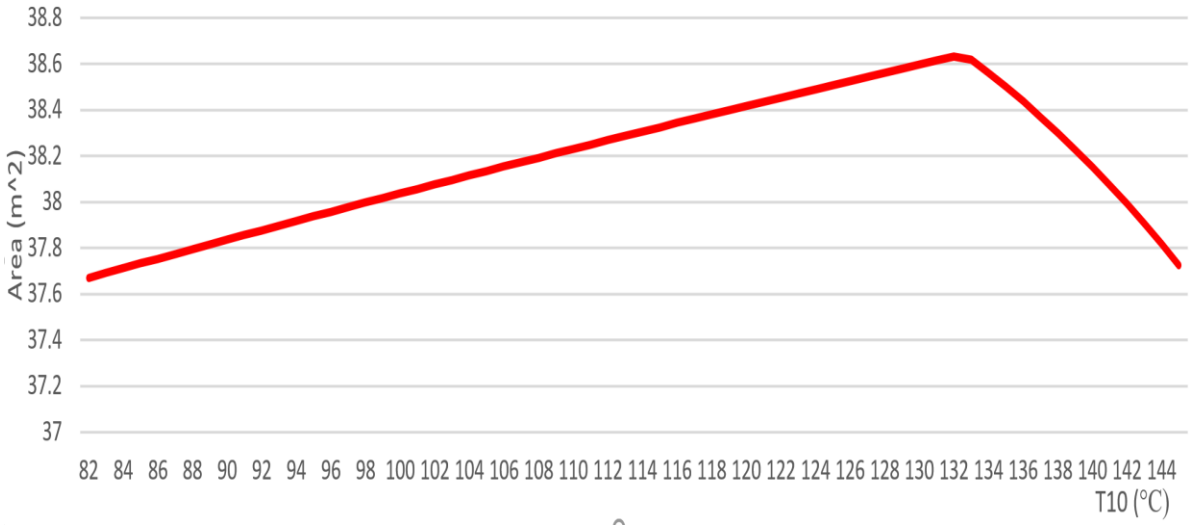

Figure 4-6: The variation of evaporator's surface area for the reference case

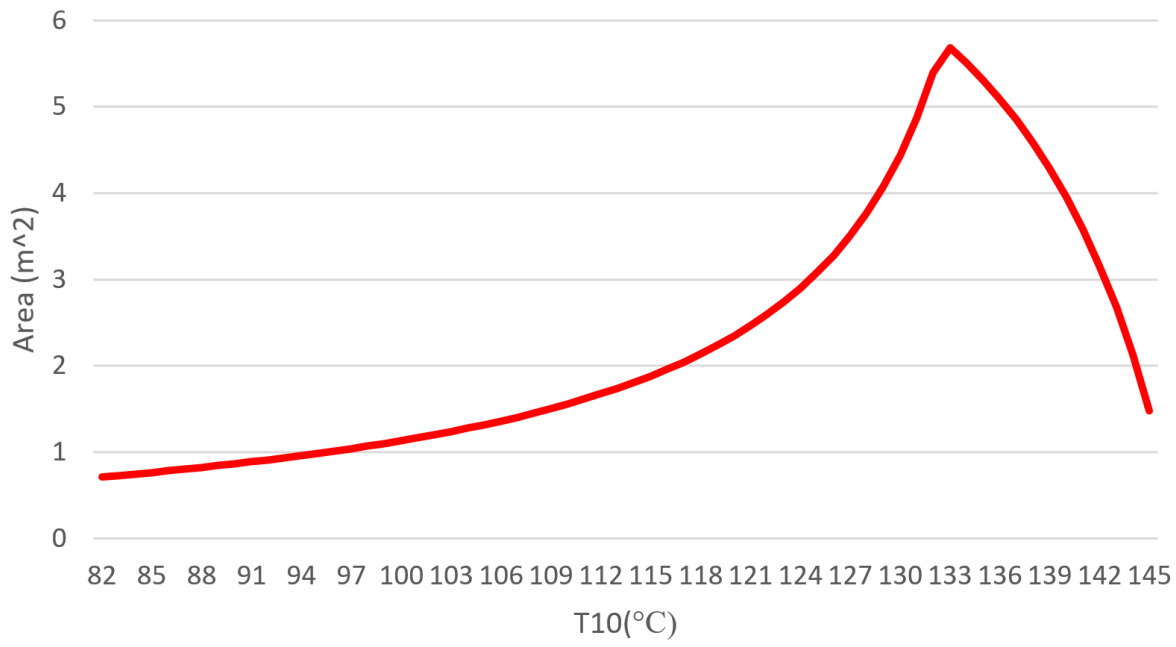

Figure 4-7: The variation of drain cooler's surface area for the reference case

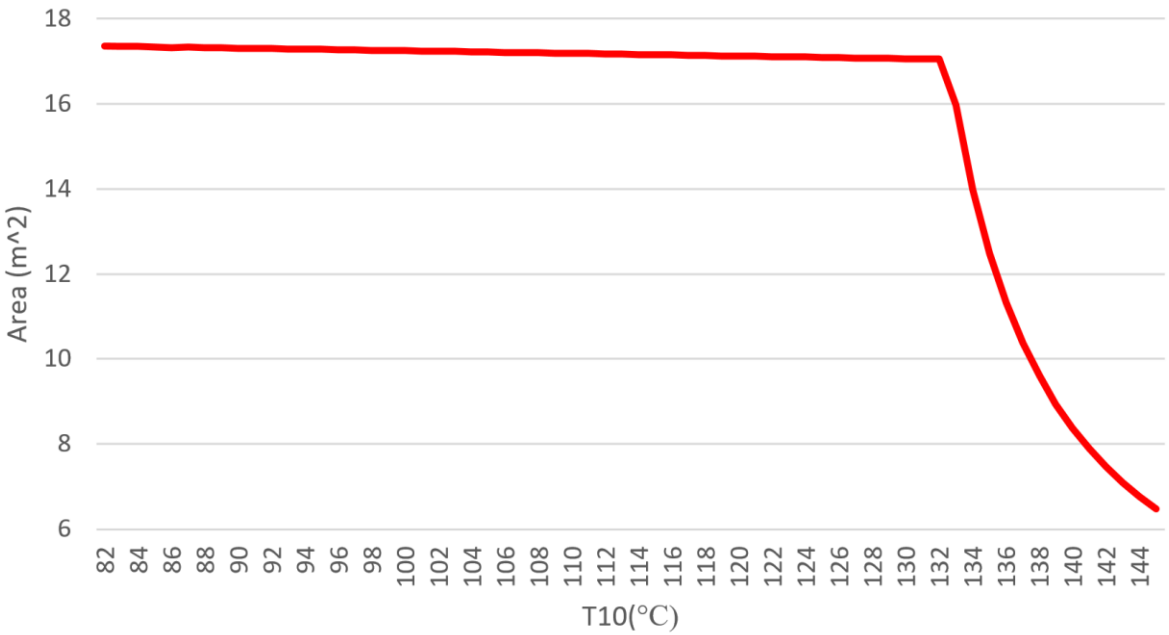

Figure 4-8: The variation of Recuperator's surface area for the reference case

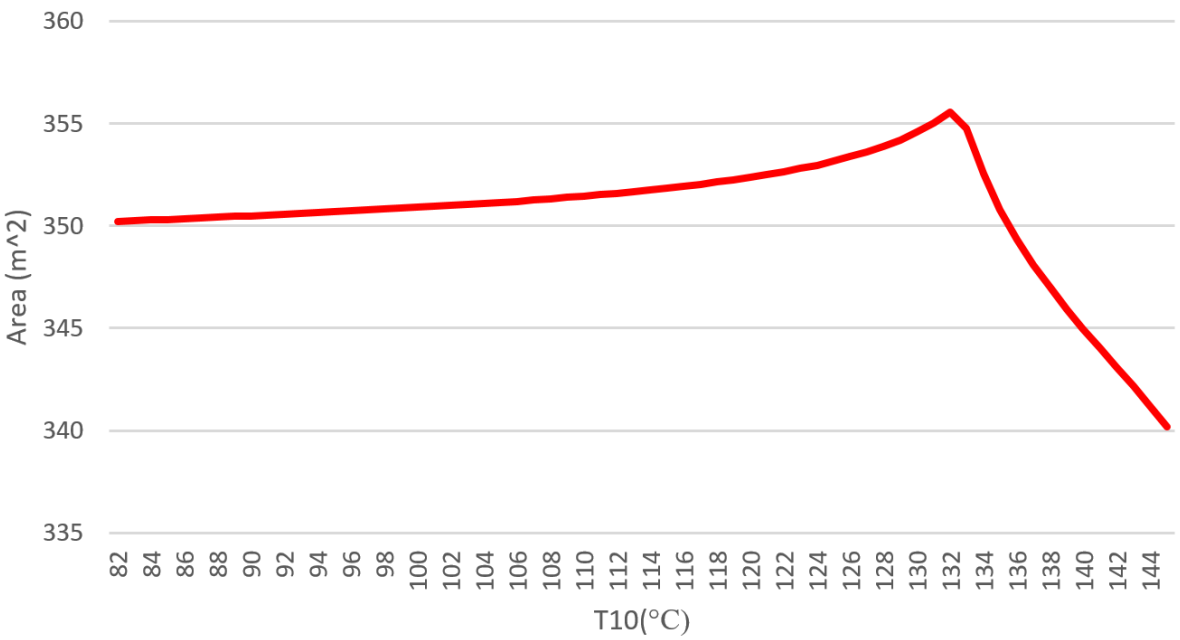

Figure 4-9: The variation of all heat exchangers' surface area for the reference case

All the effective parameters to explain the variation of each heat exchanger are explained in the Table 4-2.

According to Figure 4-5, condenser and desuperheater have the constant area due to keeping T_7 constant. As a result, the high-pressure heat exchanger area remains constant.

Next, Figure 4-6 illustrates that evaporator's surface area fluctuation is negligible. The difference is less than one [m^2]. However, to justify the changes: it should be mentioned that the fluctuation is similar to COP variation. By giving greater attention to the parameters, it can be asserted that $\dot{Q}_{eva\_HP}$ is the determined parameter in this formula; for the T_{10} lower than $T_{10\_optimum}$ there are two parameters in the co-direction and $\dot{Q}_{eva\_HP}$ decreases rapidly; but for the T_{10} larger than $T_{10\_optimum}$ two parameters have counter-effects and $\dot{Q}_{eva\_HP}$ increases steadily.

When it comes to drain cooler, based on Figure 4-7, the variation is different from the others; for the left side of $T_{10\_optimum}$, all the parameters have the same effect causes a steep decrease, while for the right side it becomes complex; decrease of h_2 exerts a more pronounced influence on $\dot{Q}_{dc\_HP}$ compared to $\dot{m}_{LP}$ which leads to increase of drain-cooler heat transfer. On the other hand, based on Figure 4-3, the pinch point

temperature of drain cooler increases; finally, the effect of transferred heat is more significant and the area of drain cooler increases.

Concerning the Recuperator, the pinch point temperature holds a significant position; so it does effect on mean logarithmic temperature, enthalpy of point 12. As indicated in Figure 4-8, in a broad sense, Recuperator experiences the constant surface area on the left side; But, by focusing more, it is revealed that it increases a bit; so that, the highest surface area at the lowest temperature of point 10 takes place; Also, the lowest area happens at the largest possible temperature.

Regarding the total heat exchangers, based Figure 4-9, on in the right of diagram, as T_{10} decreases the surface area increases, reaching the maximum at $T_{10\_optimum}$. Then, in the left side, it reduces smoothly. Considering all heat exchangers' surface area, Recuperator and drain cooler are determinative; in other words, to anticipate the total heat exchanger surface area, Recuperator and drain cooler variation should be monitored.

4.2.3 COP/Area parameter

In this section the results of COP in Figure 4-1 and surface area in Figure 4-9 are combined to choose the best temperature. Therefore, it is essential to define a new parameter that takes all these factors into account simultaneously. To do this, the COP/Area ratio of reference case has been computed in Figure 4-10.

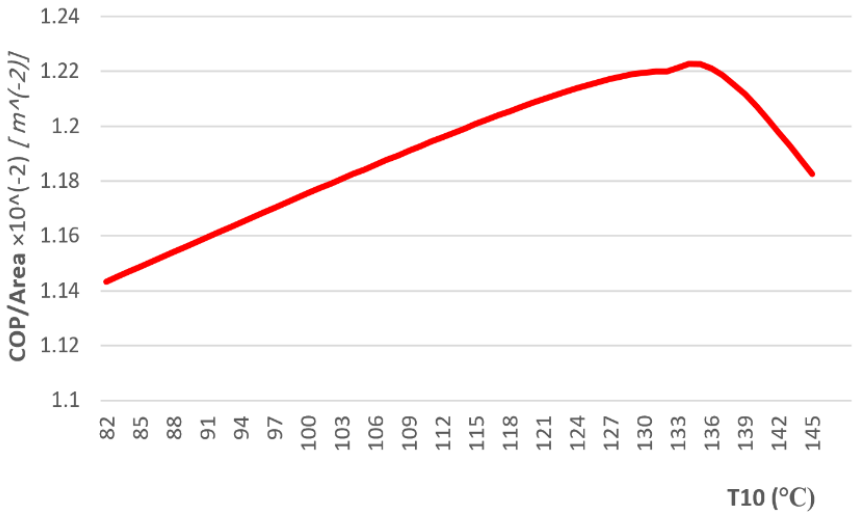

Figure 4-10: COP/Area parameter for reference case

4.3 Sensitivity Analysis

4.3.1 Maximum Temperature effect

It is clear that maximum temperature of cycle has significant effect on all outcomes. Among different results, COP, variables, area of heat exchangers and COP/area parameter are the main. So, in this section, these parameters will be analyzed.

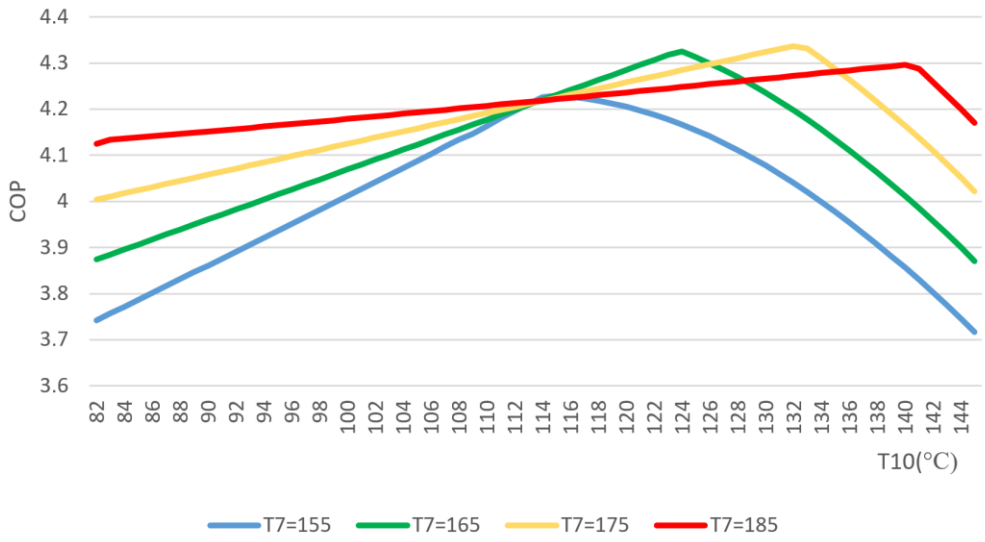

Figure 4-11: COP variation at different T_7

Figure 4-11 shows the COP variation at different maximum temperature of cycle for C1CC6. All curves at different maximum temperature of cycle follow similar trends of COP variation. By descending point of view, COP increases to reach the optimum value; then, decreasing until reach the same COP as starting point.

It is apparent that for larger T_7, the optimum temperature of T_{10} shifts to the right side. It means that improved cycle includes drain cooler with large T_7 needs high $T_{reaction}$ of system. In other words, although drain cooler help to increase the COP of cycle for large T_7, the role of drain cooler becomes fade; so that the difference of $(COP_{optimum} - COP_{start})$ is decreasing.

Despite the fact that COP of simple heat pump cycle always increase by increasing the maximum temperature of cycle, the improved heat pump cycle has different behavior. For low and medium T_7, increasing T_7yields positive results while for the large values it is reversed. More specifically, increasing the temperature of point seven from 175°C to 185 °C brings larger COP of cycle in almost all the parts, but

decrease of $COP_{optimum}$. In other words, considering the cycle works in optimal condition, increasing the temperature of point 7 has a negative effect on COP.

Moreover, it is visible that in some ranges of T_{10}, improved heat pump cycle with lower T_7 has larger COP compared to the cycle having larger T_7. For example, considering the range of $[114, 126]$, cycle with $T_7 = 165℃$ has larger COP compared to the cycle having T_7=175℃ or $T_7 = 185℃$. As a result, working with small T_7 is preferable in some ranges.

Next, the pinch point temperature of drain cooler and Recuperator are illustrated in Figure 4-12 and Figure 4-13 respectively.

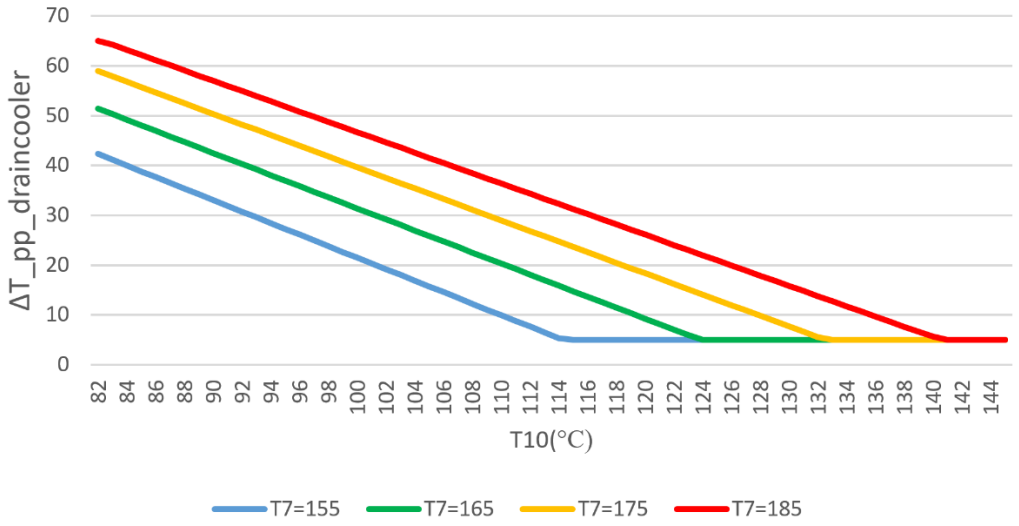

Figure 4-12: The effect of Increasing the maximum temperature on drain cooler pinch point

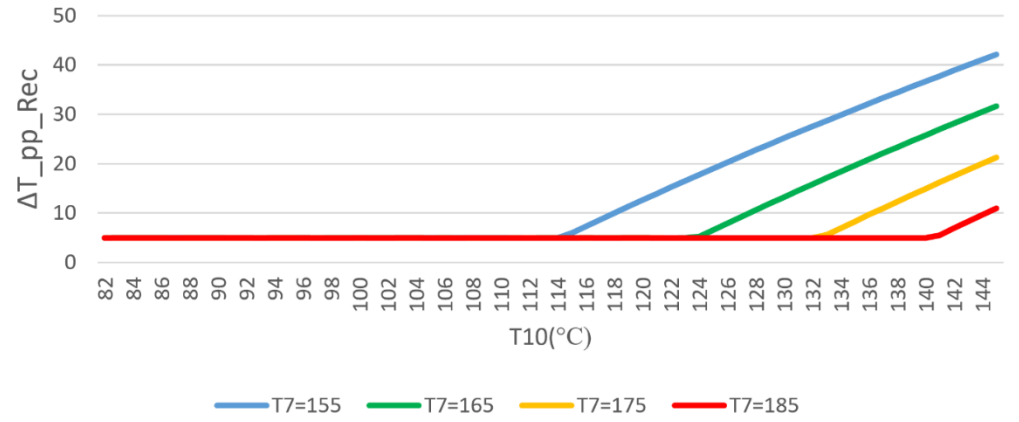

Figure 4-13: The effect of Increasing the maximum temperature on Recuperator pinch point

As can be seen above, increasing the maximum temperature of cycle increase the optimal temperature of cycle. As a result, at high T_7, the pinch point temperature of drain cooler increases at larger temperature. Therefore, it has higher values of pinch point temperatures at high T_7. It is visible that pinch point temperature of drain cooler reaches to the maximum constraint at T_7 =175 at the lowest temperature of cycle. Thus, it is expected that for T_7 larger than 175°C the curve reaches the maximum in larger temperature of cycle. This means that, for large T_7, from a certain point the constraint will limit the optimization and optimization does not happen for the low value of T_{10}.

When it comes to pinch point temperature of Recuperator, the trend is reversed. Large values of T_7 does not need the high pinch point temperature of Recuperator, Thus, the starting point is a low value and it reaches the minimum constraint at large temperatures.

Next, going through the heat exchangers surface area, all the trends follow the same manner. Nevertheless, for some HX the surface area increase while for the others decrease. Table 4-3 summarizes the variation of all HX.

	Condenser	**Desuperheater**	**Evaporator**	**Recuperator**	**Drain cooler**
Variation	Decrease	Increase	Increase	Increase	Decrease

Table 4-3: The effect of Increasing the maximum temperature on Heat exchangers area

To find the reason of heat exchangers' surface area variation the following table should be take into account. Basic parameters are computed in different T_7. The variation of basic parameters are stated in case of increasing T_7.

HX_{Cond}	$\dot{Q}_{Cond} = \dot{m}_{total}.(h_8 - h_1)$ & $UA_{cond} = \frac{\dot{Q}_{Cond}}{\Delta T_{ml\_cond}}$		
	$h_8 = const$ $h_1 = const$ $\dot{m}_{total}$ ↓	$\dot{Q}_{Cond}$ ↓ $\Delta T_{ml_{cond}} = const$	A_{cond} ↓
HX_{DSH}	$\dot{Q}_{DSH} = \dot{m}_{total}.(h_7 - h_8)$ & $UA_{DSH} = \frac{\dot{Q}_{DSH}}{\Delta T_{ml\_DSH}}$		

	$h_8 = const$, $h_7 \uparrow\uparrow$, $\dot{m}_{total} \downarrow$ → $\dot{Q}_{DSH} \uparrow\uparrow$, $\Delta T_{ml_{DSH}} \uparrow$ → A_{DSH}
Evaporator	$\dot{Q}_{eva\_HP} = \dot{m}_{LP}.(h_4 - h_3)$ & $UA_{eva} = \frac{\dot{Q}_{eva\_HP}}{\Delta T_{ml\_eva}}$
	$h_4 = const$, $h_3 \downarrow$, $\dot{m}_{LP} \downarrow$ → $\dot{Q}_{eva_{HP}} \uparrow$, $\Delta T_{ml\_eva} = const$ → $A_{eva} \uparrow$
Recuperator	$\dot{Q}_{rec\_HP} = \dot{m}_{LP}.(h_{12} - h_4)$ & $UA_{rec} = \frac{\dot{Q}_{rec\_HP}}{\Delta T_{ml\_rec}}$
	$h_4 = const$, $h_{12} \uparrow\uparrow$, $\dot{m}_{LP} \downarrow$ → $\dot{Q}_{rec_{HP}} \uparrow\uparrow$, $\Delta T_{ml\_rec} \uparrow$ → $A_{rec} \uparrow$
Drain Cooler	$\dot{Q}_{dc\_HP} = \dot{m}_{LP}.(h_1 - h_2)$ & $UA_{dc} = \frac{\dot{Q}_{dc\_HP}}{\Delta T_{ml\_dc}}$
	$h_1 = const$, $h_2 \uparrow$, $\dot{m}_{LP} \downarrow$ → $\dot{Q}_{dc\_HP} \downarrow$, $\Delta T_{ml\_dc} \uparrow$ → $A_{dc} \downarrow$

Table 4-4: The effect of Increasing the maximum temperature on Basic parameters

Considering all HXs' variation the sensitivity of total surface area to maximum temperature of cycle is as Figure 4-14. It is apparent that increasing the maximum temperature of cycle has a positive effect on surface area; so that, the surface area difference of $T_7 = 155$ and $T_7 = 185$ reaches 37 $[m^2]$.

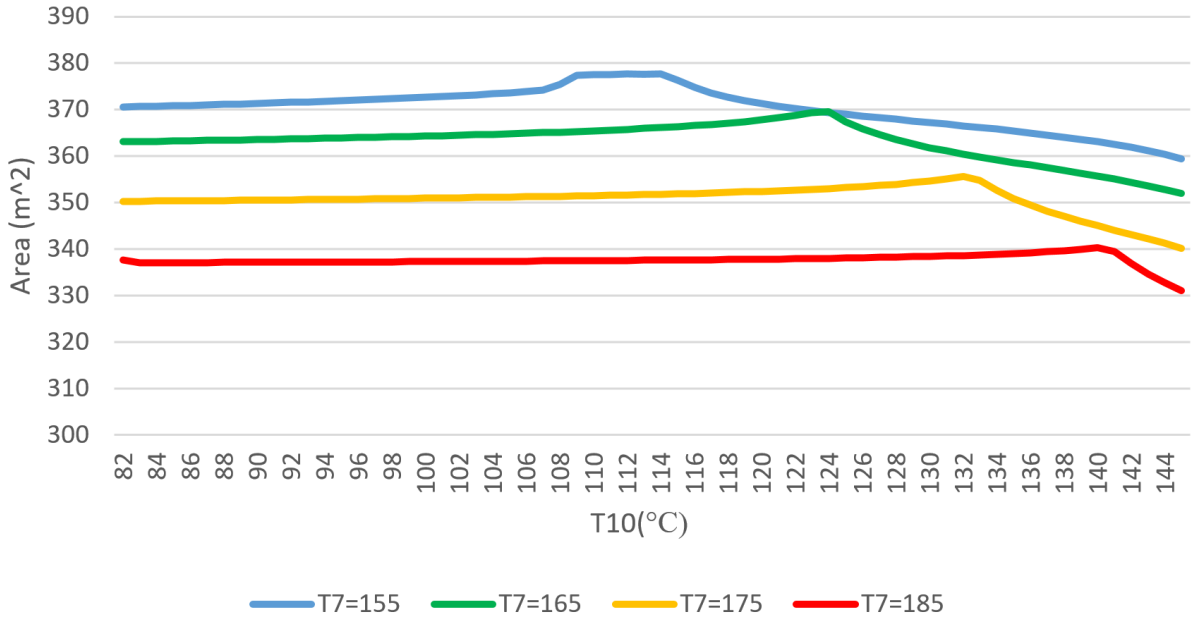

Figure 4-14: The effect of Increasing the maximum temperature on total HXs' surface area

Finally, the COP/Area parameter is shown in Figure 4-15.

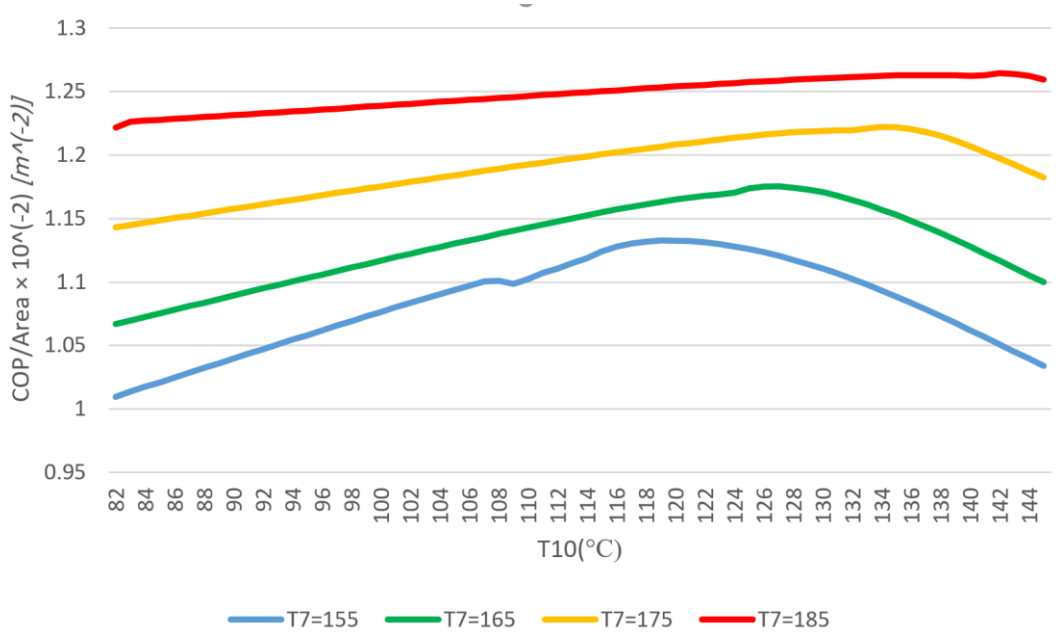

Figure 4-15: The effect of Increasing the maximum temperature on COP/Area parameter

It is obvious that increasing the maximum temperature of cycle leads to increase of COP as well as decrease of surface area. Consequently, the ratio of COP/Area will increase. Increasing T_7 from 155 °C to 185°C increase the ratio by 12%.

4.3.2 Fluid effect

The second part of sensitivity analysis dedicates to fluid effect. Initial fluids that were introduced in 3.2.2.2 Working Fluid, are compared in terms of COP as Figure 4-16.

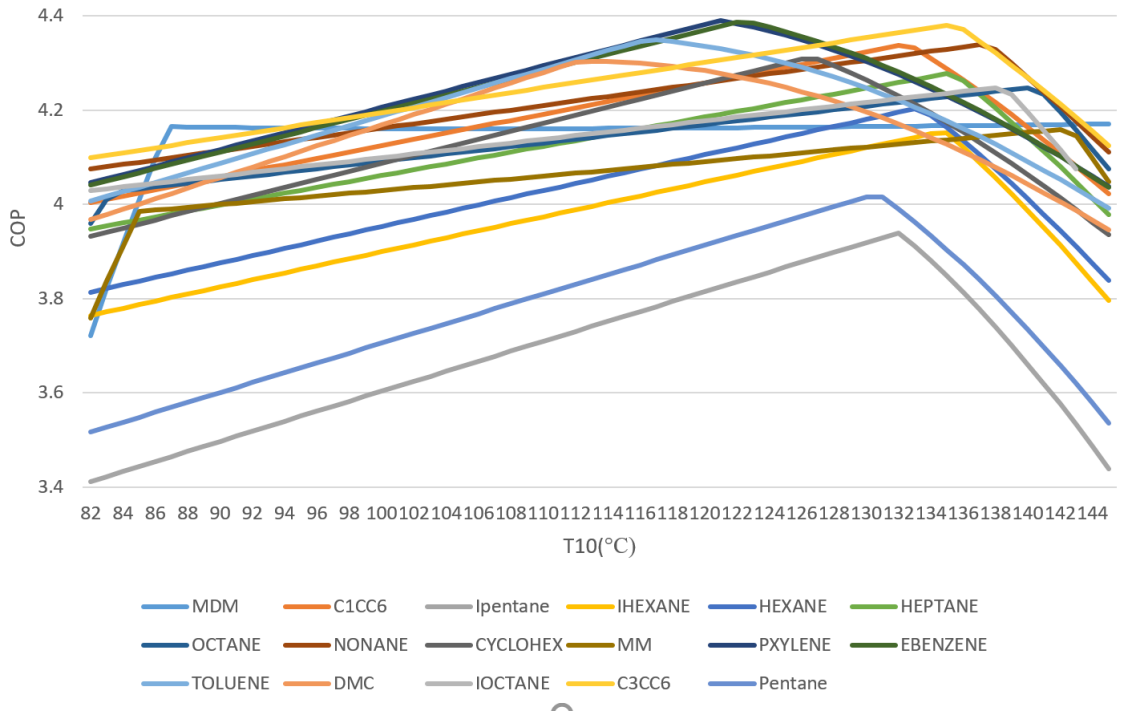

Figure 4-16: Fluid Comparison

The graph illustrates that almost all fluids (Except MDM and MM) follow a similar trend of COP. More specifically, in descending approach, fluids experience COP increase at first, then reaching the maximum one in the range of [120℃, 145℃]. After that, they decrease linearly reaching the same value of COP as starting point with the negligible tolerance as equation (4- 1).

Additionally, based on the Figure 4-16 there is a discontinuity for MDM and MM for the low values of T_{10}. The reason is related to constraints' variables, equation (3. 7), which limits the optimization for the temperatures near boundaries. Thus, it starts to solve the optimization, but the goal of optimization is not reached completely. To be more specific, there is a deviation of T_7 from the imposed value. Table 4-5 shows the deviation for low values of T_{10} for MDM. It can be seen that the deviation increases

dramatically when T_{10} becomes too small, so that the discontinuity takes place. Moreover, for large T_7 deviation increase and it starts from a larger T_{10} to the lowest temperature.

T10	82	83	84	85	86	87	88	89
T7	158.1586	161.5266	164.9783	168.5161	172.1422	175.0002	175.0002	175.0002

Table 4-5: T_7 deviation of MDM optimization

To have a better perspective of how different fluids behave in the proposed cycle Table 4-6 is given. It is divided into two parts: first, the optimum condition of COP takes place. Second, the optimum condition of COP/Area happens. Due to surface area variation, the optimum temperature of point 10 increases one or two degree.

Going to the left side of table, in the second column the optimum temperature of all fluids are listed. It is visible that optimal value takes place in the range of $[120℃ - 140℃]$ for hydrocarbons and $[140℃ - 145℃]$ for siloxanes. It can be perceived that hydrocarbons match better with the temperature of reaction compared to Siloxanes. Indeed, Siloxanes are appropriate for high reaction temperature.

In the third column, the optimum COP of each fluid is shown. Pxylene, Ebenzene and C3CC6 with the COP of 4.40, 4.39 and 4.39 are the best fluids in the optimum condition. Similarly, IHEXANE, PENTANE and IPENTANE are the worst fluids having COP of 4.16, 4.02, 3.94 respectively.

Before going to the fourth and fifth column, an important parameter should be defined. The effectiveness of the improved cycle compared to simple heat pump cycle is defined as following equation.

$$\varepsilon = \frac{COP_{optimum} - COP_{T_{10\_max}}}{COP_{T_{10\_max}}} \times 100 \qquad (4\text{- }3)$$

The effectiveness of all fluids are calculated in the fifth column. It is clear that the COP is increased more in hydrocarbons (linear and cyclo) compared to siloxanes. In other words, hydrocarbons perfectly react to adding drain cooler to simple heat pump cycle. For instance, Ipentane and Pentane have the highest increase with 14.5% and 13.5% respectively. Siloxanes such as MM and MDM show the lowest increase with 2.7% and zero percent.

Next column, the total surface area is computed. All area are almost the same; they are in the range of [346,360] square meters. MDM sets a maximum area while Ipentane has the lowest surface area.

Going to COP/Area parameter in column seven, Ebenzene, Toluene and Pxylene are the best fluids having the largest ratio. The effect of total surface area is clear in in this column. In fact, Pxylene that has the largest COP among all fluids, becomes the third best fluid because of larger area. As for the lowest COP/Area, MM, MDM, Pentane, Ipentane could be mentioned. Despite the fact that MDM set a suitable COP, the COP/Area becomes small so that it becomes one of the worst fluids.

Considering the right part of table, COPs and total area decrease compared to the left side at the same time, so that the COP/Area experiences negligible variation.

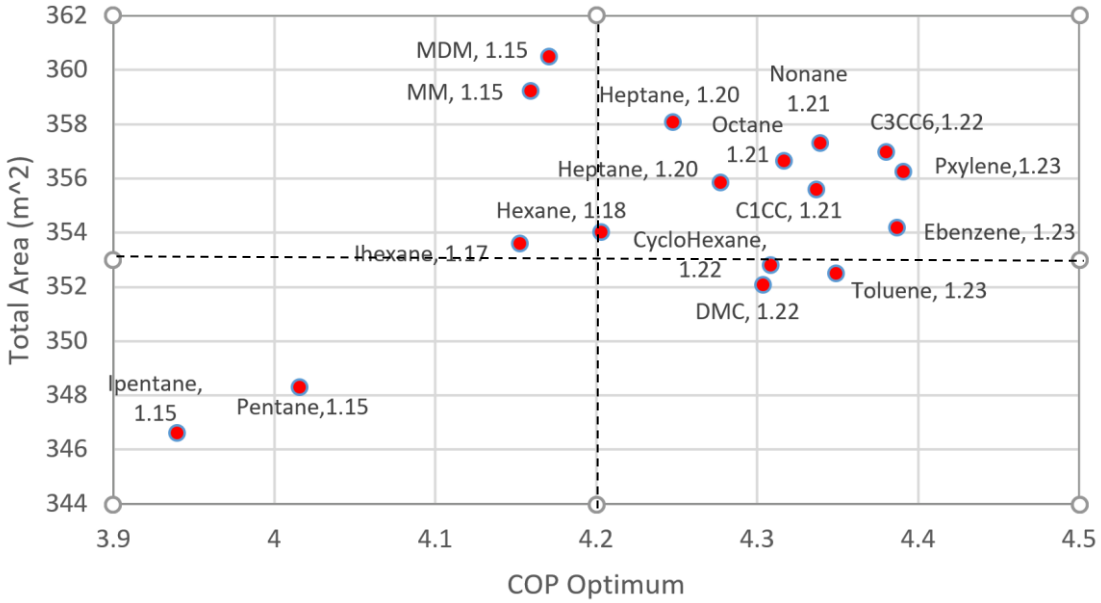

Figure 4-17: Optimum temperature of different fluids

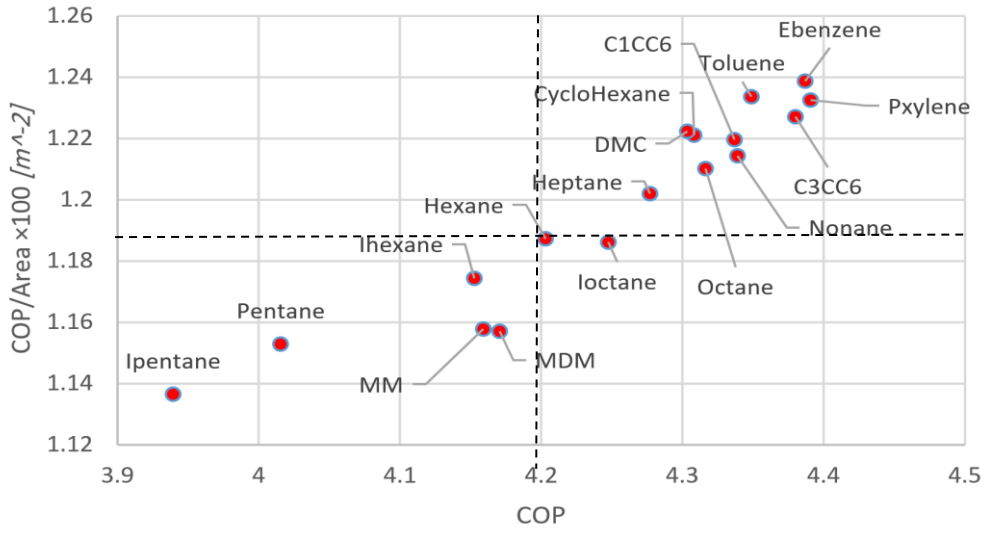

Figure 4-18: Trade off COP and COP/Area for different fluids

	Optimum temperature of COP						Optimum temperature of COP/Area			
Fluid	T_{10_opt} [°C]	$\mathbf{COP_{OPT}}$	COP_{simple}	ε	**Area total** $[m^2]$	$\frac{COP}{Area} \times 100[m^{-2}]$	T_{10_opt} [°C]	$\frac{COP}{Area} \times 100[m^{-2}]$	**Area total** $[m^2]$	**COP**
MDM	145	4.17	4.17	0	360.4	1.15	145	1.16	360.4	4.17
C1CC6	132	4.33	4.02	7.8	355.6	1.21	134	1.22	352.6	4.31
Ipentane	132	3.93	3.43	14.5	346.6	1.13	133	1.14	343.4	3.91
Ihexane	135	4.15	3.79	9.3	353.5	1.17	136	1.18	350.3	4.12
Hexane	133	4.2	3.83	9.5	354	1.18	135	1.19	349.9	4.16
Heptane	135	4.27	3.97	7.5	355.8	1.20	137	1.20	351.6	4.23
Octane	136	4.31	4.06	6.3	356.6	1.21	138	1.21	353.1	4.28
Nonane	137	4.33	4.11	5.5	357.3	1.21	139	1.22	353.5	4.30
CycloHexane	127	4.3	3.93	9.4	352.8	1.22	129	1.22	349.9	4.28
MM	142	4.15	4.04	2.7	359.2	1.16	144	1.16	352.9	4.10
Pxylene	121	4.39	4.03	8.7	356.2	1.23	125	1.24	350.3	4.36
Ebenzene	122	4.38	4.03	8.6	354.1	1.24	125	1.24	351.2	4.37
Toluene	117	4.34	3.99	8.9	352.5	1.23	121	1.24	349.6	4.33
DMC	113	4.3	3.94	9	352	1.22	118	1.23	349.4	4.29
Ioctane	140	4.24	4.07	4.2	358	1.19	142	1.19	352.8	4.20
C3CC6	135	4.38	4.12	6.1	356.9	1.23	137	1.23	353.5	4.35
Pentane	130	4.01	3.53	13.5	348.3	1.15	132	1.16	345.2	3.99

Table 4-6: Optimum values of different fluids

Figure 4-17 shows the optimum COP versus the total surface area for all the fluids. Also, the COP/Area parameter is written close to each points.

The figure is divided into four segments: the top-right (1), top-left (2), bottom-left (3), bottom-right (4) areas. In general, area 4 is the best place for fluids in which large COP and low surface have positive effect leading large COP/Area. On the other hand, area 2 is the worst place in which low COP and large surface area have negative effects on COP/Area. Area 1 and 3 have counter effect parameters. It means that one of them can have a stronger effect leading to high or low COP/Area.

In area 4, Toluene, DMC and Cyclohexane have the high COP/Area ratio. Going to area 1, almost all fluids are presented; They still have suitable COP while the total area increases. Thus, they have lower COP/Area compared to the previous area. Area 2 is the worst place for the fluids in which COP is low and total area is large; MM and MDM are presented in this group. Finally, area 4 dedicates to fluids in which area and COP are low.

Figure 4-18 shows the relation between COP and COP/Area parameter. It should be mentioned that the COP/Area variation is negligible in the optimal temperature of COP and COP/Area; as a result, this figure is plotted in the optimized temperature of COP.

Similar to previous figure, it is divide into 4 parts. Area 1 is the best having large COP and COP/Area at the same time. Area 2 is related to fluids having low COP while COP/Area is large. As can be seen, this area is empty, which means that there is no fluid with low COP and low surface area. Area 3 the worst place in which COP and COP/Area are low. Finally, area 4 shows the fluids with large COP as well as large surface area so that the COP/Area becomes small. However, this information could be understood from the previous figure.

The important note is related to trade-off between COP and COP/Area. Indeed, in this paragraph, fluids having the same COP with different COP/Area are discussed. Also, fluids with equal COP/Area but different COP are introduced.

For instance, Nonane and Toluene have similar COPs while the COP/Area for Tuluene is higher than Nonane. On the other hand, MDM and MM have similar COP/Area compared to Ipentane and Pentane but COP is larger for MM and MDM.

5.Conclusion and Future development

5.1 Conclusion

There has never been a more compelling need to switch to greener, more sustainable energy sources. Renewable energy has received a lot of attention as a result of the ongoing rise in carbon emissions and their negative consequences on the environment. Moreover, as the world's population continues to grow, accompanied by escalating energy needs, transitioning from fossil fuels to renewable sources has become an absolute necessity.

As the generation of power/energy from renewable sources continues to increase, it becomes increasingly crucial to explore strategies and methods for energy storage.

Among the various available options, thermochemical heat storage systems have emerged as a groundbreaking innovation. These systems have the capacity to tackle the intermittency associated with renewable energy sources, bolster grid stability, and contribute to a cleaner and more dependable energy infrastructure. It also has a bunch of advantages such as addressing the energy gap, long duration energy storage, high energy density, reduced thermal losses. In this regard, synchronizing the thermochemical storage system with organic Rankin cycle and heat pump cycle is utilized perfectly.

In this study, the improved heat pump cycle is being optimized; drain cooler and Recuperator are added to simple heat pump cycle. For the optimization, there are some inputs for the optimization such as temperature of heat sources, working fluid, and some fixed assumption such as the efficiencies of components.

The goal of the optimization was to compute how adding a drain cooler could be worthy for the heat pump cycle. The coefficient of performance of system was the parameter to check this goal. The temperature of drain cooler changes between the maximum and minimum temperature of cycle to find the optimized condition.

In this procedure, there were some problems such as controlling the inlet and outlet temperature of compressor in order to prevent ending inside the two-phase domain.

Another challenge was pertained to controlling the maximum temperature of cycle due to thermal limitation.

Considering all the challenges ended up to new optimization; in this optimization, the maximum temperature keeps fixed to assess its worthiness with respect to simple heat pump cycle. Also the maximum coefficient of performance was an objective.

C1CC6 at maximum temperature of cycle equals to 175°C was chosen as a reference case. Then all the results such as COP variation, heat exchanger surface area and COP/area parameter obtained.

Then in the sensitivity analysis, the effect of maximum temperature of cycle, working fluid on optimization was analyzed.

Increasing the maximum temperature brings positive effect as increasing COP and deceasing the surface area of heat exchanger.

Regarding the working fluid, PXYLENE, EBENZENE, C3CC6 and Toluene are the best fluids while IHEXANE, PENTANE and IPENTANE are the worst ones. Besides, hydrocarbons are the most effective types of fluids in terms of adding drain cooler to simple heat pump cycle.

5.2 Future developments

Upon analyzing the results several other features and aspects deserve further scrutiny. These areas should become the focus of future research. This will enable us to create a comprehensive methodology capable of yielding more in-depth and detailed results.

- **Economic calculation**: economic computation related to the cost of fluid,cost of fuels, cost of components, cost of heat exchanger could be done in order to have a optimization close to reality.
- **Heat exchangers design**: instead of assuming some fixed parameters to calculate the global heat transfer coefficient, the HXs could be design in order to increase the efficiency of cycles.
- **Round-trip-efficiency**: considering the procedure of charge and discharge, it is much better to analyze the effect of drain cooler on round trip efficiency.
- **Efficiency of components:** despit the fact that the values of efficiency was based on literature, the better modelling of components like volumetric machines efficiency could be formulated and becomes more accurate.

- **Sensitivity analysis:** 1) analysing other fluids could provide a classification of fluids and could be helpful. 2) effect of diffrent district systems and temperature of low heat source could also be checked.
- **Data validation:** In order to check the results and the optimization other methods and solvers should be carried out; for example, using the multi-objective function or using Patternsearch solver of matlab could also be beneficial.
- **Reversible Machines:** using reversible machine could decrease the cost and increases the simplicity. However, they are often used for small scale cycles.
- **Material and Chemistry:** Developing suitable and cost-effective thermochemical storage material with long cycle life remains a research challenge.
- **Scalling:** Adopting the technology for various scales requires different engineering approaches.

The future of reversible heat pump-ORC systems coupled with thermochemical heat storage holds a great potential for sustainable energy solution. Continued research and development, along with collaboration between industry and academia, will be essential in addressing these challenges and unlocking the full potential of this innovative technology.

References

1. *Eurostat Renewable energy statistics*.
2. Olabi, A., *Renewable energy and energy storage systems*. 2017, Elsevier. p. 1-6.
3. Linden, D. and B. Reddy, *TB, Handbook of Batteries*. 2002, McGraw-Hill Professional, New York.
4. Daniel, C. and J.O. Besenhard, *Handbook of battery materials*. 2012: John Wiley & Sons.
5. Mensah-Darkwa, K., et al., *Recent advancements in chalcogenides for electrochemical energy storage applications.* Energies, 2022. **15**(11): p. 4052.
6. Gogus, Y., *Energy storage systems-Volume I*. 2009: EOLSS Publications.
7. Commission, I., *Electrical energy storage white paper.* Geneva, Switzerland: International Electrotechnical Commission, 2011: p. 1-78.
8. Jouhara, H., et al., *Latent thermal energy storage technologies and applications: A review.* International Journal of Thermofluids, 2020. **5**: p. 100039.
9. Wagner, L., *Overview of energy storage methods.* Analyst, 2007.
10. Uner, D., *Storage of chemical energy and nuclear materials.* Energy Storage Systems, Encyclopaedia of Life Support Systems, 2015: p. 119-139.
11. Chen, H., et al., *Progress in electrical energy storage system: A critical review.* Progress in natural science, 2009. **19**(3): p. 291-312.
12. Zakeri, B. and S. Syri, *Electrical energy storage systems: A comparative life cycle cost analysis.* Renewable and sustainable energy reviews, 2015. **42**: p. 569-596.
13. Nikolaidis, P. and A. Poullikkas, *A comparative review of electrical energy storage systems for better sustainability.* Journal of power technologies, 2017. **97**(3).
14. Hadjipaschalis, I., A. Poullikkas, and V. Efthimiou, *Overview of current and future energy storage technologies for electric power applications.* Renewable and sustainable energy reviews, 2009. **13**(6-7): p. 1513-1522.

15. Amiryar, M.E. and K.R. Pullen, *Analysis of standby losses and charging cycles in flywheel energy storage systems.* Energies, 2020. **13**(17): p. 4441.

16. H Abedin, A. and M. A Rosen, *A critical review of thermochemical energy storage systems.* The open renewable energy journal, 2011. **4**(1).

17. Jerz, J., P. Tobolka, V. Michenka, and T. Dvorák, *Heat storage in future zero-energy buildings.* International Journal of Innovative Research in Science, Engineering and Technology, 2015. **4**(8).

18. Mongird, K., et al., *Energy storage technology and cost characterization report*. 2019, Pacific Northwest National Lab.(PNNL), Richland, WA (United States).

19. Thess, A., *Thermodynamic efficiency of pumped heat electricity storage.* Physical review letters, 2013. **111**(11): p. 110602.

20. Steinmann, W.-D., D. Bauer, H. Jockenhöfer, and M. Johnson, *Pumped thermal energy storage (PTES) as smart sector-coupling technology for heat and electricity.* Energy, 2019. **183**: p. 185-190.

21. Olympios, A.V., et al., *Progress and prospects of thermo-mechanical energy storage—a critical review.* Progress in Energy, 2021. **3**(2): p. 022001.

22. Thiele, E., A. Jahnke, and F. Ziegler, *Efficiency of the Lamm–Honigmann thermochemical energy storage.* Thermal Science and Engineering Progress, 2020. **19**: p. 100606.

23. Meroueh, L. and G. Chen, *Thermal energy storage radiatively coupled to a supercritical Rankine cycle for electric grid support.* Renewable Energy, 2020. **145**: p. 604-621.

24. Dumont, O., et al., *Carnot battery technology: A state-of-the-art review.* Journal of Energy Storage, 2020. **32**: p. 101756.

25. Desrues, T., J. Ruer, P. Marty, and J.-F. Fourmigué, *A thermal energy storage process for large scale electric applications.* Applied Thermal Engineering, 2010. **30**(5): p. 425-432.

26. McTigue, J.D., A.J. White, and C.N. Markides, *Parametric studies and optimisation of pumped thermal electricity storage.* Applied Energy, 2015. **137**: p. 800-811.

27. Wang, L., et al., *Cyclic transient behavior of the Joule–Brayton based pumped heat electricity storage: Modeling and analysis.* Renewable and Sustainable Energy Reviews, 2019. **111**: p. 523-534.

28. White, A., G. Parks, and C.N. Markides, *Thermodynamic analysis of pumped thermal electricity storage.* Applied Thermal Engineering, 2013. **53**(2): p. 291-298.

29. Steinmann, W.-D., *The CHEST (Compressed Heat Energy STorage) concept for facility scale thermo mechanical energy storage.* Energy, 2014. **69**: p. 543-552.

30. Vinnemeier, P., M. Wirsum, D. Malpiece, and R. Bove. *Integration of pumped-heat-electricity-storage into water/steam cycles of thermal power plants*. in *5th International Symposium-Supercritical CO2 Power Cycles. Institute for Power Plant Technology RWTH Aachen*. 2016.

31. Frate, G.F., L. Ferrari, and U. Desideri, *Analysis of suitability ranges of high temperature heat pump working fluids.* Applied Thermal Engineering, 2019. **150**: p. 628-640.

32. Jockenhöfer, H., W.-D. Steinmann, and D. Bauer, *Detailed numerical investigation of a pumped thermal energy storage with low temperature heat integration.* Energy, 2018. **145**: p. 665-676.

33. Eppinger, B., et al., *Carnot battery: Simulation and design of a reversible heat pump-organic Rankine cycle pilot plant.* Applied Energy, 2021. **288**: p. 116650.

34. Antonelli, M., et al., *Liquid air energy storage: Potential and challenges of hybrid power plants.* Applied energy, 2017. **194**: p. 522-529.

35. Laue, H.J., *Renewable Energy · 9 Heat pumps: Datasheet from Landolt-Börnstein - Group VIII Advanced Materials and Technologies · Volume 3C: "Renewable Energy" in SpringerMaterials (https://doi.org/10.1007/10858992_21)*, K. Heinloth, Editor., Springer-Verlag Berlin Heidelberg.

36. Chua, K., S. Chou, J. Ho, and M. Hawlader, *Heat pump drying: recent developments and future trends.* Drying technology, 2002. **20**(8): p. 1579-1610.

37. Bertsch, S.S. and E.A. Groll, *Two-stage air-source heat pump for residential heating and cooling applications in northern US climates.* International journal of refrigeration, 2008. **31**(7): p. 1282-1292.

38. Chen, L., J. Li, F. Sun, and C. Wu, *Performance optimization for a two-stage thermoelectric heat-pump with internal and external irreversibilities.* Applied Energy, 2008. **85**(7): p. 641-649.

39. Agrawal, N. and S. Bhattacharyya, *Studies on a two-stage transcritical carbon dioxide heat pump cycle with flash intercooling.* Applied Thermal Engineering, 2007. **27**(2-3): p. 299-305.

40. Tanaka, N. and S. Kotoh, *The current status of and future trends in heat pump technologies with natural refrigerants.* Mitsubishi Electric Advance, 2007. **120**: p. 2-5.

41. Wang, W., et al., *Field test investigation of a double-stage coupled heat pumps heating system for cold regions.* International Journal of Refrigeration, 2005. **28**(5): p. 672-679.

42. Wang, X., Y. Hwang, and R. Radermacher, *Two-stage heat pump system with vapor-injected scroll compressor using R410A as a refrigerant.* International Journal of Refrigeration, 2009. **32**(6): p. 1442-1451.

43. Winandy, E.L. and J. Lebrun, *Scroll compressors using gas and liquid injection: experimental analysis and modelling.* International Journal of Refrigeration, 2002. **25**(8): p. 1143-1156.

44. Ma, G. and X. Li, *Exergetic optimization of a key design parameter in heat pump systems with economizer coupled with scroll compressor.* Energy Conversion and Management, 2007. **48**(4): p. 1150-1159.

45. Ma, G.-Y. and H.-X. Zhao, *Experimental study of a heat pump system with flash-tank coupled with scroll compressor.* Energy and Buildings, 2008. **40**(5): p. 697-701.

46. Wang, X., Y. Hwang, and R. Radermacher, *Investigation of potential benefits of compressor cooling.* Applied thermal engineering, 2008. **28**(14-15): p. 1791-1797.

47. Alexis, G., *Estimation of ejector's main cross sections in steam-ejector refrigeration system.* Applied Thermal Engineering, 2004. **24**(17-18): p. 2657-2663.

48. Abdulateef, J., K. Sopian, M. Alghoul, and M. Sulaiman, *Review on solar-driven ejector refrigeration technologies.* Renewable and Sustainable Energy Reviews, 2009. **13**(6-7): p. 1338-1349.

49. Sarkar, J., *Optimization of ejector-expansion transcritical CO2 heat pump cycle.* Energy, 2008. **33**(9): p. 1399-1406.

50. Wongwises, S. and S. Disawas, *Performance of the two-phase ejector expansion refrigeration cycle.* International journal of heat and mass transfer, 2005. **48**(19-20): p. 4282-4286.

51. Chaiwongsa, P. and S. Wongwises, *Experimental study on R-134a refrigeration system using a two-phase ejector as an expansion device.* Applied Thermal Engineering, 2008. **28**(5-6): p. 467-477.

52. Kairouani, L., M. Elakhdar, E. Nehdi, and N. Bouaziz, *Use of ejectors in a multi-evaporator refrigeration system for performance enhancement.* International Journal of Refrigeration, 2009. **32**(6): p. 1173-1185.

53. Yapıcı, R. and C. Yetişen, *Experimental study on ejector refrigeration system powered by low grade heat.* Energy Conversion and Management, 2007. **48**(5): p. 1560-1568.

54. Meyer, A., T. Harms, and R. Dobson, *Steam jet ejector cooling powered by waste or solar heat.* Renewable Energy, 2009. **34**(1): p. 297-306.

55. Yari, M. and M. Sirousazar, *Performance analysis of the ejector-vapour compression refrigeration cycle.* Proceedings of the Institution of Mechanical Engineers, Part A: Journal of Power and Energy, 2007. **221**(8): p. 1089-1098.

56. Chen, W., *A comparative study on the performance and environmental characteristics of R410A and R22 residential air conditioners.* Applied thermal engineering, 2008. **28**(1): p. 1-7.

57. Han, D.-H., K.-J. Lee, and Y.-H. Kim, *Experiments on the characteristics of evaporation of R410A in brazed plate heat exchangers with different geometric configurations.* Applied thermal engineering, 2003. **23**(10): p. 1209-1225.

58. Park, K.-J., Y.-B. Shim, and D. Jung, *Performance of R433A for replacing HCFC22 used in residential air-conditioners and heat pumps.* Applied Energy, 2008. **85**(9): p. 896-900.

59. Park, K.-J. and D. Jung, *Performance of heat pumps charged with R170/R290 mixture.* Applied energy, 2009. **86**(12): p. 2598-2603.

60. Nuntaphan, A., C. Chansena, and T. Kiatsiriroat, *Performance analysis of solar water heater combined with heat pump using refrigerant mixture.* Applied Energy, 2009. **86**(5): p. 748-756.

61. Chata, F.G., S. Chaturvedi, and A. Almogbel, *Analysis of a direct expansion solar assisted heat pump using different refrigerants.* Energy Conversion and Management, 2005. **46**(15-16): p. 2614-2624.

62. Lazzarin, R.M. and F. Castellotti, *A new heat pump desiccant dehumidifier for supermarket application.* Energy and Buildings, 2007. **39**(1): p. 59-65.

63. Aynur, T.N., Y. Hwang, and R. Radermacher, *Field performance measurements of a heat pump desiccant unit in dehumidification mode.* Energy and Buildings, 2008. **40**(12): p. 2141-2147.

64. Mohanraj, M., S. Jayaraj, and C. Muraleedharan, *Performance prediction of a direct expansion solar assisted heat pump using artificial neural networks.* Applied Energy, 2009. **86**(9): p. 1442-1449.

65. Gang, P., J. Jie, H. Chongwei, and F. Wen, *Performance of solar assisted heat pump using PV evaporator under different compressor frequency.* 2008.

66. Tangwe, S., P. Mukumba, and G. Makaka, *An Installed Hybrid Direct Expansion Solar Assisted Heat Pump Water Heater to Monitor and Modeled the Energy Factor of a University Students' Accommodation.* Energies, 2023. **16**(3): p. 1159.

67. Chow, T.T., et al., *Modeling and application of direct-expansion solar-assisted heat pump for water heating in subtropical Hong Kong.* Applied Energy, 2010. **87**(2): p. 643-649.

68. Li, H. and H. Yang, *Study on performance of solar assisted air source heat pump systems for hot water production in Hong Kong.* Applied energy, 2010. **87**(9): p. 2818-2825.

69. Chua, K. and S. Chou, *A modular approach to study the performance of a two-stage heat pump system for drying.* Applied Thermal Engineering, 2005. **25**(8-9): p. 1363-1379.

70. Colak, N. and A. Hepbasli, *A review of heat pump drying: Part 1–Systems, models and studies.* Energy conversion and management, 2009. **50**(9): p. 2180-2186.

71. Colak, N. and A. Hepbasli, *A review of heat-pump drying (HPD): Part 2–Applications and performance assessments.* Energy Conversion and Management, 2009. **50**(9): p. 2187-2199.

72. Hepbasli, A., et al., *A review of gas engine driven heat pumps (GEHPs) for residential and industrial applications.* Renewable and Sustainable Energy Reviews, 2009. **13**(1): p. 85-99.

73. Aly, N.H. and A.K. El-Figi, *Mechanical vapor compression desalination systems—a case study.* Desalination, 2003. **158**(1-3): p. 143-150.

74. Adak, A., G. Kishore, V. Srivastava, and P. Tewari, *Mechanical vapour compression desalination plant at Trombay.* International Journal of Nuclear Desalination, 2007. **2**(4): p. 353-362.

75. Gao, P., L. Zhang, and H. Zhang, *Performance analysis of a new type desalination unit of heat pump with humidification and dehumidification.* Desalination, 2008. **220**(1-3): p. 531-537.

76. Hawlader, M., P.K. Dey, S. Diab, and C.Y. Chung, *Solar assisted heat pump desalination system.* Desalination, 2004. **168**: p. 49-54.

77. *HD Service LTD Website (https://www.hdservicesltd.co.uk/ground-source-energy/ground-source-heat-pumps/).*

78. Zamfirescu, C. and I. Dincer, *Performance investigation of high-temperature heat pumps with various BZT working fluids.* Thermochimica Acta, 2009. **488**(1-2): p. 66-77.

79. Granovskii, M., I. Dincer, M.A. Rosen, and I. Pioro, *Thermodynamic analysis of the use a chemical heat pump to link a supercritical water-cooled nuclear reactor and a thermochemical water-splitting cycle for hydrogen production.* Journal of Power and Energy Systems, 2008. **2**(2): p. 756-767.

80. Yang, H., P. Cui, and Z. Fang, *Vertical-borehole ground-coupled heat pumps: A review of models and systems.* Applied energy, 2010. **87**(1): p. 16-27.

81. Sarkar, J., S. Bhattacharyya, and M.R. Gopal, *Simulation of a transcritical CO2 heat pump cycle for simultaneous cooling and heating applications.* International Journal of Refrigeration, 2006. **29**(5): p. 735-743.

82. Hosoz, M. and M. Direk, *Performance evaluation of an integrated automotive air conditioning and heat pump system.* Energy conversion and management, 2006. **47**(5): p. 545-559.

83. Yaïci, W., E. Entchev, P.T. Sardari, and M. Longo, *Recent developments of combined heat pump and organic Rankine Cycle energy systems for buildings.* Product Design, 2020.

84. Steger, D., et al., *Design aspects of a reversible heat pump-Organic rankine cycle pilot plant for energy storage.* Energy, 2020. **208**: p. 118216.

85. Eppinger, B., L. Zigan, J. Karl, and S. Will, *Pumped thermal energy storage with heat pump-ORC-systems: Comparison of latent and sensible thermal storages for various fluids.* Applied Energy, 2020. **280**: p. 115940.

86. Abarr, M., J. Hertzberg, and L.D. Montoya, *Pumped thermal energy storage and bottoming system part B: sensitivity analysis and baseline performance.* Energy, 2017. **119**: p. 601-611.

87. Montozzi, S., *Thermodynamic analysis and optimal working fluid selection of a reversible Heat Pump-Organic Rankine Cycle coupled to a renewable energy based thermo-chemical energy storage.* 2022.

88. Astolfi, M., *An innovative approach for the techno-economic optimization of organic rankine cycles.* 2014.

89. Nam, K.W., J.H. Jeong, K.S. Kim, and M.Y. Ha. *The effects of heat transfer evaluation methods on Nusselt number for mini-channel tube bundles*. in *2010 3rd*

International Conference on Thermal Issues in Emerging Technologies Theory and Applications. 2010. IEEE.

90. Calise, F., A. Macaluso, P. Pelella, and L. Vanoli, *A comparison of heat transfer correlations applied to an Organic Rankine Cycle.* Engineering science and technology, an international journal, 2018. **21**(6): p. 1164-1180.
91. Salimpour, M.R., *Heat transfer coefficients of shell and coiled tube heat exchangers.* Experimental thermal and fluid science, 2009. **33**(2): p. 203-207.
92. Bandhauer, T.M., A. Agarwal, and S. Garimella, *Measurement and modeling of condensation heat transfer coefficients in circular microchannels.* 2006.
93. *National Institute of Standards and Technology*.
94. Göktun, S.n., *Selection of working fluids for high-temperature heat pumps.* Energy, 1995. **20**(7): p. 623-625.
95. Macchi, E. and M. Astolfi, *Organic rankine cycle (ORC) power systems: technologies and applications*. 2016: Woodhead Publishing.
96. VEAL, L., *United States environmental protection agency*. 2021.
97. Sai, T., *Organic Rankine cycle as waste heat recovery system for marine application: Screening methodology, modelling and analysis*, in *Mechanical, Maritime and Materials Engineering*. 2019, TU Delft

List of Figures

List of Tables

List of abbreviation

Abbreviation	Full description
CFC	Chlorochloro fluro carbon
CHP	Combined heat and power
CMP	Compressor
Cond	Condenser
COP	Coefficient of performance
CSP	Concentrated solar power
DC	Drain cooler
DSH	Desuperheater
ESS	Energy storage system
EU	European union
EV	Electric vehicle
Eva	Evaporator
GCHP	Ground-coupled heat pump
GDH	Generation of district heating
GEHP	Gas engine driven heat pump
GSHP	Ground-source heat pump
GWP	Global warming potential
HCFC	Hydro chloroflur carbon
HP	Heat pump
HPD	Heat pump desiccant

HPD	Heat pump drying
HX	Heat exchanger
LP	Low-pressure
ML	Mean logarithm
MP	Mid-pressure
MVC	Mechanical vapor compressor
ODP	Ozone depletion potential
OPT	Optimum
ORC	Organic Rankine cycle
PC	Power cycle
PP	Pinch point
PTES	Pumped thermal energy storage
PVT	Photovoltaic Thermal
Rec	Recuperator
RES	Renewable energy source
Wh	Waste heat
SAHP	Solar-assisted heat pump
Sat	Saturation
SMER	Specific Moisture extraction ratio
SMES	Superconducting Magnetic energy storage
TCES	Thermochemical energy storage
TCS	Thermochemical storage

List of Symbols

Variable	Description	SI unit
T	Temperature	K
S	Entropy	m
h	Enthalpy	J/Kg
h	Heat transfer coefficient	$\frac{W}{k \cdot m^2}$
P	Pressure	Pa
Q	Quality	-
$\dot{Q}$	Heat transfer	W
ε	Drain cooler effectiveness	-
η	Efficiency	-
A	Area	m^2
R	Anti-fouling ability	$\frac{k \cdot m^2}{W}$
COP	Coefficient of performance	-
U	Global heat transfer coefficient	$\frac{W}{k \cdot m^2}$
$\dot{m}$	Mass flow rate	$\frac{Kg}{s}$